CONDUCTION BAND STRUCTURE OF GALLIUM ANTIMONIDE

by

Hartley Bruce Harland

Submitted in partial fulfillment

of the requirements for the degree of

Doctor of Philosophy

Department of Physics,
Faculty of Pure and Applied Science,
The University of Ottawa,
Ottawa, Canada.

1965

ABSTRACT

The dependencies of the Hall coefficient and the magnetoresistance upon the magnetic flux density were determined for Te-doped GaSb for temperatures in the range $4.2^{o}K \leq T \leq 300^{o}K$. The data was analysed on the basis of the two-band model. The density-of-states effective mass for the ⟨111⟩ minima, the energy separation between the (000) and ⟨111⟩ minima at $4.21^{o}K$, and the temperature coefficient of this energy separation, were determined.

$M_1^*/M = 1.10 \pm 0.06$ $\qquad$ $(M_1^*/M)/4^{2/3} = 0.44 \pm 0.03$

$\Delta E_{4.21^{o}K} = 0.0845 \pm 0.0003$ ev.

$d(\Delta E)/dT_{T \geq 78^{o}K} = (8.4 \pm 1.7) \times 10^{-5}$ ev./K^{o}

The total number of observable electrons, $N_0 + N_1$, increased monotonically with increasing temperature for all specimens. The mobility ratio, μ_0/μ_1 , was a function of both the temperature and the impurity concentration. The values obtained varied from 5 to 21 . The dependence of μ_0 upon the electron density in the ⟨111⟩ minima and the temperature agreed very well with the theoretical predictions of Robinson and Rodriguez (64:7) , (65:1) .

ACKNOWLEDGEMENTS

I wish to express my appreciation to Dr. J. C. Woolley for suggesting this problem and for his advice throughout. I also wish to thank the National Research Council for the support of an N.R.C. Studentship and an N.R.C. research grant.

TABLE OF CONTENTS

LIST OF FIGURES

LIST OF TABLES

CHAPTER 1

INTRODUCTION

1. STATEMENT OF THE PROBLEM

The purpose of this research project was to investigate the conduction band structure of GaSb, in particular, the properties of the (000) and ⟨111⟩ bands. The electrical resistivity and the Hall coefficient were determined for a number of Te-doped, single crystal specimens, as functions of the temperature, $2^{\circ}K \leq T \leq 300^{\circ}K$, and the magnetic induction, $0 \leq B \leq 2.4\ w/m^2$. These results were analysed on the basis of the two-band model to give the electron concentrations in the two bands, N_0 and N_1 , and their respective mobilities, μ_0 and μ_1 . The results for N_0 and N_1 at $4.2^{\circ}K$ determined the energy separation of the minima of these two bands, $\Delta E_{1,0}$, and their effective mass ratio, M_1^*/M_0^* . The value for M_0^* was obtained from the literature. This allowed the value for M_1^* to be determined. Assuming a form for the scattering relaxation time, the temperature dependence of $\Delta E_{1,0}$ was determined.

The dependence of μ_0 upon the temperature and the carrier densities of the two bands was analysed on the basis of a recent theory by S. Rodriguez, which predicts that μ_0 will be very sensitive to the screening of the ionized impurities by

the slower moving electrons in the ⟨111⟩ band. Also, the position in energy, with respect to the (000) minimum, of the impurity levels or band, if the term be applicable, was investigated.

2. ELEMENTARY BAND THEORY

In the following discussion, algebraic relations will be stated without proof, since their derivation may be found in almost any book dealing with Band Theory, such as "The Theory of Metals" by A. H. Wilson. Consider an infinite, one dimensional, periodic lattice having an interatomic spacing "a". The Schrödinger equation for an electron moving in the field of the lattice is $d^2\psi/dx^2 + (8\pi^2M/h^2)(E - V(x))\psi = 0$ where $V(x) = V(x + a)$. According to Floquet's Theorm, a solution of this equation is $\psi = \exp(ikx) \cdot u_k(x)$ where $u_k(x) = u_k(x + a)$ and k is real or complex. In order that the wave function correspond to a state of motion in an infinite crystal, it is necessary that k be real. ψ is then a plane wave modulated by a function having the periodicity of the lattice.

The eigenvalues corresponding to this solution may be shown to consist, in general, of bands of allowed energies separated by forbidden gaps. Consider the following case.

Let $V(x) = 0$, $n(a + b) \leq x \leq n(a + b) + a$

$V(x) = V_o$, $n(a + b) + a \leq x \leq (n + 1)(a + b)$

where n is an integer.

Consider two particular solutions of the Schrödinger equation, $\psi_1(x)$ and $\psi_2(x)$, which satisfy the following relations.

$\psi_1(0) = 1$, $\psi_1'(0) = 0$; $\psi_2(0) = 0$, $\psi_2'(0) = 1$

The following relation between k and ψ_1 , ψ_2 may be established by manipulation of linear combinations of wave functions. $\cos(k(a + b)) = (\psi_1(a + b) + \psi_2'(a + b))/2$

Upon solution of the Schrödinger equation for $\psi_1(x)$ and $\psi_2(x)$, and substitution into the above relation, one obtains

$$\cos(k(a+b)) = \cos(\beta a)\cdot\cosh(\gamma b) + \left(\frac{\gamma^2 - \beta^2}{2\beta\gamma}\right)\sin(\beta a)\cdot\sinh(\gamma b)$$

where $\beta^2 = 8\pi^2 ME/h^2$ and $\gamma^2 = 8\pi^2 M(V_0 - E)/h^2$. Now let $b \rightarrow 0$ and $V_0 \rightarrow \infty$ in such a manner that $\lim(bV_0)$ remains finite. Then β and γ are always real and we may write

$\lim(4\pi^2 MabV_0/h^2) = P$.

Then $\cos(ka) = (P/\beta a)\sin(\beta a) + \cos(\beta a)$.

Only values of βa, such that the magnitude of the right hand side is less than or equal to one, correspond to allowed values of energy. The net result is an infinite set of allowed and forbidden ranges of energy. The quantity designated by the symbol P, is a measure of the "tightness" of binding of the electrons. When $P = 0$, $\beta a = 2n\pi \pm ka$ where "n" is an integer, and all values of energy from zero to infinity are allowed. This is the case for perfectly "free" electrons. When P is infinite, the allowed energy levels are independent of k, and are given by $\beta a = n\pi$ for $n \geq 1$, that is, $E = n^2h^2/8Ma^2$. These energy levels are discrete, and the electrons are considered to be completely bound. Returning

to the equation relating k and E, that is, k and β , it will be seen that the discontinuities which occur in the energy spectrum for intermediate values of P, occur when $ka = \pm n\pi$ and n is an integer.

Many of the results obtained from the one dimensional approach carry over into three dimensions. For example, the condition $ka = \pm n\pi$ corresponds to the three dimensional condition for Bragg reflection. The major difference is that in one dimension, for intermediate values of P, the allowed bands of energy are always separated by a forbidden energy gap, whereas in three dimensional crystals it is possible to have energy bands which overlap.

In order to simplify the following discussion, assume that a set of three orthogonal axes (x,y,z) may be chosen in the crystal in such a manner that the lattice is periodic in (x,y,z). This is the case for most of the common semiconducting elements and compounds. Let (d_1,d_2,d_3) represent the periodic spacings along the axes of the crystal, that is, the unit cell is a parallelopiped whose sides are d_1,d_2,d_3 . The potential, V, is then a periodic function such that $V(\underline{r}) = V(\underline{r} + \underline{d})$, where $\underline{d} = n_1 d_1 \underline{i} + n_2 d_2 \underline{j} + n_3 d_3 \underline{k}$, n_1,n_2,n_3 are integers and $\underline{i},\underline{j},\underline{k}$ are unit vectors along the x,y,z axes. The solution of the Schrödinger equation is

$\psi(x,y,z) = u_k(x,y,z) \cdot \exp(i\underline{k}\cdot\underline{r})$ where $\underline{k}$ is a constant vector whose components are k_x, k_y, k_z and $u_k(x,y,z)$ is a function having the periodicity of the lattice. The energy is now a function of k_x, k_y, k_z and will show discontinuities when the value of k_i is an integral multiple of $2\pi/d_i$. Since the energy shows a type of periodicity in k_x, k_y, k_z one may restrict the values of $\underline{k}$ in k-space to a certain zone, and consider E to be a multivalued function of $\underline{k}$. This zone is usually taken as the smallest volume of k-space, centered on the origin, which includes all non-equivalent values of $\underline{k}$. It is more convenient to consider that the components of $\underline{k}$ lie in the range $-\pi/d_i$ to $+\pi/d_i$ instead of the range 0 to $2\pi/d_i$. The shape of this zone depends on the crystal structure and the zone is termed the first Brillouin zone.

The energy cannot now be represented as a function of a single variable, except when E is a function only of k, the magnitude of $\underline{k}$. It is customary to draw diagrams of E as a function of $\underline{k}$ along several of the principle directions in a crystal. Along any particular direction there is generally an energy gap between adjacent bands, but the minimum in one direction may overlap the maximum of the next lowest band in another direction. Overlapping bands are quite common in three dimensional problems. A crystal can only be a semi-

conductor or insulator when there is a finite energy gap between the highest filled band and the lowest empty band.

Theoretical evaluation of $E(\underline{k})$ for even the simplest crystalline form is a formidable problem. Frequently it is only necessary to know the form of the energy bands near the extrema of energy. Since $E(\underline{k})$ and its first and second derivatives must be continuous when the allowed bands do not overlap, and because $E(\underline{k})$ is an even function, it must contain only quadratic terms near $k = 0$. Therefore, when the bands are non-degenerate at $k = 0$, $E = A_0 + A_x k_x^2 + A_y k_y^2 + A_z k_z^2$ for k near zero, and $dE/dk = 0$ at $k = 0$. Therefore $k = 0$ must be an extremum. It may also be shown that for non-degenerate bands, $\partial E/\partial k_i = 0$ at every point on the surface of the Brillouin zone, since these points correspond to standing waves which have a group velocity equal to zero.

3. REVIEW OF THE LITERATURE

The purpose of this section is to collect and briefly discuss the existing theoretical and experimental information which is pertinent to the investigation of the conduction band structure of GaSb. In order to facilitate the comparison of the properties of GaSb with those of certain other semiconductors, the available values for the band parameters of GaSb and these other semiconductors will be tabulated. The results of theoretical investigations of possible electron scattering mechanisms will be discussed, since this information will be required in the analysis of the experimental data.

A. REVIEW OF BAND STRUCTURE INFORMATION

(1) CHOICE OF SEMICONDUCTORS TO BE COMPARED WITH GaSb

It has been predicted theoretically (57:4), and verified experimentally (63:2), that many of the properties of a semiconductor can be predicted with reasonable accuracy by consideration of the properties of neighbouring elements, and compounds of these elements, in the periodic table. The elemental semiconductors are found in group 4A of the periodic table. The simple compound semiconductors are composed of elements from groups 3A and 5A . Consider the elements of groups 3A , 4A and 5A for periods 3 , 4 and 5 of the periodic

table.

	GROUP		
	3A	4A	5A
PERIOD 3	Al	Si	P
4	Ga	Ge	As
5	In	Sn	Sb

The most intensively investigated elemental and compound semiconductors consist, respectively, of one or two elements from this set of nine elements.

It has been found that in many 3-5 compound semiconductors the lowest conduction band minimum is centered upon (000) . However, only Gray Sn of the elemental semiconductors has its lowest conduction band minimum centered upon (000) . The lowest sets of minima in Si and Ge are oriented along the ⟨100⟩ and ⟨111⟩ directions, respectively. The $\underline{k}\cdot\underline{p}$ perturbation calculations [57:2] predict that GaAs should be very similar to Ge . However, the second lowest set of minima in GaAs is oriented along the ⟨100⟩ directions, as is the case for the lowest set of minima in Si . It is found that GaSb is similar to Ge in that its second lowest set of minima is oriented along the ⟨111⟩ directions. As a result of this, GaSb has been frequently compared with Ge . One would also

expect that the properties of GaSb would lie somewhere between those of GaAs and InSb . Therefore, the properties of Ge , GaAs and InSb will be compared with those of GaSb .

(2) ENERGY BAND STRUCTURE IN k-SPACE

The first theoretical calculations of band structure were by Herman (54:6) . He calculated the shapes of the various conduction and valence bands in Ge . His qualitative predictions of the shapes of the bands were very good. However, he was unable to predict the relative energy separations of the extrema with reasonable accuracy. It is still very difficult to accurately predict the positions of the extrema with respect to energy.

The accepted energy band schemes of the four semiconductors under consideration are shown in figure F1:01 . The energy bands of all four semiconductors have the same general shapes. Only the curvatures and energies of the extrema are different for the individual semiconductors. Certain features may be noted. The three highest valence band maxima are centered upon (000) , while the three lowest conduction band minima are oriented along (000) , ⟨100⟩ and ⟨111⟩ . The bands which are centered upon (000) will each consist of a single extremum. Since the ⟨100⟩ conduction bands are not centered upon the Brillouin zone boundary, each of these bands will

ENERGIES ARE QUOTED IN ELECTRON-VOLTS

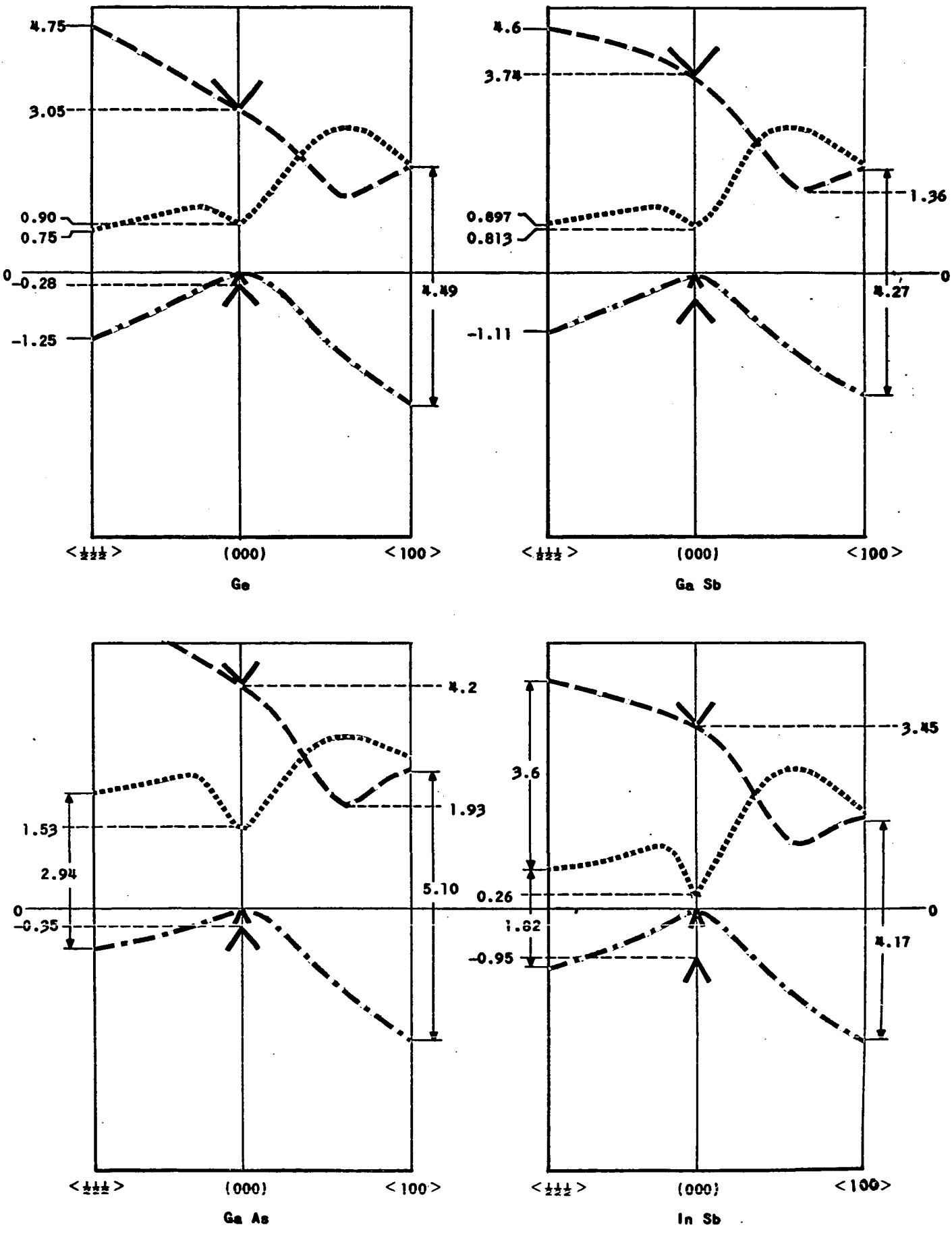

FIGURE F1:01 - ENERGY BAND SCHEMES

consist of a set of six equivalent minima. However, there is good evidence that the ⟨111⟩ conduction bands are centered upon the zone boundary, so will consist of a set of four equivalent minima. It is possible that the ⟨111⟩ conduction bands, in the 3-5 compound semiconductors, could have an energy term which was linear in k . This would remove the centers of the equivalent minima from the zone boundary, and would result in a band having eight equivalent minima. However, this condition has never been observed experimentally.

The energy band schemes which are shown in figure F1:01 were derived from the experimentally determined values of the energy gaps between the various pairs of extrema. These experimental results are tabulated in table T1:01 . In this table and the tables which are to follow, the type of experimental measurement is recorded, whenever it is known, along with the reference number. The abbreviations which were used to designate these experimental effects or types of measurements are as follows.

E	= electrical	O	= optical
C	= electrical conductivity	R	= optical reflectivity
H	= Hall effect	A	= optical absorption
MR	= magnetoresistance	F	= Faraday rotation
HS	= de Haas-Shubnikov effect	V	= Voigt effect

TABLE T1:01 - ENERGY GAPS IN ELECTRON-VOLTS

Ge

$E_{C\langle 111\rangle} - E_{V(000)}$

.785@ 0°K	(54:9 -H,C)
.62 @300°K	(54:11-PEM)
.72 @ 77°K	(55:5 -A)
.62 @300°K	
.670@291°K	(57:6 -A)
.744@ 4°K	(57:10-MA)
.89	(59:5)

$E_{C(000)} - E_{V(000)}$

.88 @ 77°K	(55:5 -A)
.81 @300°K	
.803@300°K	(57:9 -MA)
.897@4.2°K	
.890@ 77°K	(57:10-MA)
.803@298°K	

$E_{C\langle 111\rangle} - E_{V\langle 111\rangle}$

2.0	(60:2)

$E_{C\langle 100\rangle} - E_{V\langle 100\rangle}$

4.49	(62:3)

$E_{V(000)H} - E_{V(000)S}$

.28	(59:7 -A)

GaSb

$E_{C(000)} - E_{V(000)}$

.798@4.2°K	(55:16-A)
.704@290°K	
.81	(59:5)
.82 @ 0°K	(59:7 -O)
.70 @300°K	
.813@4.2°K	(59:14-MA)
.81 @4.2°K	
.80 @ 80°K	(61:1 -A)
.725@300°K	
.82 @ 77°K	(62:8 -F)
.74 @296°K	

$E_{C\langle 111\rangle} - E_{C(000)}$

.074@300°K	(60:11-H,PR)
.08 @4.2°K	(61:1 -H,MR)
.08 - .1	(61:10-PR)

$E_{C\langle 100\rangle} - E_{C(000)}$

>.35	(59:2 -A)
.3 - .4	(61:5 -A)

$E_{C\langle 100\rangle} - E_{V\langle 100\rangle}$

4.21	(60:12-R)
4.33	(62:4)

$E_{C\langle 111\rangle} - E_{V\langle 111\rangle}$

2.00	(60:12-R)

GaAs

$E_{C(000)} - E_{V(000)}$

1.5 @ 0°K	(59:11)
1.35@300°K	
1.53	(61:9 -CR)
1.55	(62:10)

$E_{C\langle 100\rangle} - E_{C(000)}$

>.5	(59:2 -A)
.38 @ 0°K	(60:1 -H)
.5	(60:6)

$E_{C\langle 100\rangle} - E_{V\langle 100\rangle}$

5.08	(60:12-R)
5.12	(62:4)

$E_{C\langle 111\rangle} - E_{V\langle 111\rangle}$

2.94	(60:12-R)

$E_{C\langle 111\rangle} - E_{C(000)}$

.25	(60:6)

InSb

$E_{C(000)} - E_{V(000)}$

.262@ 0°K	(55:18-S)
.18 @298°K	(56:10-MA)
.180@298°K	(57:10-MA)
.26 @ 0°K	(59:7 -E,O)
.18 @300°K	
.225	(61:9 -CR)
.24	(61:12)

$E_{C\langle 100\rangle} - E_{V\langle 100\rangle}$

4.13	(60:12-R)
4.20	(62:4)

$E_{C\langle 111\rangle} - E_{V\langle 111\rangle}$

1.82	(60:12-R)

$E_{V(000)H} - E_{V(000)S}$

1.0	(57:4 -TH)
.9	(61:6 -TH)

PR = piezoresistance
N = Nernst effect
S = magnetic susceptibility
TEP = thermo-electric power
MA = magneto-absorption
CR = cyclotron resonance
PEM = photoelectric lines
TH = theoretical

For each of the materials discussed, the relative positions of the various energy band extrema were established over a number of years from the results of various types of measurements. Even now the energy of the <100> minima in Ge is not known. It is relatively easy to determine the symmetry of the lowest set of conduction band minima and the highest set of valence band maxima by means of angular magnetoresistance measurements. The main band gap can be established from the intrinsic Hall effect, and all direct gaps from direct transition optical measurements. However, it is usually very difficult to establish the symmetry of the subsidiary conduction band minima.

These subsidiary minima can be observed by optical transitions, but it is frequently very difficult to determine which set of minima lie lowest. For each of the three 3-5 compound semiconductors which are being considered, the second lowest set of conduction band minima lies only a few tenths of an electron-volt above the main conduction band minimum. As a result, the thermal energy at room temperature is suf-

ficient to excite an appreciable number of electrons into this subsidiary conduction band. It is then possible to establish the symmetry of this subsidiary set of minima by means of angular magnetoresistance measurements, and the energy separation by means of a two-band analysis or optical measurements. Becker, Ramdas and Fan (61:1) showed from the magnetoresistance anisotropy that the second lowest set of conduction band minima in GaSb had <111> symmetry. Kravchenko and Fan(62:6) also used the anisotropy of the magnetoresistance in GaAs to show that its subsidiary minima had <100> symmetry.

It has been found, mainly by means of optical measurements, that the energy separations between the various band extrema are functions of the temperature. The available values for the temperature dependencies of the energy gaps, for the four semiconductors under consideration, are tabulated in table T1:02 . Only the main or "intrinsic" gap has been investigated in detail for these semiconductors. The temperature dependencies of the inter-band gaps are not as well known as the energy separation of these gaps. It may be seen from table T1:02 that as the temperature rises the minima of the conduction bands move towards the valence bands. However, since these bands move at different rates it is

TABLE T1:02 - TEMPERATURE COEFFICIENTS OF THE ENERGY GAPS IN ev./K°

Ge

$d(E_{C\langle 111\rangle} - E_{V(000)})/dT$

-4×10^{-4} (54:9 -H,C)
-4.5×10^{-4} (55:5 -A)
-4.4×10^{-4} (56:3 -A)
-3.7×10^{-4} (57:6 -A)
-3.9×10^{-4} (59:11-A)

$d(E_{C(000)} - E_{V(000)})/dT$

-6.3×10^{-4} (57:10-MA)

$d(E_{C(000)} - E_{C\langle 111\rangle})/dT$

5×10^{-5} (58:3)

GaSb

$d(E_{C(000)} - E_{V(000)})/dT$

-3.5×10^{-4} (59:4 -O)
-4.1×10^{-4} (59:7 -O)
-3.7×10^{-4} (62:8 -F)

$d(E_{C\langle 111\rangle} - E_{C(000)})/dT$

-3×10^{-4} (60:11-PR,H)
1×10^{-4} (61:3)
1.1×10^{-4} (63:3 -F,H)

GaAs

$d(E_{C(000)} - E_{V(000)})/dT$

-4.9×10^{-4} (56:9)

InSb

$d(E_{C(000)} - E_{V(000)})/dT$

-4.0×10^{-4} (53:4 -A)
-2.6×10^{-4} (54:2 -A)
-2.6×10^{-4} (55:11-A)
-2.9×10^{-4} (55:17-A)
$-(2.9 - 3.9) \times 10^{-4}$ (59:7 -A,PEM)
-3.5×10^{-4} (60:12-O)

possible for some of the inter-conduction band gaps to have positive temperature coefficients. In particular, for GaSb

$$d(\Delta E_{c\langle 111\rangle} - c(000))/dT \approx 10^{-4} \text{ev./K}^{o} .$$

(3) ELECTRON AND HOLE EFFECTIVE MASSES

The energy of a free electron may be expressed as follows: $E = p^2/2M = h^2k^2/8\pi^2M$. Upon differentiation and rearrangement one obtains:

$$M = h^2k^2/8\pi^2E = h^2k/4\pi^2(\partial E/\partial k) = h^2/4\pi^2(\partial^2E/\partial k^2)$$

Many of the equations for free electrons may be applied to the quasi-free carriers in semiconductors by replacing M by M^* , the effective mass. In general, M^* is a tensor, the components of which could be defined by either $h^2k_i/4\pi^2(\partial E/\partial k_i)$ or $h^2/4\pi^2(\partial^2E/\partial k_i^2)$. The most common choice is $M_i^* = h^2/4\pi^2(\partial^2E/\partial k_i^2)$. The theory of band structure predicts that, for a semiconductor which has cubic symmetry, the constant energy surfaces of an extremum in k-space may be approximated by ellipsoids of revolution about the direction along which the extremum is oriented. The effective mass tensor then reduces to three components $M_1 = M_L$ and $M_2 = M_3 = M_T$, where L and T are respectively the longitudinal and transverse components. When the extremum is centered upon (000) , the constant energy surfaces may be approximated by spheres and $M_1 = M_2 = M_3 = M^*$.

The total effective mass may be expressed in terms of the tensor components. There are several different functional forms for the total effective mass. The functional form which is chosen depends upon the particular experimental effect being investigated. The two effective masses which are most commonly employed are the "conductivity" and "density of states" effective masses. They are defined as follows: $1/M_c^* = ((1/M_L) + (2/M_T))/3$ and $M_D^* = (M_L M_T^2)^{1/3}$. When the extremum is centered upon (000) , $M_D^* = M_c^* = M^*$.

The values for the effective masses of the various extrema may be determined from several experimental effects. The effective mass anisotropy, $K = M_L/M_T$, has usually been determined by means of angular magnetoresistance measurements. The experimental effects which are most commonly used to determine the values of the effective mass components are Faraday rotation, de Haas-Shubnikov oscillation, cyclotron resonance and magneto-optical absorption. Faraday rotation measurements probably yield the most reliable values for the effective masses.

The effective mass values which have been determined for Ge , GaSb , GaAs and InSb are recorded in table T1:03 . Because of the relative positions of Ga , In , As and Sb in the periodic table, one would expect the properties of GaSb

TABLE T1:03 - EFFECTIVE MASSES

Ge

$M^*_{C\langle 111\rangle}/M$

Dens.-of-states
.22 (56:1 -CR)
Conductivity
.12 - .16 (55:13-A)
.12 (56:1 -CR)
Longitudinal
.082(56:1 -CR)
.081(57:5)
Transverse
1.64(56:1 -CR)
1.6 (57:5)
Anisotropy
20 (54:1)
14.5(55:1 -MR)
11.9(55:11)
20.0(56:1 -CR)

$M^*_{C(000)}/M$

.041(55:7)
.042(57:9 -MA)
.033(57:10-MA)
.036 - .041 (60:9)

$M^*_{V(000)}/M$

Heavy
.32 (54:5)
.35 (55:7)
.28 (59:11)
Light
.042(54:5)
.045(55:7)
.044(59:11)
.044(62:7)
Split-off
.077(59:7)
.077(59:11)
.066(62:7)
.10 (63:1)
Dens.-of-states
.39 (59:11)

GaSb

$M^*_{C(000)}/M$

.047(59:14-MA)
.052(61:1 - MR,H,A)
.047(61:3)
.047(62:2)
.049(63:3)
.052(64:1 -HS)

$M^*_{C\langle 111\rangle}/M$

Dens.-of-states
.4 (60:8 - PR,H)
.55 (60:11- PR,H)
.90 (61:1 - MR,H,A)
.70 (63:3-F,H)
Anisotropy
8.6 (64:6 -F)

$M^*_{V(000)}/M$

Heavy
.23 (58:4 -A)
.38 (59:14-MA)
.3 (62:2)
.39 (62:5-H,T)
Light
.06 (61:4)
.065(62:2 -TH)
Split-off
.298(62:2 -TH)
.16 (63:2 -TH)

GaAs

$M^*_{C(000)}/M$

.024 - .032 (54:3 -TEP)
.06 (56:2 -TEP)
.043(58:1 -R)
.03 (58:2 -TEP)
.06 (58:7 -H,C)
.065(59:1 -R)
.072(59:9 -F)
.078(59:12-R)
.067 - .083 (61:2 -R,F)
.07 (61:4)
.024(61:8 -TEP)
.071 - .076 (61:9-F,CR)

$M^*_{V(000)}/M$

Heavy
.68 (61:4)
Light
.12 (61:4)
Split-off
.20 (61:4)
Dens.-of-states
.5 (55:8 -TEP)

InSb

$M^*_{C(000)}/M$

.013(55:7 -CR)
.013(55:8 -CR)
.014 - .015 (55:10- H,C,TEP)
.014(56:10-MA)
.015(57:1-MA,CR)
.010(57:3 -HS)
.013 - .04 (57:8 -O)
.013(59:7 -CR)
.013 - .029 (59:8 -F)
.014 - .023 (61:9 -CR,F)
.016(62:9)

$M^*_{V(000)}/M$

Heavy
.13 - .18 (55:10-TEP)
.18 (56:9 -TEP)
.18 (57:4 -TH)
.2 (57:8 -O)
.25 (61:4)
.60 (61:6 -TEP)
Light
.012(60:7 -O)
.015(61:6 -TH)
.012(62:2)
Split-off
.12 (63:2 -TH)

to lie somewhere between those of GaAs and InSb . This is definitely the case for the (000) conduction band effective mass. The experimental values for the minima of the bands are: $(M_0^*/M)_{GaAs} = 0.07$, $(M_0^*/M)_{GaSb} = 0.047$ and $(M_0^*/M)_{InSb} = 0.013$. It may be seen from table T1:01 that the (000) energy gaps, between the conduction and valence bands of these three semiconductors, follow this same sequence. The experimental values for these gaps at the absolute zero of temperature are: $\Delta E_{GaAs} = 1.5ev.$, $\Delta E_{GaSb} = 0.813ev.$ and $\Delta E_{InSb} = 0.26ev.$

Cardona (63:2) and Woolley and Thompson (64:8) discussed the dependence of the various effective masses upon the relative positions of the band extrema. They compared the values of the experimentally determined effective masses with the values calculated using energy gap data. The agreement was very good.

(4) IMPURITY LEVELS

Many experiments have been conducted in order to determine the activation energies of donors and acceptors in semiconductors. Consider a group 5 impurity atom in a group 4 semiconducting crystal. If the impurity atom replaces one of the group 4 atoms, only four of its five valence electrons are required to complete the tetrahedral bonding configuration. The extra electron is only loosely bound to the

impurity atom site and its motion is very similar to that of the electron in a hydrogen atom. If one considers as a model for group 3 and 5 impurities, a hydrogen atom with an electron or hole of mass M^* in a medium having the dielectric constant, ϵ , of the host crystal, the ionization energy is given by:

$$E_I = 2\pi^2 M^* e^4/\epsilon^2 h^2 = 13.53 M^*/M\epsilon^2 ev. \quad ....(1:01)$$

Unfortunately, it is not obvious what value to use for M^* . The usual choice is the value of M^* for the extremum into which the electron or hole can be activated. This tacitly assumes that the wave function, which describes the donor or acceptor state, is a linear combination of the wave functions which describe the extremum into which the electron or hole can be activated. This will be discussed in more detail later.

The dielectric constant for Ge is 16 , and if one uses 0.22 as the value of M^*/M for the <111> conduction band, the predicted value for E_D is 0.0116ev. This prediction agrees reasonably well with the experimentally determined values for As and Sb impurities, namely 0.0127ev. and 0.0096ev. (59:11) respectively. Assuming that $M^*/M = 0.39$ for holes in Ge , the predicted acceptor activation energy is 0.0206ev. The experimentally determined values for B , Ga and In are 0.0104ev. , 0.0108ev. and 0.0112ev. respectively. Although

the agreement is not very good, the difference may be partly due to using the combined value, of the density-of-states effective mass of the three hole bands, in the calculation. Equation (1:01) is an approximation and does not take into account the differences in the activation energy due to the differences in the properties of the individual impurity atoms.

G. Rickayzen (55:16) showed theoretically that equation (1:01) should predict the activation energies of impurities in 3-5 compound semiconductors to approximately the same degree of accuracy obtained for group 4 semiconductors. Groups 2 and 6 impurities in 3-5 semiconductors are the equivalent of groups 3 and 5 impurities in group 4 semiconductors. The experimentally determined values for acceptor ionization energies in the 3-5 semiconductors are in reasonable agreement with theoretical predictions. Since the effective masses of the (000) bands in GaAs , GaSb and InSb are relatively small, their donor activation energies will also be relatively small. Assuming values of 0.07 , 0.047 and 0.013 for M^*/M for the (000) conduction bands in GaAs , GaSb and InSb , and assuming that $\varepsilon = 16$, one predicts donor activation energies of 0.0037ev. , 0.0025ev. and 0.0007ev. respectively.

The Bohr radius of a donor impurity electron in InSb

is relatively large, resulting in an appreciable overlap of the donor wave functions and the formation of an impurity band at donor concentrations as small as 10^{14}cm.$^{-3}$. This impurity band is broad enough to overlap the (000) minimum, resulting in a "zero" activation energy. A donor activation energy has not been observed in InSb except in the presence of a magnetic field which was large enough to shrink the donor wave functions until the impurity band no longer overlapped the conduction band. Although the impurity band in GaAs should not overlap the (000) minimum at low concentrations, no one has been able to determine the activation energies of Te and Se in GaAs .

GaSb is different from most other semiconductors in that its purest form has a hole concentration of approximately 1.5×10^{17}cm.$^{-3}$. Therefore it is not surprising that the activation energies of Te and Se have not been detected. Sagar (60:11), Strauss(61:11) and Bate (62:1) observed relatively large positive Fermi energies for heavily Te- and Se- doped GaSb at low temperatures. This large Fermi energy was much too large to be explained by a conventional impurity band which overlapped the (000) conduction band. Bate attempted to explain these results by postulating a set of impurity levels or an impurity band which was associated with

and immediately below the <111> subsidiary minima of GaSb . This assumption implies that the wave functions of the impurity levels or band are composed of linear combinations of the <111> wave functions. It also implies that the impurity levels or band are/is localized in k-space and therefore would not appear merely as a distortion of the (000) band. This assumption, if valid, explains the behavior of Te-doped GaSb . It allows filling of the (000) minimum, up to the energy of the impurity band, even at low temperatures.

The energy difference between the impurity levels, at low concentrations, and the <111> minima can be estimated from equation (1:01) . The density of states effective mass of the <111> minima is approximately twice [64:5] that of Ge . Therefore, one would expect an energy separation of approximately 0.02ev. The energy separation of the (000) and <111> minima in GaSb is approximately 0.08ev. [61:10] . The impurity levels must lie approximately 0.06ev. above the (000) minimum. Since it is possible to obtain conduction in both the (000) and <111> minima at low temperatures in heavily Te-doped GaSb , the impurity levels must have broadened into a band which overlaps the <111> minima.

B. REVIEW OF THE SCATTERING MECHANISMS IN SEMICONDUCTORS

The purpose of this section is to discuss the electron and hole scattering mechanisms which can occur in semiconductors and the carrier relaxation times, τ , and mobilities, μ, which result from these scattering mechanisms. Quantitative discussions of carrier mobilities require detailed knowledge of the relaxation times involved. However, it is usually only necessary to know the energy and temperature dependencies of the relaxation time in order to be able to analyse experimental data. In order to analyse the experimental data which will be presented in chapter 4 it is only necessary to know the energy dependence of the relaxation time.

The following is a list of the scattering mechanisms which are considered to be important in determining the electrical, optical and thermal properties of semiconductors.

(1) Lattice or phonon scattering

  (a) Acoustical mode scattering

  (b) Optical mode scattering

(2) Impurity scattering

  (a) Ionized impurity scattering

  (b) Neutral impurity scattering

(3) Dislocation scattering

(4) Inter-valley scattering

(5) Electron-electron and electron-hole scattering

The results of theoretical calculations of the relaxation times and conductivity mobilities will be discussed for the types of scattering listed above. The relaxation time and conductivity mobility are defined by the following equations.

$$\sigma = Ne\mu \quad \text{and} \quad \mu = e\langle\tau\rangle / M_c^* \qquad \ldots.(1:02)$$

where: σ = electrical conductivity

N = carrier density

e = magnitude of the charge of an electron

μ = conductivity or drift mobility

τ = carrier relaxation time

M_c^* = conductivity effective mass

$\langle\ \rangle$ denotes the expected average with respect to energy, taken over all occupied states.

(1) LATTICE OR PHONON SCATTERING

Quantum mechanics is frequently used in theoretical investigations of scattering mechanisms in conducting solids. It predicts that the periodic potential of a perfect crystal lattice and the "zero-point" vibrational energy of the atoms in the lattice produce no scattering of the charge carriers. Scattering is produced by deviations from perfect periodicity of the crystal potential. One source of these deviations is

lattice vibration, which is produced by the thermal energy of the lattice. There are two basic modes of lattice vibration, the acoustical and optical modes.

(a) ACOUSTICAL MODE SCATTERING

For acoustical mode vibration the wave length is large compared to the inter-atomic lattice spacing, and the vibrational energy is relatively small. Shockley and Bardeen (49:1), using a wave-mechanical treatment, showed that for the longitudinal acoustic mode:

$$\tau_1 = \rho u_1^2 h^4 / 8\pi^3 (2M_D^*)^{3/2} kT E_1^2 E^{1/2} \quad \ldots.(1:03)$$

where: ρ = density of semiconductor

u_1 = velocity of long compressional waves in the crystal

$E_1 = dE_c/(dV/V)$

E_c = energy of the extremum, measured with respect to an arbitrary zero of energy, of the band in which conduction occurs.

V = volume of the crystal

The drift or conductivity mobility is obtained by substituting equation (1:03) into equation (1:02) .

$$\mu_1 = (\rho u_1^2 eh^4 / 8\pi^3 (2M_D^*)^{3/2} M_C^* E_1^2) \langle E^{-1/2} \rangle / kT \quad \ldots.(1:04)$$

where: $M_D^{*3/2} M_C^* = 3 M_T M_L^{1/2} / (2/M_T + 1/M_L)$

Smith (59:11), page 111 , shows that the expected average of a function may be expressed as follows:

$$\langle X \rangle = \int_0^\infty XE^{3/2} f_0 dE \Big/ \int_0^\infty E^{3/2} f_0 dE \qquad \ldots.(1:05)$$

where: f_0 = Fermi function

$= 1/(1 + \exp((E - E_F)/kT))$ for electrons

$= 1/(1 + \exp((E_F - E)/kT))$ for holes

The energy and temperature dependencies of τ_1 and μ_1 are:

$$\tau_1 \propto (kTE^{1/2})^{-1} \qquad \ldots.(1:06)$$

$$\mu_1 \propto (kT)^{-3/2} F_1(\eta^*)/F_{3/2}(\eta^*)$$

$$= (4/3\pi^{1/2})(kT)^{-3/2} \quad \text{for } \eta^* \ll 1$$

$$= (5/4E_F^{1/2})(kT)^{-1} \quad \text{for } \eta^* \gg 1 \qquad \ldots.(1:07)$$

$F_n(\eta^*)$ and η^* are defined in equations (4:15) and (4:16) .

Note: $F_n(\eta^*) = \Gamma(n + 1) \cdot \exp(\eta^*)$ for $\eta^* \ll 1$

$= \eta^{*(n + 1)}/(n + 1)$ for $\eta^* \gg 1$

$\Gamma(n)$ = mathematical Gamma Function

Equation (1:06) has the form: $\tau \propto E^S$ where $S = -1/2$.

It may be seen from equations (1:07) that for longitudinal acoustical mode lattice scattering, the mobility decreases with increasing temperature.

Herring (55:12) discussed scattering by transverse acoustical shear modes. He showed that the temperature and energy dependencies of τ_S and μ_S were the same as those for τ_i and μ_i , but the expression for the absolute value of τ_S was complex. He also showed that for spherical constant

energy surfaces the scattering due to transverse modes is smaller than that due to longitudinal modes, whereas for bands having multiple extrema, these two types of scattering modes produce relaxation times which are approximately equal.

(b) OPTICAL MODE SCATTERING

For optical mode vibration, adjacent atoms have a vibrational phase difference of 180^{o} . Therefore, the minimum frequency for optical mode vibration is higher than the maximum frequency for acoustical mode vibration. According to Putley (60:10), page 142, the energy associated with the optical modes is greater than that associated with the acoustical modes and is approximately equal to $k\theta_D$. θ_D , which is the Debye temperature, is a few hundred ^{o}K for semiconductors. Putley also states that scattering by optical modes will be less important at low temperatures and will have a temperature variation of approximately $\exp(-\theta_D/T)$.

The "relaxation time approximation" is not reliable for optical mode scattering, because the energy change upon scattering need not be small compared with the total energy of the scattered electron or hole. At relatively high temperatures, $T \gg \theta_D$, and in degenerate specimens, the average energy of a carrier will be large compared to θ_D so the relaxation time approximation should hold. Howarth and

Sondheimer (53:1) showed that for optical scattering, when a relaxation time exists, S = 1/2 in $\tau \propto E^S$. Their expressions for τ and μ were very complex. Fröhlich, Pelzer and Zienau (50:4) obtained similar results.

Herring (55:12) showed that, contrary to earlier ideas, optical mode scattering can be important in group 4 semiconductors below room temperature. However, optical scattering will be more important in 3-5 compound semiconductors where adjacent atoms are dissimilar.

(2) IMPURITY SCATTERING

(a) IONIZED IMPURITY SCATTERING

The Coulomb field of an ionized impurity atom scatters electrons and holes very efficiently. It would be relatively easy to calculate the relaxation time for ionized impurity scattering if it were not necessary to take account of the screening of the Coulomb field by the "quasi-free" charge carriers. There have been several calculations of the relaxation time for ionized impurity scattering. These calculations took account of the screening in different ways.

Conwell and Weisskopf (50:2) assumed that the Coulomb field ceased to be effective at a radius $r_m = N_I^{-1/3}/2$, where N_I is the density of ionized impurity atoms. They obtained the following expression for τ_I :

$$\tau_I = 16\pi(2M_D^*)^{1/2}\varepsilon^2 E^{3/2}/(Z^2e^4N_I \cdot \mathrm{LOG}_e(1 + (4\pi\varepsilon N_I^{1/3}E/Ze^2)^2)) \quad \ldots.(1:08)$$

where: ε = dielectric constant of the semiconductor

Z = number of electrons which were lost or gained by the impurity atom

The most important feature of equation (1:08) is that τ_I is approximately proportional to $E^{3/2}$, so $S = 3/2$ for ionized impurity scattering. It is necessary to evaluate $\langle\tau_I\rangle$ in order to determine the expression for μ_I. The logarithmic term can be taken outside of the integral, since it changes relatively slowly compared to $E^{3/2}$. E, in the logarithmic term, must be replaced by the value of E, E_m, which makes the integrand, $E^3 f_0$, a maximum.

The resulting expression for μ_I is:

$$\mu_I = \frac{16\pi(2M_D^*)^{1/2}\varepsilon^2}{Z^2e^3N_IM_C^* \cdot \mathrm{LOG}_e(1 + (4\pi\varepsilon N_I^{1/3}E_m/Ze^2)^2)} \cdot \frac{(kT)^{3/2}F_3(\eta^*)}{F_{3/2}(\eta^*)} \quad \ldots.(1:09)$$

$$\mu_I \propto (kT)^{3/2}F_3(\eta^*)/F_{3/2}(\eta^*)$$

$$= 8\pi^{-1/2}(kT)^{3/2} \text{ and } E_m = 3kT \quad \text{for } \eta^* \ll 1$$

$$= 5E_F^{3/2}/8 \quad \text{and } E_m = E_F \quad \text{for } \eta^* \gg 1 \quad \ldots.(1:10)$$

Another approach to the problem of how to cut-off the Coulomb field from an ionized impurity atom has been invest-

igated by Dingle (55:6) and by Brooks (55:2) . They took account of the screening of the Coulomb field by the free electrons and holes. They assumed that the potential, ϕ , in the neighbourhood of an ionized impurity had the form:

$$\phi = (Ze/4\pi\varepsilon r)\cdot\exp(-r/d) \qquad \ldots.(1:11)$$

where: r = radial distance from ionized impurity atom

$d = (\varepsilon kT/e^2N)^{1/2}$ = Debye length

N = carrier density

They obtained the following expression for τ_I :

$$\tau_I = 16\pi(2M_D^*)^{1/2}\varepsilon^2E^{3/2}/Z^2e^4N_I(\text{LOG}_e(1 + (h^2e^2N/32\pi^2M_D^*\varepsilon kTE)) - 1) \qquad \ldots.(1:12)$$

Only the logarithmic terms are different in equations (1:08) and (1:12) . It therefore seems reasonably certain that S = 3/2 for ionized impurity scattering. Also, the temperature dependencies of μ_I , which are given by equations (1:10) , are reasonably well established. According to Smith (59:11) , page 151 , equation (1:12) is more reliable than equation (1:08) since (1:12) was developed from a better theoretical foundation.

(b) NEUTRAL IMPURITY SCATTERING

The term, "neutral impurity scattering", refers to scattering by impurities which could be, but are not, ionized. Therefore, Si atoms, in a crystal of Ge , are not considered

to be "neutral impurities". Bardeen and Pearson [49:1] showed that the scattering of electrons and holes by neutral impurities was very similar to the scattering of electrons by neutral hydrogen atoms. The two important scattering processes are direct elastic scattering and exchange scattering in which an incident electron changes places with the loosely bound electron of an impurity atom. These are very "weak" scattering mechanisms compared to scattering by the Coulomb field of an ionized impurity atom. However, in non-degenerate semiconductors at low temperatures, neutral impurity scattering can dominate since there are very few ionized impurities and lattice scattering is insignificant. Neutral impurity scattering should not be important in degenerate semiconductors since they usually possess a relatively "high" density of ionized impurity atoms.

Erginsoy [50:3] considered the collisions of "slow" electrons with neutral impurity atoms and obtained the following expression for the relaxation time.

$$\tau_N = 2\pi^3 M_D^* e^3 / 5\varepsilon N_N h^3 \qquad \ldots.(1:13)$$

where N_N = density of neutral impurities. Equation (1:13) is independent of E and T , and S = 0 . The expression for the mobility is also independent of E and T .

$$\mu_N = 2\pi^3 M_D^{*4} e^4 / 5\varepsilon N_N h^3 M_C^* \qquad \ldots.(1:14)$$

Although equations (1:13) and (1:14) were derived with the aid of a number of approximations, they do indicate that neutral impurity scattering could be dominant in non-degenerate semiconductors at low temperatures.

Sclar (56:8) calculated the scattering of free charge carriers by neutral impurities in semiconductors using the "partial wave technique". He considered the source of scattering to be an attractive potential caused by a negative-energy state associated with the neutral impurity. His treatment predicts a mobility which differs from that of the Erginsoy (50:3) treatment by only a few percent, but predicts a slight temperature dependence. The results of the calculations by Sclar and Erginsoy indicate that τ_N and μ_N are essentially independent of E and T .

(3) DISLOCATION SCATTERING

Distortions of the crystalline lattice due to dislocations cause scattering of the conduction electrons and holes. This form of scattering was discussed theoretically by Dexter and Seitz (52:2) . They showed that dislocation scattering is negligible, at room temperature, unless the dislocation density exceeds 10^8 $cm.^{-2}$. Read (54:10) postulated that dislocations act as acceptor centers. A dislocation, in an n-type crystal, would therefore behave like a negative line

charge and would have around it a positive space charge. This line charge would repel electrons and so would cause scattering. He showed that dislocation scattering is isotropic, unless produced by plastic bending, and has associated with it a relaxation time which may be expressed as follows:

$$\tau_D = 3(M^*/2E)^{1/2}/8R_D N_D \qquad \ldots.(1:15)$$

where: R_D = effective radius of the line charge

N_D = dislocation density in $cm.^{-2}$

τ_D has the same energy dependence as the relaxation time for acoustical lattice scattering. Read also predicted that dislocation scattering will only be important for very heavily strained semiconductors.

(4) INTER-VALLEY SCATTERING

The term, "inter-valley scattering", refers to scattering in which an electron is transferred from one minimum to an equivalent minimum of the same band. The change in the crystal momentum is approximately $h(\underline{k}_1 - \underline{k}_2)/2\pi$ where $\underline{k}_i$ is the wave vector of the electron in the i^{th} minimum. If the change in the crystal momentum is different from zero, a phonon must be emitted or absorbed. The process will therefore be inelastic and unlikely to occur at low temperatures. Herring (55:12) showed that the relaxation time for inter-valley scattering is given by:

$$\tau_{IV} = 1/(\tau_a + \tau_e)$$

$$\tau_a = (1 + E/h\nu)^{1/2}/(\exp(h\nu/kT) - 1)$$

$$\tau_e = (E/h\nu - 1)^{1/2}\exp(h\nu/kT)/(\exp(h\nu/kT) - 1) \quad , E \geq h\nu$$

$$= 0 \quad , E < h\nu$$

....(1:16)

where: "a" refers to absorption of a phonon

"e" refers to emission of a phonon

τ = constant having the dimension of time

$h\nu$ = energy of the phonon involved

E = energy of the electron prior to scattering

This scattering mechanism can only occur for a band having multiple equivalent extrema. It therefore does not apply to bands which are centered upon (000) . A similar type of scattering process could occur between different bands if the electron could be transferred without a large change in its energy. This process can therefore occur between the (000) and ⟨111⟩ conduction bands of GaSb when the Fermi energy is above the bottom of the ⟨111⟩ band. Intervalley scattering can also occur amongst the equivalent minima of the ⟨111⟩ conduction band in GaSb .

(5) ELECTRON-ELECTRON AND ELECTRON-HOLE SCATTERING

Smith (59:11) , page 156, states that collisions between electrons are unimportant in determining the mobility except

under highly degenerate conditions. Even then the contribution must be small since such collisions have very little effect in determining the resistivity of metals. However, collisions between electrons and between electrons and holes may play an important role in establishing a steady state under "high field" conditions. Because of the similarity of the masses of the colliding particles, energy is exchanged much more rapidly between them than between electrons and impurity centers or lattice vibrations.

(6) SCATTERING IN GaSb

It is usually assumed that the overall relaxation time for scattering may be expressed approximately in terms of the relaxation times of the individual scattering mechanisms, by the following equation:

$$1/\tau = \sum_i (a_i/\tau_i) \qquad \text{where: } 0 < a_i \leq 1 \qquad \ldots.(1:17)$$

It is therefore theoretically possible to predict the energy dependence of the resultant relaxation time. Although one can predict the energy dependence of each τ_i, its magnitude and the value of its weighting coefficient, a_i, are very difficult to predict with sufficient accuracy to allow use of equation (1:17). Therefore, equation (1:17) can rarely be applied to the analysis of semiconductors. In practise it is necessary to have one dominant scattering mechanism in

order to be able to predict the dependence of τ upon E with reasonable accuracy.

In order to analyse the experimental data, which will be presented in chapter 4, it is necessary to know the energy dependence of τ . It was mentioned earlier in this chapter that the purest GaSb which has been obtained had a hole concentration of approximately 10^{17} $cm.^{-3}$. n-Type GaSb is obtained by doping with an element, such as Te , to an atomic concentration greater than 10^{17} $cm.^{-3}$. The resulting material is compensated, and will have at least 10^{17} ionized impurities per cubic centimeter. It is also found that n-type impurities have a zero activation energy with respect to the (000) conduction band. This may be due to the impurity states lying above the bottom of the (000) band. For every electron in the (000) band there must be an ionized impurity. As a result, at all temperatures below $300^{o}K$, the highest temperature investigated, ionized impurity scattering will probably be the dominant scattering mechanism.

CHAPTER 2

THEORY

1. "LOW-FIELD" HALL EFFECT AND MAGNETORESISTANCE FOR CONDUCTION IN A SINGLE BAND.

The purpose of this section is to act as an introduction to the theory for the two-band model, and to clarify an assumption which will be made in deriving mathematical relations for the two-band model. In this section, all equations will be stated without proof, since they may be found in any standard semiconductor book such as "Semiconductors" by R. A. Smith.

A. SINGLE EXTREMUM HAVING SPHERICAL CONSTANT ENERGY SURFACES.

This is the case for a non-degenerate band centered upon $k = 0$. For this case plots of constant energy in k-space are assumed to be spheres even when the energy, E , is not parabolic with respect to k . The derivations of equations (2:01) and (2:02) may be found in "Smith", pages 118 and 124, equations (121) , (122) , (166) and (167) .

$$R_0 = \pm r/Ne \ , \ r = \mu_H/\mu = \langle\tau^2\rangle/\langle\tau\rangle^2 \qquad \ldots.(2:01)$$

$$(\Delta\rho/\rho_0)_T = \xi R_0^2 \sigma_0^2 B^2 \ , \ (\Delta\rho/\rho_0)_L = 0 \ , \ \xi + 1 = \langle\tau^3\rangle\langle\tau\rangle/\langle\tau^2\rangle^2 \qquad \ldots.(2:02)$$

where: R_0 = Hall coefficient extrapolated to zero magnetic field

$\rho_0 = 1/\sigma_0$ = electrical resistivity in zero magnetic field

N = carrier density

B = magnetic induction

$\Delta\rho$ = increase in resistivity due to increased scattering in a magnetic field

e = electronic charge

τ = scattering relaxation time

μ_H = Hall mobility

μ = drift mobility

T = transverse

L = longitudinal

$\langle\ \rangle$ = expected average with respect to the energy

When $\langle\tau^n\rangle = \tau^n$, which is the case for infinite degeneracy or when τ is independent of the energy of the carriers, $r = 1$ and $\beta = 0$. Then $R = \pm 1/Ne$ and $(\Delta\rho/\rho_0)_T = 0$.

B. MULTIPLE EQUIVALENT MINIMA OR MAXIMA HAVING CONSTANT ENERGY SURFACES WHICH ARE ELLIPSOIDS OF REVOLUTION.

When a band is not centered upon $k = 0$, it is composed of a number of equivalent extrema which are oriented along a certain set of equivalent axes of symmetry in the crystal. In a material having cubic symmetry, such as GaSb , the most important sets of directions are $\langle 100\rangle$ and $\langle 111\rangle$. In general there is an extremum for each equivalent direction in the set, however, when these extrema are centered on a Brillouin

zone boundary there are only one-half as many extrema as there are equivalent directions. This is because a direction such as [111] and its opposite, $[\bar{1}\bar{1}\bar{1}]$, combine at the zone boundary to produce only one extremum between them. It may also be shown that the constant energy surfaces in k-space, for each extremum, may be approximated by ellipsoids of revolution about the direction along which the extremum is oriented. This is discussed in more detail by Smith in chapter 2.

Equations (2:03) to (2:06) inclusive, which immediately follow, are derived by Smith on pages 120 to 135 .

$$R_0 = \pm (r/Ne)\cdot(3K(K + 2)/(2K + 1)^2) \quad , \quad K = M_L/M_T \qquad \ldots.(2:03)$$

where M_T and M_L are respectively the transverse and longitudinal effective masses of any of the extrema.

$$\Delta\rho/\rho_0 = (b + c(il + jm + kn)^2 + d(i^2l^2 + j^2m^2 + k^2n^2))\cdot B^2 \qquad \ldots.(2:04)$$

where (ijk) and (lmn) are the direction cosines of the electric current and the magnetic induction, respectively, referred to the crystal axes. When the equivalent extrema lie along the $\langle 100 \rangle$ directions, $b + c = -d$, where:

$$b = R_0^2\sigma_0^2\wp_{100}^{001} \quad , \quad c = R_0^2\sigma_0^2(2\wp_{110}^{110} - \wp_{100}^{001}) \quad , \quad d = -2R_0^2\sigma_0^2\wp_{110}^{110}$$

$$\wp_{100}^{001} = (1 + \xi)\cdot((K^2 + K + 1)(2K + 1)/K(K + 2)^2) - 1$$

$$\wp_{110}^{110} = (1 + \xi)\cdot(K - 1)^2(2K + 1)/2K(K + 2)^2 \qquad \ldots.(2:05)$$

When the equivalent extrema lie along the ⟨111⟩ directions, $b + c = 0$ and $d > 0$, where:

$$b = R_0^2 \sigma_0^2 \wp^{001}_{100} \quad , \quad c = -R_0^2 \sigma_0^2 \wp^{001}_{100} \quad , \quad d = R_0^2 \sigma_0^2 \wp^{100}_{100}$$

$$\wp^{001}_{100} = ((1 + \xi) \cdot (2K + 1)^2 / 3K(K + 2)) - 1$$

$$\wp^{100}_{100} = 2(1 + \xi) \cdot (K - 1)^2 (2K + 1) / 3K(K + 2)^2 \qquad \ldots.(2:06)$$

The superscript denotes the magnetic induction direction in the crystal, and the subscript, the electric current direction.

When $K = 1$, the constant energy surfaces are approximately spherical, and the above expressions reduce to those given in the previous section, A. For $K \neq 1$, the magnetoresistance need not be zero for infinite degeneracy or an energy independent relaxation time.

2. TWO-BAND MODEL

The equations of motion of an electron in crossed electric and magnetic fields are:

$$\dot{V}_x = -eE_x/M^* - \omega V_y \qquad \text{where: current density, } J = J_x$$

$$\dot{V}_y = -eE_y/M^* + \omega V_x \quad \ldots.(2:07) \qquad \text{magnetic induction, } B = B_z$$

$$\omega = eB/M^*$$

Let $Z = V_x + iV_y$ ....(2:08)

Then $\dot{Z} - i\omega Z = -e(E_x + iE_y)/M^*$ ....(2:09)

The general solution is

$$Z = Z_0 + e(E_x + iE_y)(1 - \exp(i\omega t))/i\omega M^* \quad \text{where } Z_0 = V_{x_0} + iV_{y_0}$$

This equation is completely general. However, it is necessary to make simplifying assumptions, in order to average Z over all possible collision times.

(1) On collision, the electron loses all knowledge of its previous direction of travel. Therefore, for $t = 0$, V_x and V_y have an isotropic distribution of directions and magnitudes. Therefore $\bar{Z}_0 = \bar{V}_{x_0} + i\bar{V}_{y_0} = 0$. The "bar" denotes the average with respect to time.

(2) A relaxation time for collisions, τ, exists.

(3) τ is direction independent. This limits discussion to

cases of isotropic τ , which can only be strictly true for motion in bands centered upon k = 0 .

The validity of these assumptions will be discussed in section 3. No assumption has been made, as yet, about the energy dependence of τ . This will be considered later. The time average of Z , for a given τ , is:

$$\bar{Z} = \bar{V}_x + i\bar{V}_y$$

$$= e((E_x + iE_y)/i\omega M^*)\cdot\int_0^\infty (1 - \exp(i\omega t))\exp(-t/\tau)dt \Big/ \int_0^\infty \exp(-t/\tau)dt \quad \ldots.(2:11)$$

Equation (2:11) reduces to:

$$\bar{Z} = -e(E_x + iE_y)\tau(1 + i\omega\tau)/(M^*(1 + \omega^2\tau^2)) \quad \ldots.(2:12)$$

Therefore: $\bar{V}_x = -e(E_x - \omega\tau E_y)\tau/(M^*(1 + \omega^2\tau^2))$

$$\bar{V}_y = -e(E_y + \omega\tau E_x)\tau/(M^*(1 + \omega^2\tau^2)) \quad \ldots.(2:13)$$

The current densities for two types of electrons are:

$$J_x = -e(N_1\bar{V}_{x_1} + N_2\bar{V}_{x_2}) \quad , \quad J_y = -e(N_1\bar{V}_{y_1} + N_2\bar{V}_{y_2}) \quad \ldots.(2:14)$$

It is now necessary to average τ with respect to energy. The bra-ket signs will denote the expected average.

Let: $C_i = e^2N_i\langle\tau_i/(1 + \omega_i^2\tau_i^2)\rangle/M_i^*$

$$D_i = e^2N_i\omega_i\langle\tau_i^2/(1 + \omega_i^2\tau_i^2)\rangle/M_i^* \quad \ldots.(2:15)$$

Then: $J_x = (C_1 + C_2)E_x - (D_1 + D_2)E_y$

$$J_y = (C_1 + C_2)E_y + (D_1 + D_2)E_x \quad \ldots.(2:16)$$

Since: $J = J_x$ and $J_y = 0$, $E_y = -(D_1 + D_2)E_x/(C_1 + C_2)$

Therefore: $\rho = E_x/J_x = (C_1 + C_2)/((C_1 + C_2)^2 + (D_1 + D_2)^2)$

$$BR = E_y/J_x = -(D_1 + D_2)/((C_1 + C_2)^2 + (D_1 + D_2)^2) \quad \ldots.(2:17)$$

CASE 1. The relaxation time, τ_i , is not a function of the energy, E .

Then: $\langle \tau_i/(1 + \omega_i^2\tau_i^2) \rangle = \tau_i/(1 + \omega_i^2\tau_i^2) \quad \ldots.(2:18)$

This is the case for τ_i a constant with respect to the carrier energy and also for extreme degeneracy, that is, $E_f/kT \gg 1$. Under these conditions $\langle \tau_i^n \rangle = \tau_i^n$. The conductivity, σ_i , and the Hall coefficient, R_i , for each band, have the following simple forms:

$$\sigma_i = N_i e \mu_i \quad , \quad R_i = 1/N_i e \quad \text{where:} \quad \mu_i = e\tau_i/M_i^* \quad \ldots.(2:19)$$

The drift mobility, μ_i , is the carrier velocity per unit electric field when B = 0 .

Introduce the following sign convention:

$e > 0$

$N, \mu < 0$ for electrons

$N, \mu > 0$ for holes

Equations (2:15) and (2:17) may be transformed into the more useful form of equations (2:20) and (2:21) by introduction of the sign convention and substitution of equations (2:19) into equations (2:15) and (2:17).

Then: $$\rho = (A_0 + A_1B^2)/e(A_0^2 + A_2B^2)$$

$$R = (A_3 + A_4B^2)/e(A_0^2 + A_2B^2) \qquad \ldots.(2:20)$$

Where:

$$A_0 = (\sigma_{000} + \sigma_{111})/e = N_0\mu_0 + N_1\mu_1$$

$$A_1 = \sigma_{000}\sigma_{111}(\sigma_{000}R_{000}^2 + \sigma_{111}R_{111}^2)/e = (N_0\mu_1 + N_1\mu_0)\mu_0\mu_1$$

$$A_2 = \sigma_{000}^2\sigma_{111}^2(R_{000} + R_{111})^2/e^2 = (N_0 + N_1)^2\mu_0^2\mu_1^2$$

$$A_3 = (\sigma_{000}^2R_{000} + \sigma_{111}^2R_{111})/e = N_0\mu_0^2 + N_1\mu_1^2$$

$$A_4 = \sigma_{000}^2\sigma_{111}^2R_{000}R_{111}(R_{000} + R_{111})/e = (N_0 + N_1)\mu_0^2\mu_1^2 \qquad \ldots.(2:21)$$

In order to evaluate the experimental results for σ and R in terms of N_i and μ_i, it is necessary to do a "low-field" expansion of the equations for ρ and R.

Then: $$\rho \simeq \rho_0 + \rho_1B^2 + \rho_2B^4$$

$$\simeq \frac{1}{e}\left[\frac{1}{A_0} + \frac{(A_0A_1 - A_2)B^2}{A_0^3} - \frac{A_2(A_0A_1 - A_2)B^4}{A_0^5}\right]$$

$$R \simeq R_0 + R_1 B^2$$

$$\simeq \frac{1}{e}\left[\frac{A_3}{A_0^2} + \frac{(A_0^2 A_4 - A_2 A_3)B^2}{A_0^4}\right] \qquad \ldots.(2:22)$$

Five coefficients, ρ_0 , ρ_1 , ρ_2 , R_0 and R_1 , may be determined from measurements of ρ and R as functions of B. However, there are only four independent band parameters to be determined, N_0 , N_1 , μ_0 and μ_1 . These may be evaluated by using ρ_0 , ρ_1 , R_0 and either ρ_2 or R_1 . These latter two are related by the relation $R_1^2 = -\rho_1\rho_2$. The A_i's are related to the experimental parameters as follows:

$$A_0 = 1/e\rho_0$$

$$A_1 = A_0((\rho_1/\rho_0) - (\rho_2/\rho_1)) \quad = A_0((\rho_1/\rho_0) + (R_1^2/\rho_1^2))$$

$$A_2 = -A_0^2\rho_2/\rho_1 \quad = A_0^2 R_1^2/\rho_1^2$$

$$\sqrt{A_2} = -A_2^{1/2} \quad = -A_0 R_1/\rho_1$$

$$A_3 = eA_0^2 R_0 \qquad \ldots.(2:23)$$

A_4 is not expressed in terms of the experimental parameters since it is not required in solution for the band parameters.

Define: $\alpha = A_3\sqrt{A_2} + A_2 - A_0 A_1$

$$\beta = A_3 + \sqrt{A_2}$$

$$\gamma = (\beta^2 - 4\alpha)^{1/2} \qquad \ldots.(2:24)$$

The four band parameters may be obtained by substitution of equations (2:23) and (2:24) into equations (2:21).

Then: $\mu_0 = (\beta - \gamma)/2A_0$

$$\mu_1 = (\beta + \gamma)/2A_0$$

$$N_0 = A_0^2(\sqrt{A_2}(\gamma + \beta) - 2\alpha)/2\alpha\gamma$$

$$N_1 = A_0^2(\sqrt{A_2}(\gamma - \beta) + 2\alpha)/2\alpha\gamma \qquad \ldots.(2:25)$$

The above relations have been defined so that the subscript, 0 , refers to the band having the larger mobility magnitude. In the case of n-type GaSb, and conduction by two types of electrons, 0 refers to the (000) minimum and 1 to the set of equivalent $\langle 111 \rangle$ minima. This theory was derived by considering two types of electrons. However, the sign convention built into the derivation results in the equations for N_i and μ_i being applicable to any two types of carriers.

CASE 2. τ_i is a function of the energy, E .

$$\langle \tau^n/(1 + \omega^2\tau^2) \rangle \cong \langle \tau^n \rangle - \omega^2 \langle \tau^{n+2} \rangle + \omega^4 \langle \tau^{n+4} \rangle$$

It is impossible to solve explicitly for the band parameters, in general, since the expected average of each different power of τ may be replaced by a scattering parameter, $r_{i_n} = \langle \tau_i^n \rangle / \langle \tau_i \rangle^n$, which can only be evaluated by numerical integration. Moreover, this numerical integration cannot be carried out until the "reduced Fermi energy", $\eta^* = E_f/kT$, which depends on the value of N_i and functional form of $\tau_i(E)$, has been determined.

It is necessary to make an approximation which will allow the general equations for R and ρ , (2:17), to be solved in terms of the band parameters, and yet take into account the energy dependence of τ_i . The simplest way to do this is to replace the R_i in equations (2:21) by the more general form,

$$R_i = r_i F_i(K_i)/N_i e \quad \text{where:} \quad r_i = \langle \tau_i^2 \rangle / \langle \tau_i \rangle^2$$

$$F_i(K_i) = 3K_i(K_i + 2)/(2K_i + 1)^2$$

$$K_i = (M_L^*/M_T^*)_i \qquad \ldots.(2:26)$$

It may then be shown that:

$$r_0 F_0 \mu_0 = (\beta - \gamma)/2A_0$$

$$r_1 F_1 \mu_1 = (\beta + \gamma)/2A_0$$

$$N_0/r_0F_0 = A_0^2(\sqrt{A_2}(\gamma + \beta) - 2\alpha)/2\alpha\gamma$$

$$N_1/r_1F_1 = A_0^2(\sqrt{A_2}(\gamma - \beta) + 2\alpha)/2\alpha\gamma \qquad \ldots\ldots(2:27)$$

3. VALIDITY OF THE TWO-BAND MODEL

This section is an attempt to justify the assumptions and approximations involved in the derivation of the two-band equations. The first and second assumptions, that $\bar{Z}_0 = 0$ and τ_i exists for each band, are frequently encountered in electron transport theory. Although these assumptions are probably valid, they can only be shown to be reasonable. The concept of a relaxation time for scattering is obviously valid whenever there exists a scattering mechanism which tends to return a system from a non-equilibrium to an equilibrium condition. This should be the case whenever the change in the carrier energy upon scattering is small compared to the total kinetic energy of the carrier. Most of the scattering processes which occur in semiconductors are believed to satisfy these conditions. Also, in the absence of external fields, an equilibrium becomes established which does not permit a net transfer of charge. Under these conditions $\bar{Z}_0 = 0$. This condition should still be valid in the presence of sufficiently "small" externally applied fields, particularly for "large angle" scattering.

The third assumption, that τ_i for each band is isotropic with respect to k, can only be strictly true if both bands are centered upon $k = 0$. In general, for bands not centered

upon k = 0 , this assumption can only be acceptable if the error introduced by neglect of the effects due to anisotropy is relatively small. Consider equation (2:03) for the Hall coefficient of a material having conduction in only one band. R_0 is a function of K , but not of $\underline{k}$. R_0 is isotropic for a single band, so should not introduce anisotropy into two band conduction.

The resistivity in zero magnetic field will also be isotropic for any material with cubic symmetry, but the magnetoresistance will in general be anisotropic as may be seen from equation (2:04). The two-band equations are derived in such a manner that the predicted magnetoresistance is due solely to the presence of two types of carriers, the effect of anisotropy being neglected. The contribution to the magnetoresistance due to the anisotropy of τ_i , and the variable degeneracy of each band, may be calculated in the following manner.

Let the subscripts 0 and 1 refer to the (000) and ⟨111⟩ bands respectively. Let the sub-subscript, 0 , indicate the value for B = 0 . Assume that there is no interaction of any kind between the bands. Then the magnetic-field-dependent conductivity, including the effects of anisotropy and variable degeneracy, is given by: $\sigma(B) = \sigma_0(B) + \sigma_1(B)$

The corresponding resistivity may be expressed in terms of the individual zero-magnetic-field resistivities and the individual magnetoresistances. Since $\sigma_{B=0}$ is a scaler, the tensor properties of $\sigma(B)$ may be neglected when $\Delta\sigma/\sigma \ll 1$.

$$\rho(B) = 1/\sigma(B) = \rho_0\rho_1/(\rho_0 + \rho_1)$$

$$= \rho_{0_0}\rho_{1_0}(1 + \Delta\rho_0/\rho_{0_0})(1 + \Delta\rho_1/\rho_{1_0})/(\rho_{0_0} + \rho_{1_0} + \Delta\rho_0 + \Delta\rho_1)$$

The magnetoresistance due to the anisotropy and the variable degeneracy is expressed by equation (2:28).

$$\Delta\rho/\rho_{B=0} \simeq (\rho_{0_0}(\Delta\rho_1/\rho_{1_0}) + \rho_{1_0}(\Delta\rho_0/\rho_{0_0}))/(\rho_{0_0} + \rho_{1_0}) \quad \ldots.(2:28)$$

Equation (2:28) must be compared with the term in B^2 for the two-band-model magnetoresistance, which is expressed by equation (2:29).

$$\Delta\rho/\rho_{B=0} = \sigma_0\sigma_1(\sigma_0R_0 - \sigma_1R_1)^2B^2/(\sigma_0 + \sigma_1)^2 \quad \ldots.(2:29)$$

Since the two-band model will be applied to n-type GaSb , for which the bands of interest are (000) and ⟨111⟩ , the error estimation will be carried out for a typical set of conditions in GaSb .

Let: $N_{(000)} = N_{\langle 111\rangle}$, $\mu_{(000)} = 10\mu_{\langle 111\rangle}$

Then: $\sigma_0 = 100\sigma_1$ and $R_0 \simeq R_1$ $\quad \ldots.(2:30)$

Since the k = 0 band is approximately spherical, $K_{(000)} = 1$. The only available value for $K_{\langle 111\rangle}$ was obtained by Piller [64:6], $K_{\langle 111\rangle} = 8.6$. These values will be required in the derivation of equations (2:32) and (2:33).

The two-band model deals only with the case of transverse magnetic field. Since the magnetoresistance is anisotropic, consider the following transverse cases.

CASE 1: $[ijk] = [100]$, $[lmn] = [010]$

CASE 2: $[ijk] = [111]$, $[lmn] = [11\bar{2}]$

where [ijk] and [lmn] denote, respectively, the crystal directions along which the specimen current and the magnetic field are directed. The following single-band magnetoresistances were obtained from equations (2:02) , (2:04) and (2:06).

$$\Delta\rho_0/\rho_{0_0} = \xi_0\sigma_0^2R_0^2B^2 \quad , \quad \Delta\rho_1/\rho_{1_0} = YB^2 \qquad \ldots.(2:31)$$

where: $Y = b$ for CASE 1

$Y = b + 2^{1/2}d$ for CASE 2

When K = 8.6 equations (2:06) reduce to:

$$b = (0.2111 + 1.2111\xi_1)\sigma_1^2R_1^2$$

$$d = (0.3626 + 0.3626\xi_1)\sigma_1^2R_1^2 \qquad \ldots.(2:32)$$

Upon substitution of (2:31) into (2:28), the magnetoresistance due to anisotropy and variable degeneracy reduces to:

$$\Delta\rho/\rho_{B=0} = (Y\sigma_1 + \xi_0\sigma_0^3 R_0^2)B^2/(\sigma_0 + \sigma_1) \qquad \ldots.(2:33)$$

Equations (2:34) and (2:35) are obtained by substitution of conditions (2:30) and equations (2:32) into equations (2:29) and (2:33).

Two Band Model: $\Delta\rho/\rho_{B=0} = 6.69 \times 10^{-2}\sigma_0^2 R_0^2 B^2$ ....(2:34)

Magnetoresistance Due To Anisotropy And Variable Degeneracy:

CASE 1: $\Delta\rho/\rho_{B=0} = (1.92\times10^{-4} + 1.10\times10^{-3}\xi_1 + 0.91\xi_0)\sigma_0^2 R_0^2 B^2$

CASE 2: $\Delta\rho/\rho_{B=0} = (6.58\times10^{-4} + 1.57\times10^{-3}\xi_1 + 0.91\xi_0)\sigma_0^2 R_0^2 B^2$

....(2:35)

CASE 2 is very nearly the most severe possible case, if not the most severe. The anisotropy contribution, which is given by the first term, $6.58 \times 10^{-4}\sigma_0^2 R_0^2 B^2$, is a maximum of 1% of the two-band magnetoresistance. The second and third terms give the contributions due to the variable degeneracies of the ⟨111⟩ and (000) bands, respectively. Assume that $\tau = aE^S$. In the most severe extreme, the classical limit, that is when $E_f/kT \ll 0$, it may be shown that:

$$\langle\tau^n\rangle = a^n(kT)^{nS}\cdot\Gamma(5/2 + nS)/\Gamma(5/2)$$

where $\Gamma(x)$ = Gamma Function of x .

The magnetoresistance coefficient, ξ_i , is given by:

$$1 + \xi_i = \langle \tau_i^3 \rangle \langle \tau_i \rangle / \langle \tau_i^2 \rangle^2$$

$$= \Gamma(5/2 + 3S) \cdot \Gamma(5/2 + S) / (\Gamma(5/2 + 2S))^2$$

Consider the two most important types of scattering in semiconductors.

LATTICE SCATTERING: $S = -1/2$, $\xi_i = 0.275$

IONIZED IMPURITY SCATTERING: $S = +3/2$, $\xi_i = 0.57$

Therefore, under the most severe conditions, $\xi_1 = 0.57$, and the ⟨111⟩ band degeneracy contribution is less than 1.4% of the two-band magnetoresistance. In practise, ξ_0 is very small since for all specimens measured, $E_{f_0}/kT \gg 1$ at low temperatures and $E_{f_0}/kT > 1$ even at room temperature. Therefore, assumption (3) is justified.

Although ξ_0 and ξ_1 do not appear in equation (2:34) for the two-band magnetoresistance, they are at least partially taken into account in the modified two-band equations, (2:27). These equations should produce reasonably accurate results for most of the conditions encountered in the investigation of the conduction band structure of GaSb .

4. DE HAAS-SHUBNIKOV OSCILLATIONS

The following treatment was obtained from a review article by A. H. Kahn and H. P. R. Frederikse, Solid State Physics volume 9.

Consider a conducting solid in a magnetic field which is applied in the z-direction. The motion of the quasi-free electrons is quantized in a plane normal to the field, the allowed electron energies being given by:

$$E_n = (n + 1/2)h\omega/2\pi + h^2k_z^2/8\pi^2M^* \quad , \quad \omega = eB/M^* \qquad ....(2:36)$$

The density of allowed states is:

$$N(E)dE = h\omega(2M^*/h^2)^{3/2}\sum_{n=0}^{n_{max.}}(E - (n + 1/2)h\omega/2\pi)^{-1/2}dE \qquad ....(2:37)$$

The total density of electrons is given by:

$$N = \int_{h\omega/4\pi}^{\infty} N(E)f(E)dE \quad \text{where} \quad f(E) = \text{Fermi distribution function} \qquad ....(2:38)$$

If $E_f \gg kT$, (2:38) may be integrated giving:

$$N = 2h\omega(2M^*/h^2)^{3/2}\sum_{n}(E_f - (n + 1/2)h\omega/2\pi)^{1/2} \qquad ....(2:39)$$

If $E_f \gg h\omega/2\pi$, (2:38) can be integrated approximately by means of Poisson's summation formula.

$$N = \frac{8\pi(2M^*E_f)^{3/2}}{3h^3}\left[1 - \frac{3\pi^2kT}{2^{1/2}h\omega}\left[\frac{h\omega}{2\pi E_f}\right]^{3/2}\sum_{r=1}\frac{(-1)^{r+1}\cos(4\pi^2rE_f/h\omega + \pi/4)}{r^{1/2}\sinh(4\pi^3rkT/h\omega)}\right] \qquad ....(2:40)$$

Equation (2:40) is valid for all temperatures, but the oscillatory terms are very small when $kT \gg h\omega/2\pi$. Usually N has a constant value and E_f oscillates in value. The oscillations in the electron transport properties will coincide with those in E_f , and so will have a periodicity of $h\omega/2\pi$.

$$E_f = (n + 1/2)h\omega/2\pi = (eh/2\pi M^*_{E_f})/(d(1/B)/dn)$$

$$\simeq E_{f_{B,T=0}} = (h^2/8\pi^2 M^*_D)(3\pi^2 N)^{2/3}$$

$$N \simeq (4e\pi(M^*_D/M^*_{E_f})/(d(1/B)/dn))^{3/2}/3\pi^2 \qquad \ldots.(2:41)$$

where: M^*_D = density of states effective mass averaged over all occupied states in the band

$M^*_{E_f}$ = effective mass at the Fermi level

For a parabolic band having spherical constant energy surfaces, $M^*_D/M^*_{E_f} = 1$ and equation (2:41) for N does not involve the effective mass.

The magnetoresistance of n-type GaSb shows de Haas-Shubnikov oscillations at liquid helium temperatures. It is theoretically possible to predict the amplitude of oscillation as a function of the temperature and the magnetic induction. However, the calculation is extremely difficult and requires a detailed knowledge of the scattering processes. A number of authors have shown that the oscillation

amplitude has the form:

$$\Delta\rho_{osc.amp.} = C_0 T^{C_1} B^{C_2} / \sinh(C_3(T + T')/B)$$

$$\simeq C_0 T^{C_1} B^{C_2} \exp(-C_3(T + T')/B)$$

where: $C_3 = 4\pi^3 k M^*/eh$

$T' = h/2\pi^2 k\tau$

τ^{-1} = total rate for transfer out of a state ....(2:42)

This analysis of the periodicity and the amplitude of magneto-oscillations is only valid for bands having spherical constant energy surfaces, that is, bands centered on $k = 0$. Anisotropic bands will show direction-dependent periodicity and amplitude. In general, the oscillatory behavior is a function of the extremal cross-sectional area of the Fermi surface normal to the magnetic field. Only for a spherical Fermi surface is this cross-sectional area simply related to the density of states effective mass.

CHAPTER 3

EQUIPMENT AND EXPERIMENTAL TECHNIQUES

The equipment and experimental techniques employed in the determination of certain electron transport properties of GaSb were relatively standard. All measurements were D.C. or quasi-D.C. The most important innovations were the modification of a galvanometer amplifier for use as a D.C. voltage amplifier, and the use of potential back-off techniques wherever possible in order to improve the relative accuracy of measurements of magnetic-field-dependent potentials.

1. EQUIPMENT

A. VARIABLE TEMPERATURE CRYOSTATS

(1) SPECIMEN HOLDER AND CRYOSTAT HEAD

The specimen holder and the cryostat head are shown in figure F3:01 . These units were designed to meet the following conditions:

(a) simplicity of specimen installation and initial alignment,

(b) minimal thermo-electric potential generation,

(c) good thermal contact with the controlled temperature,

(d) electrical isolation from the cryostat,

(e) minimal heat leak from room temperature,

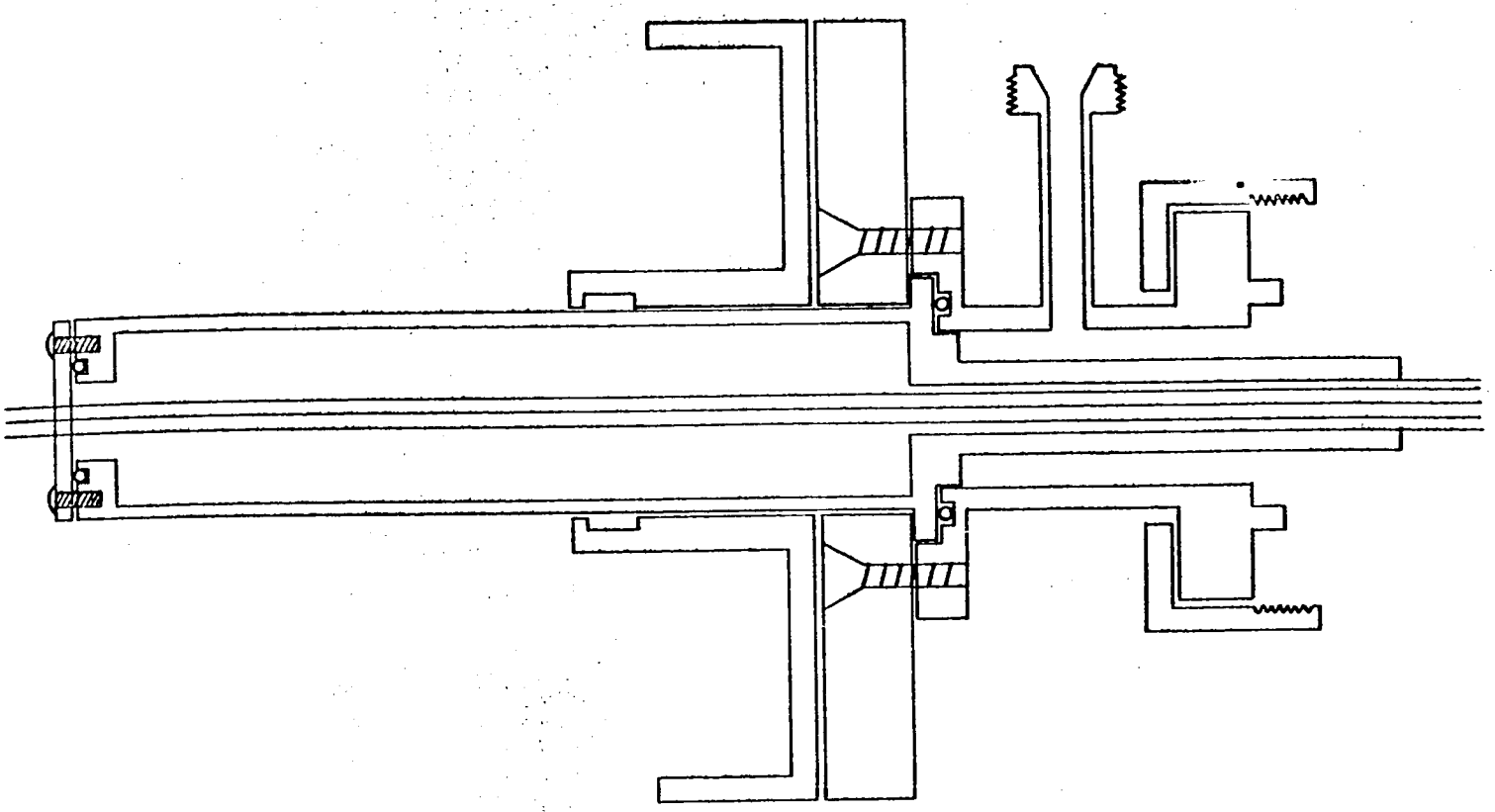

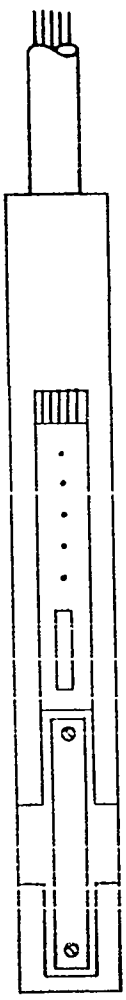

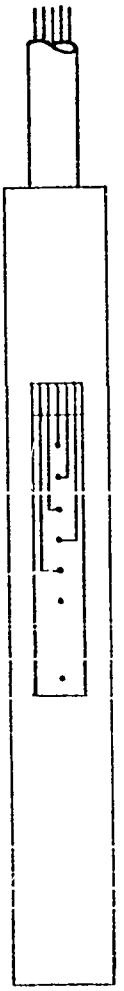

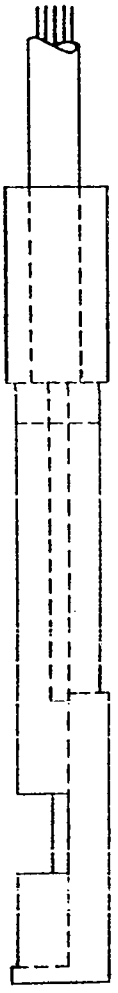

FIGURE F3:01 - SPECIMEN HOLDER AND CRYOSTAT HEAD

(f) and vacuum tight, rotatable cryostat head for specimen alignment with respect to the magnetic field.

The specimen holder was made from bakelite in order to electrically insulate the specimen from the cryostat. Its diameter was made 0.015 inch smaller than the internal diameter of the specimen chamber of the metal cryostat. This clearance was sufficient to allow the specimen holder to be easily removed from the cryostat, but still constrain the specimen holder to an accurately vertical orientation. The specimen holder was connected to the cryostat head by means of a 0.25 inch diameter, thin wall stainless steel tube, which produced a negligible heat leak. In order to minimize the generation of thermo-electric potentials in the specimen electrical leads, all wires were copper and only one set of joints was allowed within the cryostat. Contact between the set of specimen contact wires and the set of electrical leads going to the measuring equipment, was made by soldering to a set of five copper pins on the specimen holder. Since these electrical joints were within the temperature controlled specimen chamber, they generated negligible thermo-electric potentials. At the point of departure from the cryostat head, the leads were vacuum sealed into a piece of bakelite by means of baking varnish.

The cryostat head was designed so that it could be used with either the metal cryostat or the glass dewar. Two locating pins ensured accurate positioning of the cryostat head on the two cryostats. A rotatable vacuum seal allowed alignment of the specimen in the magnetic field. This rotation was calibrated in degrees for use in studies of magnetoresistance as a function of the angular orientation with respect to the magnetic field.

(2) METAL CRYOSTAT

The metal cryostat shown in figure F3:02 was based on a design by Dr. E. Sonders of Los Alamos. Basically, it consisted of an outer vacuum jacket, two refrigerant tanks, a radiation shield anchored to the liquid nitrogen tank, and a silver specimen chamber separated from the liquid helium tank by a stainless steel thermal resistance. Since most of the cryostat was constructed from brass, which outgased continuously, the high vacuum system was constantly pumped by a one inch oil diffusion pump.

The specimen was maintained at the temperature of the silver chamber by means of helium exchange gas. A 1000 ohm manganin heater and a 100 ohm copper resistance thermometer were bifilar wound, in close proximity to each other, on the specimen chamber immediately below the thermal resistance.

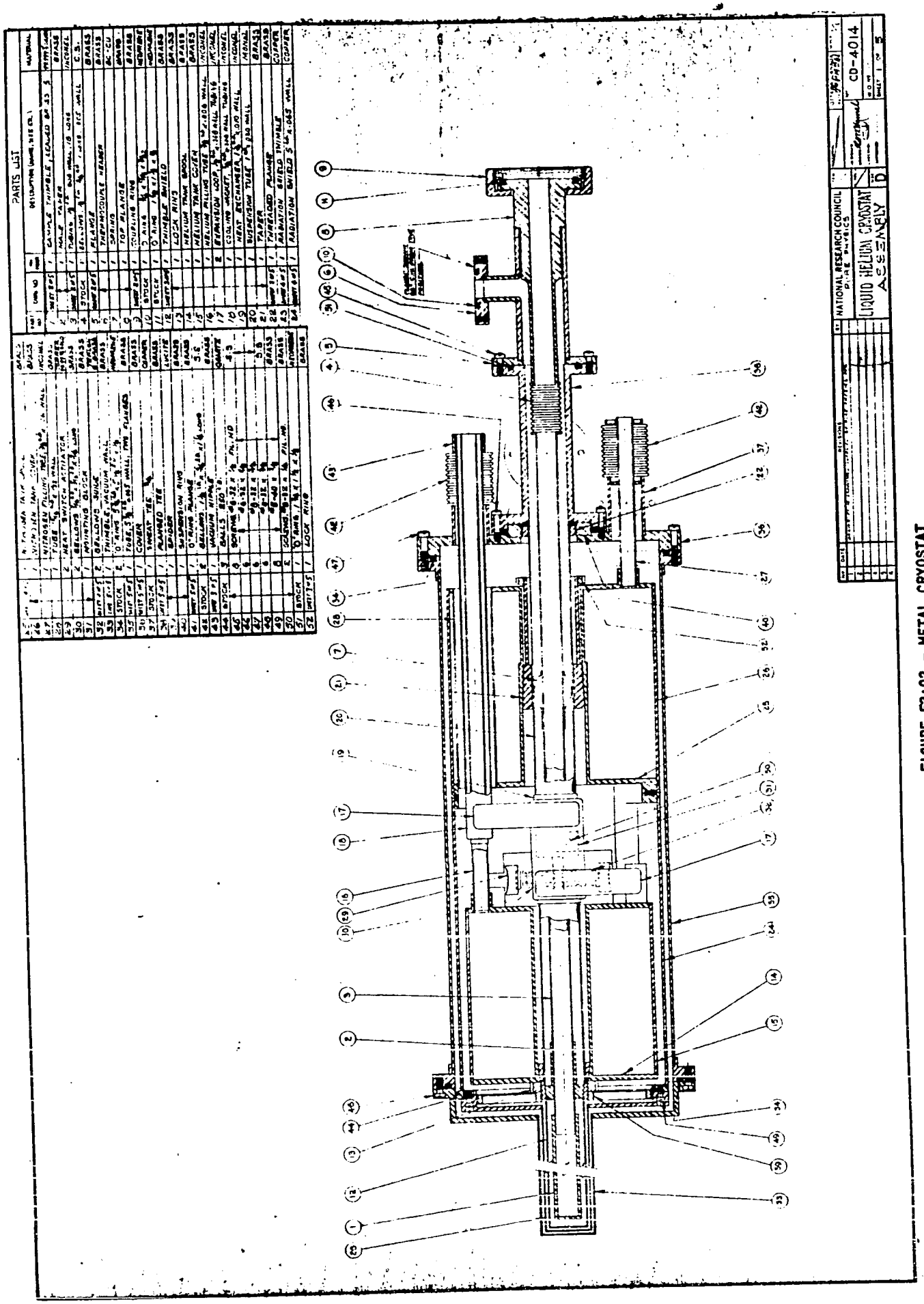

FIGURE F3:02 - METAL CRYOSTAT

The temperature of the specimen chamber was sensed, for purpose of temperature control, by a gold-cobalt versus copper thermocouple. One thermocouple junction was anchored to the specimen chamber, the other to the helium tank.

Although the cryostat was supposed to be capable of good temperature stability over the range $4.2^{o}K \leq T \leq 300^{o}K$, it was found that temperature regulation to a few hundredths of a degree was only possible above $60^{o}K$, that is, in the temperature range in which liquid nitrogen was the main refrigerant. Below this temperature, using liquid helium as the main refrigerant, fluctuations in the high vacuum surrounding the specimen chamber introduced spurious heat leaks, causing drifts in the temperature of approximately $0.2\ K^{o}$.

(3) GLASS DEWAR

A single long-tailed, completely silvered dewar was used for measurements in the range $1.8^{o}K \leq T \leq 4.2^{o}K$, and at the fixed temperatures of certain refrigerants. The small magnet-pole-gap did not allow use of a two-dewar system. The specimen holder was centered in the tail of the dewar by means of a nylon sheath. When electrically conducting refrigerants such as ice water were used, the specimen was insulated from the refrigerant by means of a long copper tube,

thermal equilibrium of the specimen and refrigerant being provided by exchange gas. The temperature of each refrigerant used was determined by measurement of its vapor pressure. The temperature of a "pumped" refrigerant was regulated by controlling its vapor pressure by means of a manostat. Below 4.2^{o}K , this allowed temperature control to about 0.002 K^{o} .

B. TEMPERATURE CONTROL EQUIPMENT

(1) THERMOCOUPLE CONTROLLER

The temperature control system which was used with the metal cryostat is shown in figure F3:03 . It was a proportional controller, that is, the change in the current supplied to the heater was proportional to the error-signal voltage. The temperature control system may be broken down into the following units: thermocouple detector and specimen chamber heater, variable potential back-off unit, D.C. chopper amplifier, and D.C. power amplifier.

The thermocouple was made from commercial (relatively high purity) number 32 copper wire and 0.003 inch gold-cobalt wire. Since temperature control was required in the presence of a variable magnetic field, a resistance thermometer could not be used as the detector for temperature control. A thermocouple is not affected by a magnetic field

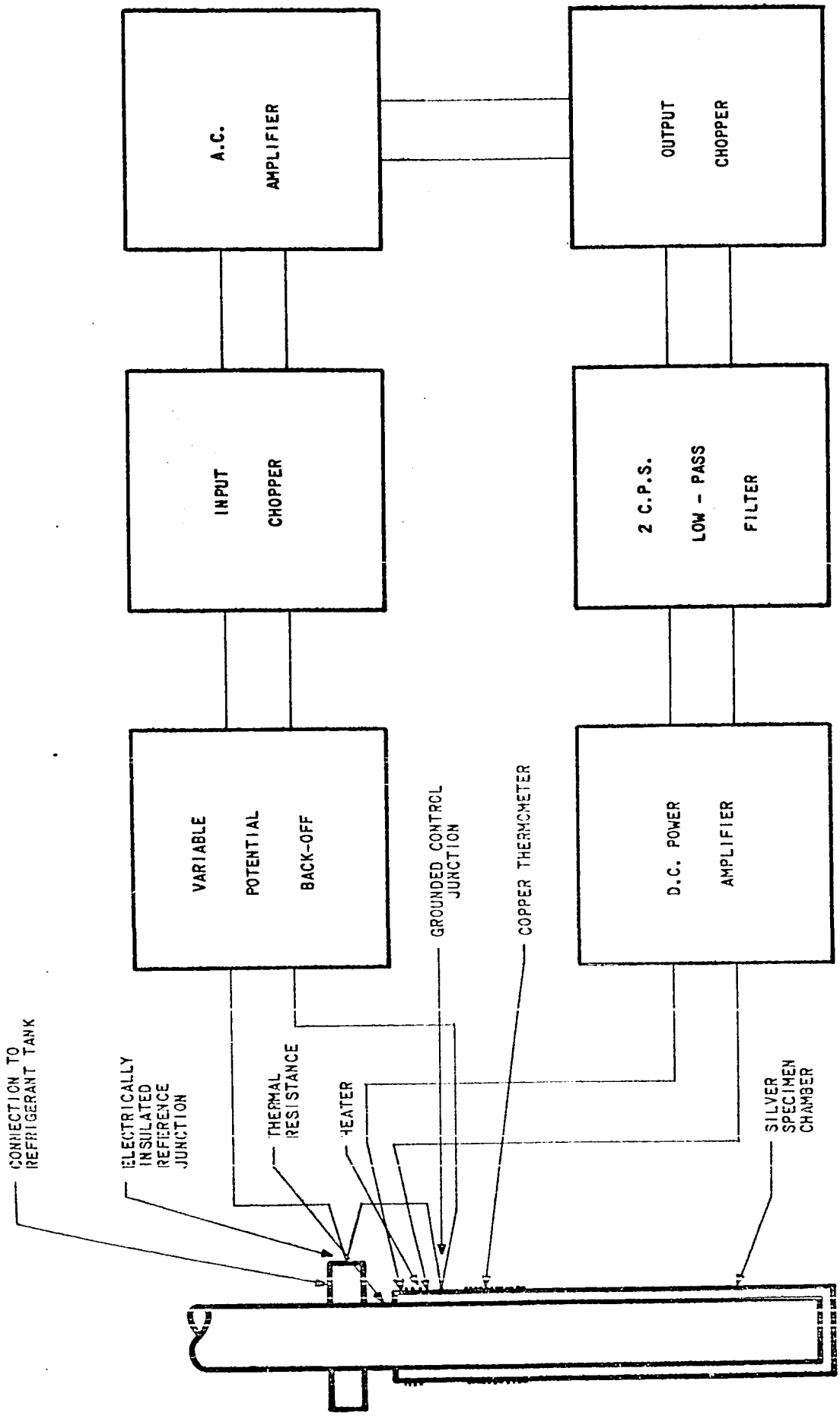

FIGURE F3:03 - THERMOCOUPLE TEMPERATURE CONTROLLER

providing its constituents are either very pure or very impure, such as a metallic alloy. This particular thermocouple was chosen because it had a larger output at low temperatures than other types of thermocouples. The reference temperature junction was anchored to the liquid helium tank with baking varnish, which is a good electrical insulator and also a fairly good thermal conductor. The control junction was indium-soldered to the specimen chamber to minimize the thermal resistance and time delay between them. In order to minimize the time delay between sensing an error signal and sensing that the error had been corrected, the thermocouple and heater were placed as close together as possible. The heater was bifilar wound on the specimen chamber, immediately below the thermal resistance, in order to reduce magnetic pickup.

Since the temperature control servo was basically a null device, the specimen temperature was fixed by the back-off potential in series with the thermocouple. The thermocouple potential was backed-off by passing a current through a small resistance which was connected in series with one of the thermocouple leads. A stable back-off current was obtained by using a 12.6 volt battery to trickle charge the

6.3 volt battery, which supplied the back-off current, and immersing the current limiting resistance decade in a grounded, oil filled metal box.

The net error signal was fed to the D.C. chopper amplifier, which was based on a circuit designed by Dr. Dauphinee of N.R.C. The input chopper, which was designed by Dauphinee and built by Tinsley Co., converted the error signal into a 38 c.p.s. square wave. This square wave was amplified by an A.C. amplifier and phase sensitive demodulated by a similar synchronous chopper. These motor driven choppers were advertised to have a noise level of less than 10^{-9} volts when adjusted for make-before-break and a time overlap of 5%. In order to amplify the extremely small signals involved, the input stage of the amplifier was a high quality transformer having an amplification of 45 and input and output impedances of 50 ohms and 100,000 ohms respectively. The A.C. amplifier was of conventional low frequency design, having an overall amplification of approximately 10^7 and a gain control for adjusting the overall servo loop gain.

The amplified D.C. signal was noisy so was passed through a low-pass filter having a time constant of 0.25 seconds, before driving the D.C. power amplifier. The power amplifier was capable of supplying 10 watts of D.C. power

into a 1000 ohm heater, and had a 10 turn helipot for manual adjustment of the power level. The helipot was adjusted for minimum error signal at the input of the power amplifier.

In the temperature range $60^{\circ}K \leq T \leq 300^{\circ}K$, the controller was capable of a short term stability of $0.001\ K^{\circ}$ and a long term stability of $0.01\ K^{\circ}$. The only major problem was electromagnetic pickup. This was reduced by encasing the chopper amplifier in a heavy iron chassis and minimizing the area between the leads which connected the thermocouple to the back-off unit.

(2) VAPOR PRESSURE REGULATOR

The temperature of a liquid refrigerant can be lowered by reducing its vapor pressure. This is accomplished by pumping on the gas-filled volume above the surface of the liquid. Since it was not possible to use a liquid nitrogen dewar around the liquid helium dewar, large heat leaks were always present. This required the use of a large orifice manostat in order to maintain temperatures below $4.2^{\circ}K$. A large orifice requires a large diaphram to generate enough force to open the orifice when it happens to close completely. A manostat was built which had an orifice of 0.5 inch diameter and a neophrene diaphram of 4 inch diameter. This manostat, which is shown in figure F3:04 , controlled the

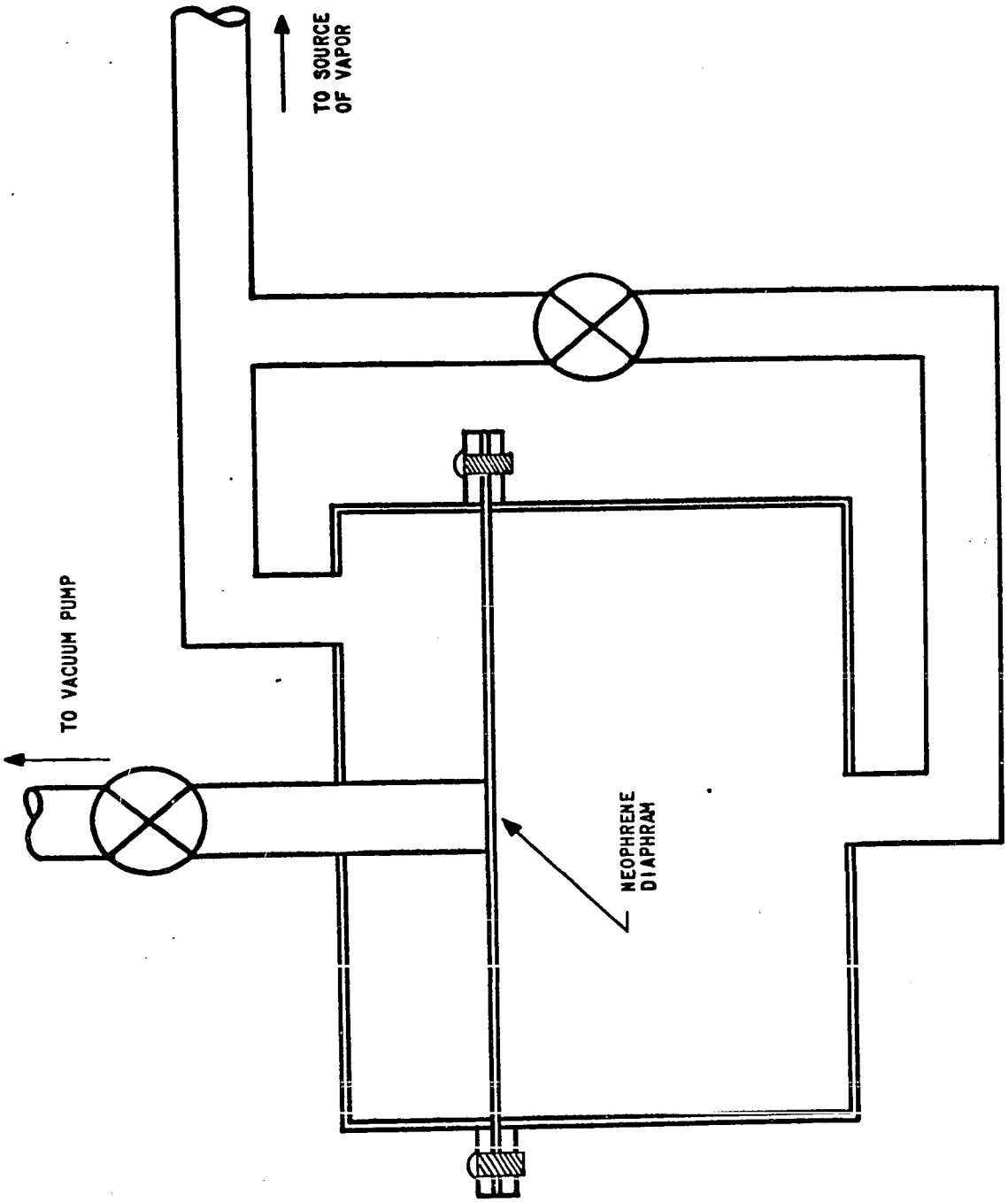

FIGURE F3:04 - MANOSTAT

temperature of pumped liquid helium in the range $1.8^{o}K \leq T \leq 4.2^{o}K$ to a stability of better than $0.002\ K^{o}$.

C. MAGNET AND MAGNETIC FIELD CONTROL EQUIPMENT

A Pacific Electric Co. magnet was used in the experimental measurements. It was powered by a 100 H.P. , D.C. motor-generator set. The magnet produced a flux density of $2.4\ w/m^2$, at a current of 225 amperes, using 3 inch pole tips and a 1.25 inch pole separation. The residual flux density was $0.0119\ w/m^2$. The magnet currents required for experimental measurements were too large to allow direct regulation of the magnet current. The magnetic field was controlled by regulating the current supplied to the field coils of the generator. The magnetic field control system is shown in figure F3:05 .

The control signal was the potential drop developed across a resistance of approximately 0.01 ohms, connected in series with the magnet coils. This resistor was constructed from manganin wire, and its resistance was stabilized by immersion in a tank of boiling water. The control voltage was compared with a variable reference voltage, and the error signal was amplified by a Philbrick chopper-stabilized D.C. operational amplifier. This amplifier had an amplification of approximately 10^{8} . The stability of this amplifier was

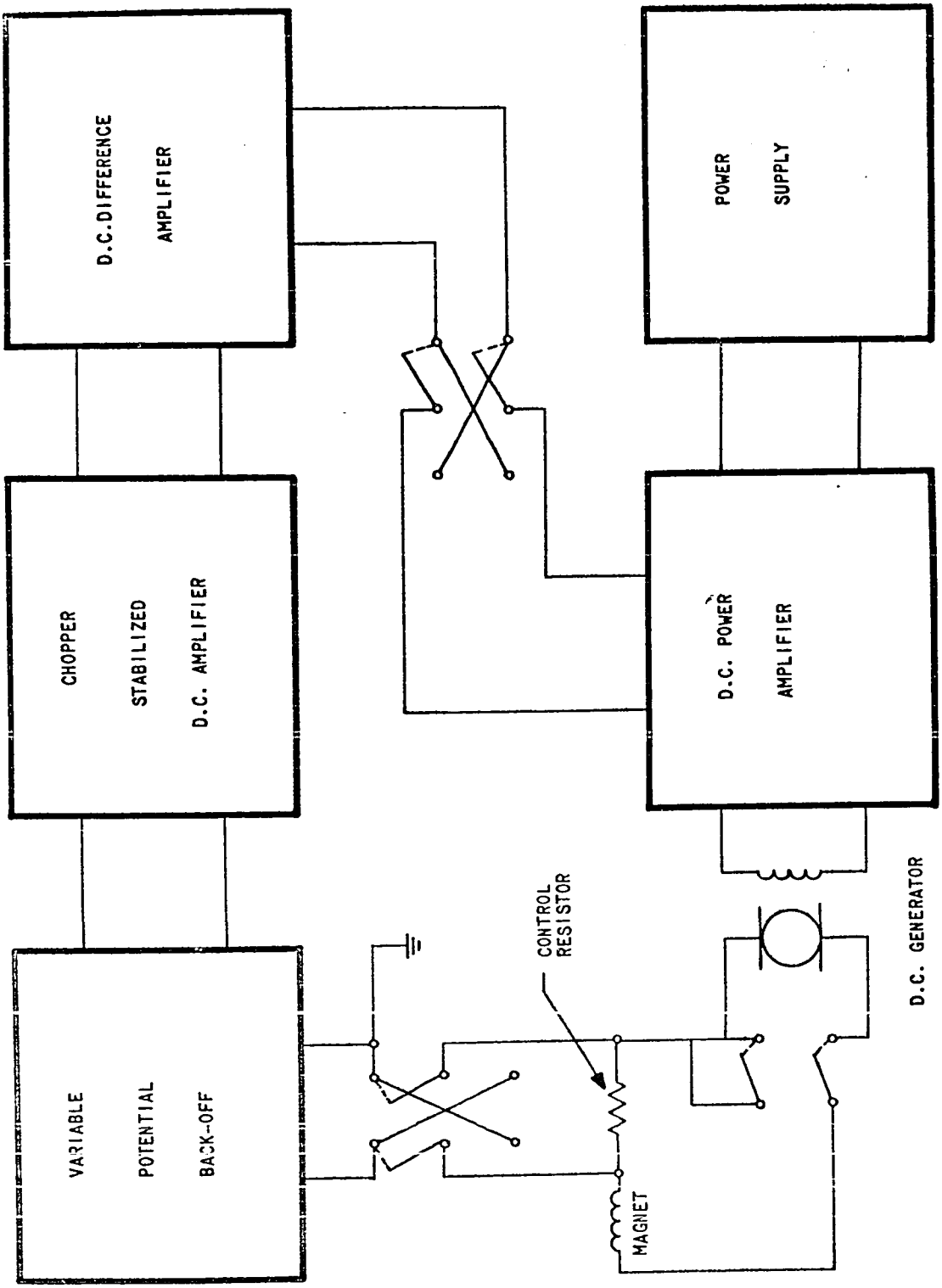

FIGURE F3:05 - MAGNETIC FLUX DENSITY CONTROLLER

improved by reducing the net amplification, by means of anode-follower-type negative feedback, to a variable range of 1 to 1000.

The output from this amplifier was connected to a conventional two stage D.C. difference amplifier which had an amplification of 4000 . The output from this stage was connected directly to the control grids of the D.C. power amplifier. The power amplifier was essentially a power cathode follower which used the generator field coil as its cathode load. The power amplifier consisted of 4 6336 dual triodes connected in parallel. Each triode could pass a current of 450 milliamperes, and each plate could dissipate 35 watts of power. At the maximum magnetic field used, the field coils required an average current of 2.7 amperes, whereas the power amplifier could supply a maximum of 3.6 amperes.

The open circuit loop gain could be varied between the limits 1 and 1000 . At maximum gain, the average magnetic field was stable to better than 0.001 w/m^2 . However, generator brush noise and electromagnetic pickup caused short term fluctuations of up to 0.01 w/m^2 . The magnetic field was varied by changing the reference potential by means of a 10 turn helipot. This helipot could be adjusted manually or varied continuously by means of a motor drive.

The motor drive could be adjusted to sweep from maximum field to zero field over a period of 10, 20 or 30 minutes.

D. MEASURING EQUIPMENT

(1) TEMPERATURE

When an experiment was performed using the glass dewar, the temperature of the specimen was assumed to be the same as that of the refrigerant in which it was immersed. The temperature of the refrigerant was determined by using mercury and oil manometers to measure its vapor pressure. The vapor pressure-temperature calibrations for He , H_2 , N_2 and O_2 are given in "Experimental Techniques in Low Temperature Physics" by G. K. White. In the range $1.8^{o}K \leq T \leq 4.2^{o}K$ the temperature of the refrigerant could be determined to an accuracy of 0.001 K^{o} . However, in the range $60^{o}K \leq T \leq 78^{o}K$, it could only be determined to an accuracy of approximately 0.005 K^{o} , since it was difficult to maintain a condition of thermal equilibrium in the liquid N_2 .

Approximately 80% of the experimental measurements were performed using the metal cryostat for production of the necessary temperatures. Two different types of thermometers were used for measurement of the temperature, depending upon which temperature range was involved. For $T < 22^{o}K$, the temperature was determined by measurement of the resistance

of a carbon resistance thermometer which was mounted on the specimen holder. For $T \geq 22^{o}K$, the temperature of the specimen chamber was measured to an accuracy of $0.005\ K^{o}$ by means of a copper resistance thermometer which was bifilar wound on the specimen chamber. Separate current and potential leads were used in order to avoid effects due to the leads themselves. The copper resistance thermometer current and potential difference were measured using a Tinsley potentiometer. After the thermometer was calibrated at $4.21^{o}K$ and $273.16^{o}K$, any intermediate temperature could be determined by using the copper thermometer calibration table in White's book. The specimen was maintained in thermal equilibrium with the specimen chamber by the introduction of a pressure of approximately 600 mm. of He exchange gas to the specimen chamber.

(2) MAGNETIC FLUX DENSITY

The magnetic flux density was calibrated, using a Rawson rotating coil gaussmeter, as a function of the potential difference developed across one-half of the magnetic field control resistor. This half of the control resistor had a resistance of approximately 0.0045 ohms, producing a potential difference of approximately 1 volt at the maximum magnet current used. The gaussmeter was calibrated to an absolute

accuracy of 0.25% of a full scale meter reading, that is, 0.01 w/m^2 for the range considered. Since the gaussmeter was a linear device requiring only a one point calibration, its relative accuracy was limited only by the accuracy of measurement of the output voltage from the rotating coil and mechanical rectifier. The magnetic flux density calibration is given in table T3:01 . The calibration was obtained by adjusting the magnet current to give specific potential differences across one-half of the control resistor, as determined by a Rubicon type K potentiometer, and at the same time measuring the gaussmeter output voltage by means of a Tinsley potentiometer. The calibration was repeated for swept magnetic fields to see if there was an appreciable difference for the two cases. The calibration for swept fields, which is the one given in table T3:01 , records very slightly higher magnetic flux densities for the same control resistor potential differences. The relative accuracy of calibration was approximately 0.001 w/m^2 . During an experiment, the calibration voltages given in T3:01 were preset on the Rubicon potentiometer. When the galvanometer indicated a null, a calibration mark was recorded on the same chart that was recording the experimental specimen signal. This calibration mark was produced by a remotely controlled marker pen.

TABLE T3:01

CALIBRATION OF THE MAGNETIC FLUX DENSITY AS A FUNCTION OF THE POTENTIAL DIFFERENCE ACROSS ONE-HALF OF THE CONTROL RESISTOR.

P.D. IN VOLTS	B IN w/m^2	P.D. IN VOLTS	B IN w/m^2
0.000	-0.012	0.325	1.749
0.900	2.343	0.300	1.696
0.850	2.321	0.275	1.638
0.800	2.299	0.250	1.577
0.750	2.275	0.225	1.499
0.700	2.245	0.200	1.389
0.650	2.213	0.175	1.253
0.600	2.166	0.150	1.096
0.550	2.113	0.125	0.922
0.500	2.049	0.100	0.743
0.475	2.012	0.090	0.670
0.450	1.974	0.080	0.599
0.425	1.934	0.070	0.526
0.400	1.890	0.060	0.456
0.375	1.845	0.050	0.382
0.350	1.797	0.000	0.012

(3) SPECIMEN ELECTRON TRANSPORT PROPERTIES

The isothermal electron transport properties of n-type GaSb were determined by D.C. and quasi-D.C. measurements. The specimen current and the resistivity voltage were measured in zero magnetic field by means of a Rubicon type K potentiometer. The magnetoresistance voltage was developed between the two resistivity probes, and the Hall voltage, between one Hall probe and one resistivity probe. These two transport voltages were separated from the experimental voltages by back-off to zero net voltage in zero magnetic field.

The two transport voltages were automatically recorded during the magnetic field sweep by means of a Phillips recorder.

Figure F3:06 is a diagram of the circuitry employed to supply and measure the specimen current, back-off the Hall and magnetoresistance voltages in zero magnetic field, and measure the resistivity, Hall and magnetoresistance voltages. The circuit was found to be sensitive to electrostatic fields, electromagnetic fields and temperature gradients. Electrostatic pickup was readily overcome by shielding. Electromagnetic pickup was considerably reduced by encasing long electrical leads in soft iron pipe. The generation of thermoelectric potentials, which is very serious when working with relatively small voltages, was reduced by more than an order of magnitude by immersion of certain of the switches in transformer oil.

Certain of the resistance decades were filled with transformer oil in order to reduce resistance changes induced by temperature drifts. The lead storage batteries, which supplied the specimen and back-off currents, produced serious current drifts unless they were operated under ideal conditions. Temperature effects were reduced by drawing a relatively constant current from each battery at all times. However, it was much more important to operate on the plateau

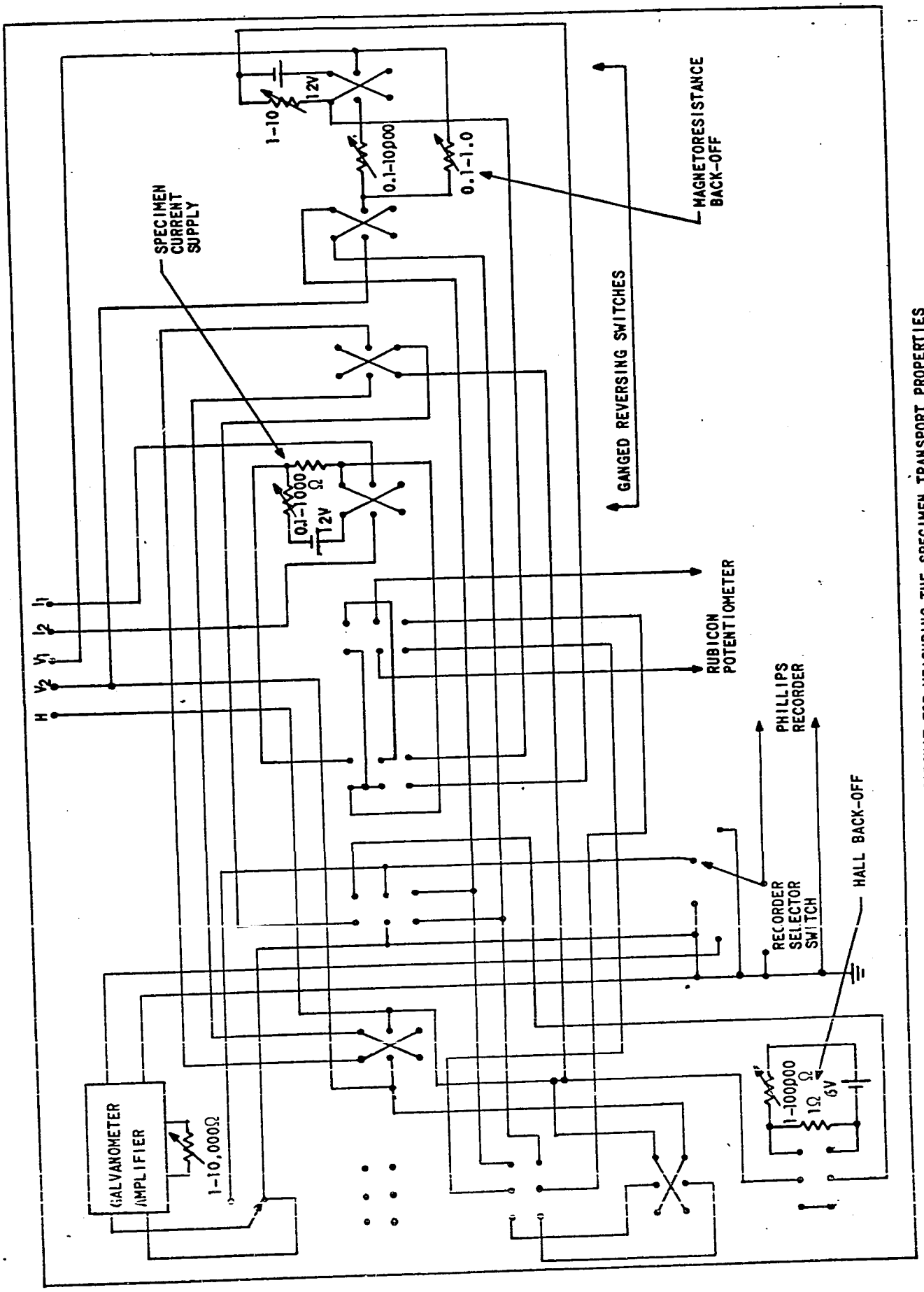

FIGURE F3:06 - CIRCUIT FOR MEASURING THE SPECIMEN TRANSPORT PROPERTIES

of the voltage versus charge curve of the battery. The batteries were charged every two weeks, and then discharged at the normal rate for at least 24 hours prior to use in actual measurements. For currents of less than 25 ma., the current was stable over a period of one hour to approximately 1 part in 50,000 . During experimental measurements, changes in the resistance of the specimen current leads inside the cryostat produced larger current variations than those due to drifts of the battery terminal voltage.

The Phillips recorder had 9 input sensitivities covering the range 1 mv. to 100 mv. The input impedance, in ohms, for each range was given by 400 x (sensitivity in mv.). The most sensitive range, 1 mv. , had an input impedance of 400 ohms. The recorder was calibrated to an absolute accuracy of 0.25% . By taking certain precautions and measuring the recorder chart by means of a travelling microscope, it was possible to obtain a relative accuracy of approximately 0.02% of a full scale reading. When either the Hall or magnetoresistance voltage, for maximum magnetic field, was too small to give a half-scale deflection on the 1 mv. range, the signal voltage was amplified by a modified galvanometer amplifier prior to being recorded by the Phillips recorder.

The modified galvanometer amplifier is shown in figure

F3:07 . A galvanometer amplifier is an impedance transformation device in which the excess current gain is internally fed back in order to improve the stability and reduce the noise generated within the amplifier. An ordinary galvanometer amplifier does not include R_o and C_o , which are shown in F3:07 . It is basically a current amplifier, the amplified current, I_o , registering on the secondary galvanometer. The modified galvanometer amplifier circuit incorporates a resistance in series with the Si split photo cell. I_o causes an amplified voltage to be developed across this resistor. The maximum allowed value for this resistance is limited only by the input impedance of the recorder, because the photo cells are current sources and therefore have a high output impedance.

The current amplification, M , is a function of the total current output from the photo cells, the primary galvanometer sensitivity, and the distance from the galvanometer mirror to the photo cells.

Now: $I_o = MI_i$, $I_R = (M + 1)I_i$

Input impedance : $Z_i = V_i/I_i = R_{P.C.} + (M + 1)R_{F.B.}$

Output impedance : $Z_o \simeq R_o$

Voltage amplification:

$$A = V_o/V_i = (R_o/R_{F.B.})(M/(M + 1 + R_{P.C.}/R_{F.B.}))$$

$$\simeq R_o/R_{F.B.}$$

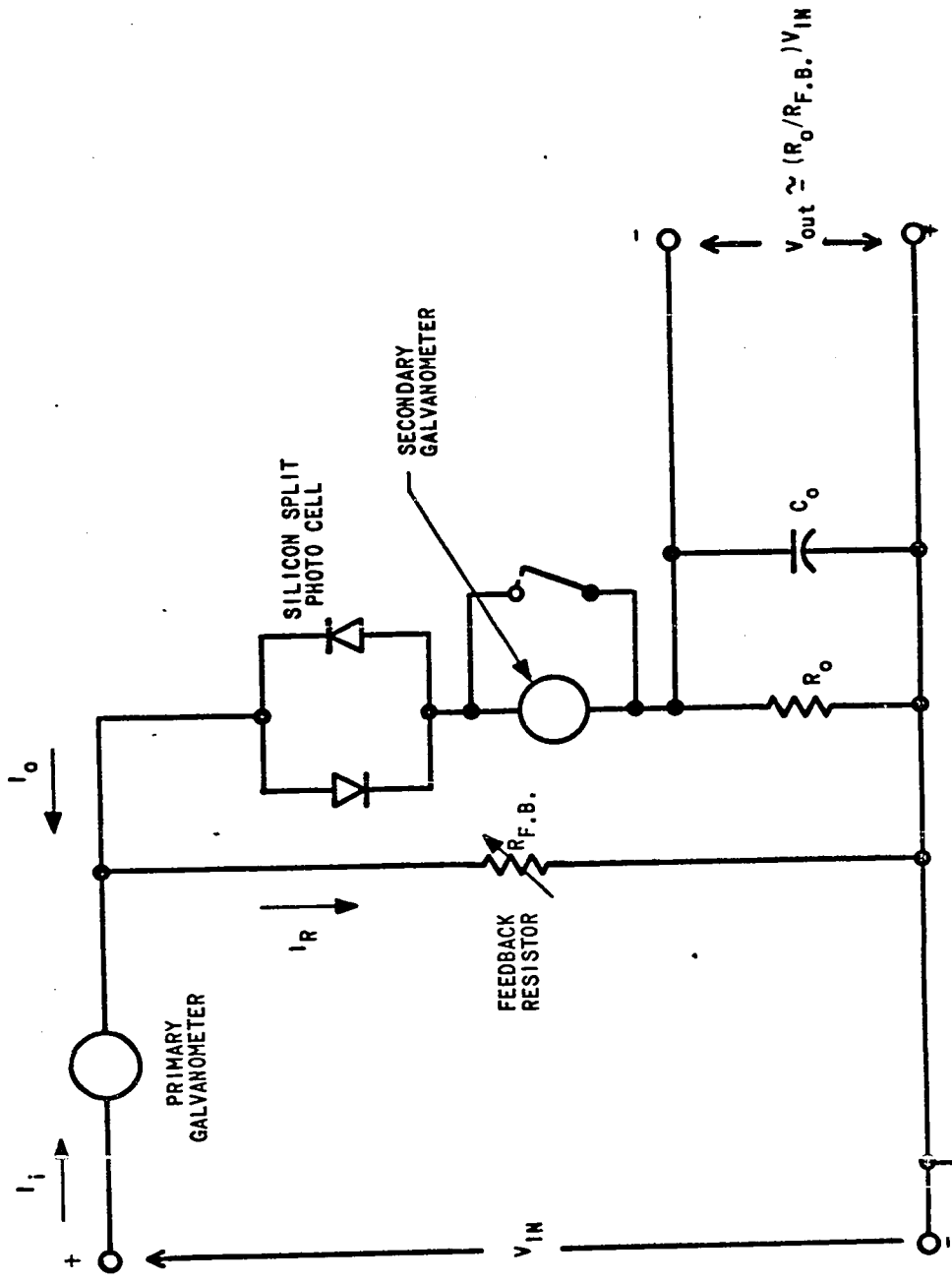

FIGURE F3:07 - MODIFIED GALVANOMETER AMPLIFIER

since M was of the order of 10,000 and $R_{P.G.}/R_{F.B.} < 1$ or at worst of the order of 1 . With R_o = 1000 ohms and C_o = 500 micro-farads, the useful range of amplification was $1 \leq A \leq 20$.

The galvanometer amplifier was very sensitive to vibration so was mounted on a damped two-stage mechanical filter. This filter had cut-off frequencies of approximately 4 c.p.s. and 60 c.p.s. This eliminated most of the noise due to vibrations. The 6.3 volt, 20 ampere light source was powered by a battery charger. A 6.3 volt lead storage battery was used as a filter for the battery charger, in order to minimize fluctuations in the light intensity. With these precautions an amplification as high as 20 could be used.

2. EXPERIMENTAL TECHNIQUES

A. SPECIMEN PREPARATION

(1) SOURCE OF MATERIAL

Six single crystal samples of Te-doped GaSb were supplied by Dr. A. Strauss of Lincoln Laboratories, M.I.T. These samples had room temperature Hall coefficients in the range -2.4×10^{-6} to -45.5×10^{-6} m^3/coul. The ingots, from which these samples were cut, were "pulled" from a melt which consisted of Te and p-type GaSb having a hole concentration of the order of 2×10^{23} m^{-3} .

(2) CUTTING AND LAPPING

The GaSb samples available were in most cases only slightly larger than the specimens to be cut from them. As a result, it was not possible to cut specimens having edges oriented in predetermined crystal directions. The samples were cut to give the maximum possible number of specimens. This was necessary because GaSb cleaves very easily, causing a high rate of specimen breakage.

The sample was lapped to give two accurately parallel surfaces and a net thickness of approximately 1.5 mm. In order to do this, the sample was glued to the adjustable lapping holder, shown in figure F3:08 , by means of glyptol thinned with acetone. The sample was then lapped on a glass

CROSS SECTIONAL VIEW

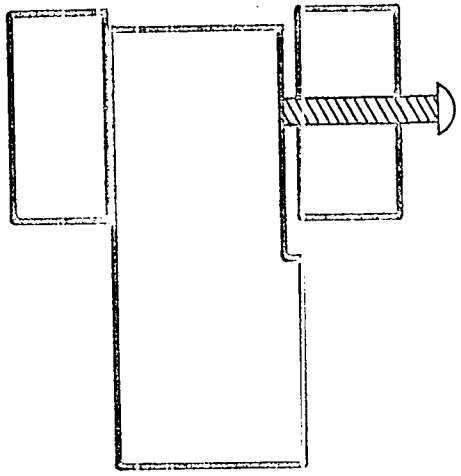

TOP VIEW

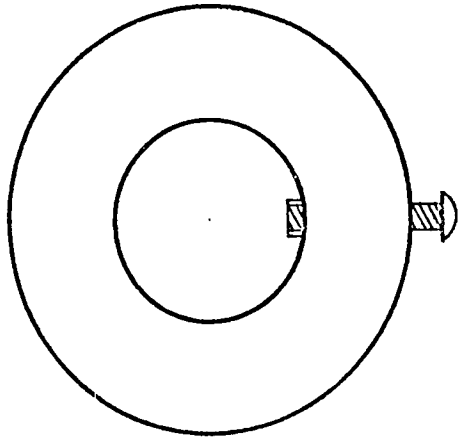

FIGURE F3:08 - LAPPING HOLDER

plate using 600 grit lapping compound moistened with distilled water. The wafer of GaSb was then cut into specimens, having widths of approximately 1 mm. , by means of a diamond-type saw using a 0.008 inch thick carborundum disk. These specimens were lapped to produce parallelopipeds having widths and thicknesses of approximately 1.5 mm. and 0.6 mm. respectively, and were then cut to a length of approximately 1.0 cm.

(3) X-RAY MEASUREMENTS

X-ray photographs, using a Laue Back-Reflection Camera, were taken for one specimen from each different sample of GaSb. These photographs showed that all the specimens were single crystals and had a zincblende structure. When the measurements on GaSb were commenced, it was not known if the two-band model for GaSb would be dependent upon the orientation of the crystal axes with respect to the specimen axes. Therefore, the orientation of the crystal axes with respect to the specimen axes was determined for specimens 5, 6, 7 and 8. The specimen was rotated by means of a goniometer until the Laue photograph corresponded to a known orientation. The three rotation angles were then read from the goniometer scales. These angles will not be given here, since the analysis in chapter 2 shows that knowledge of the precise

orientation of the crystal axes with respect to the specimen axes does not improve the two-band analysis for GaSb. Figure F3:09 is a typical Laue Back-Reflection photograph for GaSb.

(4) CONTACT PREPARATION

The specimen width and thickness were measured by means of a micrometer, the scale of which could be read to an accuracy of 2×10^{-3} mm. Then the five electrical contacts were prepared by electroplating the contact areas with tin. The specimen was held near one end by self clamping tweezers, and all areas not to be plated were masked with nail polish. The unmasked areas were etched for 15 seconds in a 1:1 solution of concentrated nitric and hydrochloric acids, and were then rinsed with distilled water. GaSb oxidizes very rapidly, so it was imperative to commence electroplating immediately after rinsing the specimen. The contact areas were electroplated in an acid tin solution for 30 minutes at a current of 2 to 4 ma. , using a platinum wire as the second electrode. The plating solution had the following composition: 50 $cm.^3$ of distilled water, 10 $cm.^3$ of anhydrous $SnCl_4$, and 5 $cm.^3$ of concentrated H_2SO_4 . The nail polish mask was then removed by dissolving it with acetone.

The metal contacts were made from Sn because it acts as a donor in GaSb, and should therefore produce a semiconductor

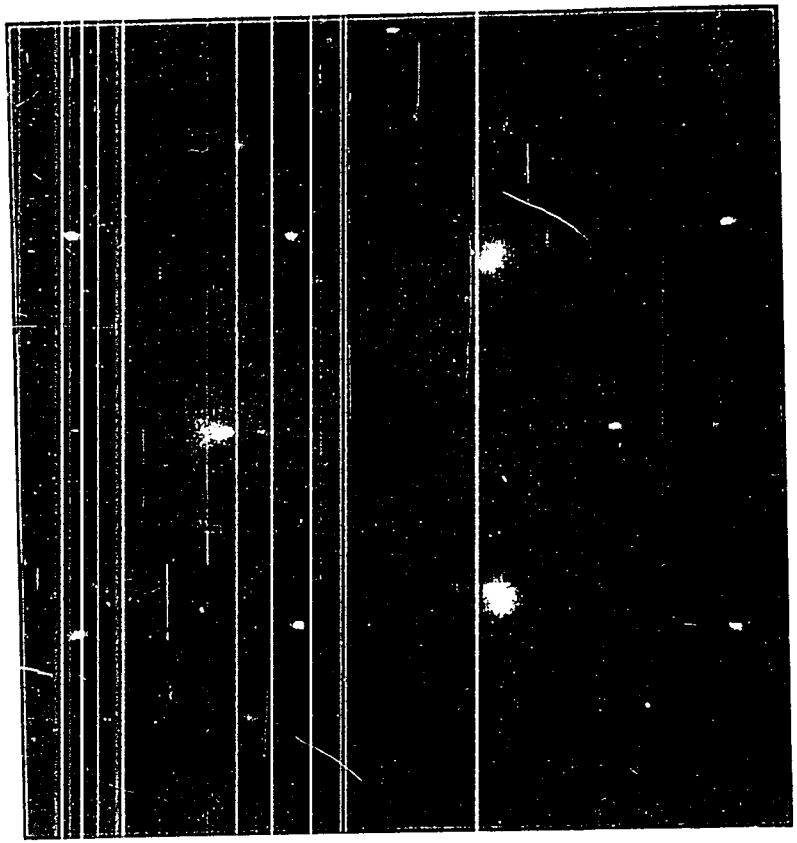

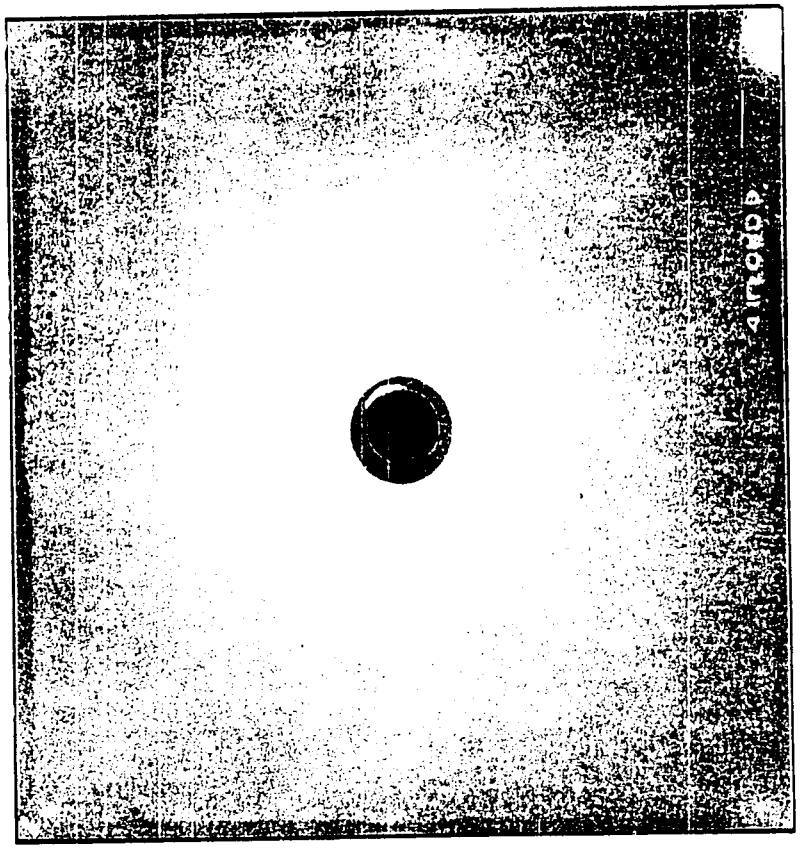

FIGURE F3:09 - LAUE PHOTOGRAPHS

to metal junction having a relatively small contact potential. These contacts were noisy and had an apparent contact resistance of approximately 5 ohms when measured on the most sensitive scale of an Avo Meter. The apparent contact resistances were reduced to approximately 0.1 ohms by heating the specimen to a temperature of approximately 250°C for a period of 20 seconds. The specimen was heated in a vacuum furnace containing He at a pressure of 10 mm. of Hg. The magnetic specimen carriage moved the specimen into and out of the heated region by means of a moveable magnet outside the vacuum furnace. The center-to-center distance between the two resistivity contacts was measured by means of a travelling microscope. The finite widths of the resistivity contacts, approximately 0.4 mm. , could introduce a larger absolute error than all other errors combined.

(5) MOUNTING

Since GaSb is very easily damaged, each specimen was mounted on a piece of glass as shown in figure F3:10 . The specimen was bonded to the glass with glyptol cement, since glyptol remained slightly fluid even at liquid He temperatures, minimizing the strain due to differential contraction between the specimen and the glass. Six #32 enamelled copper wires were attached to the glass slide with either glyptol or

TOP VIEW

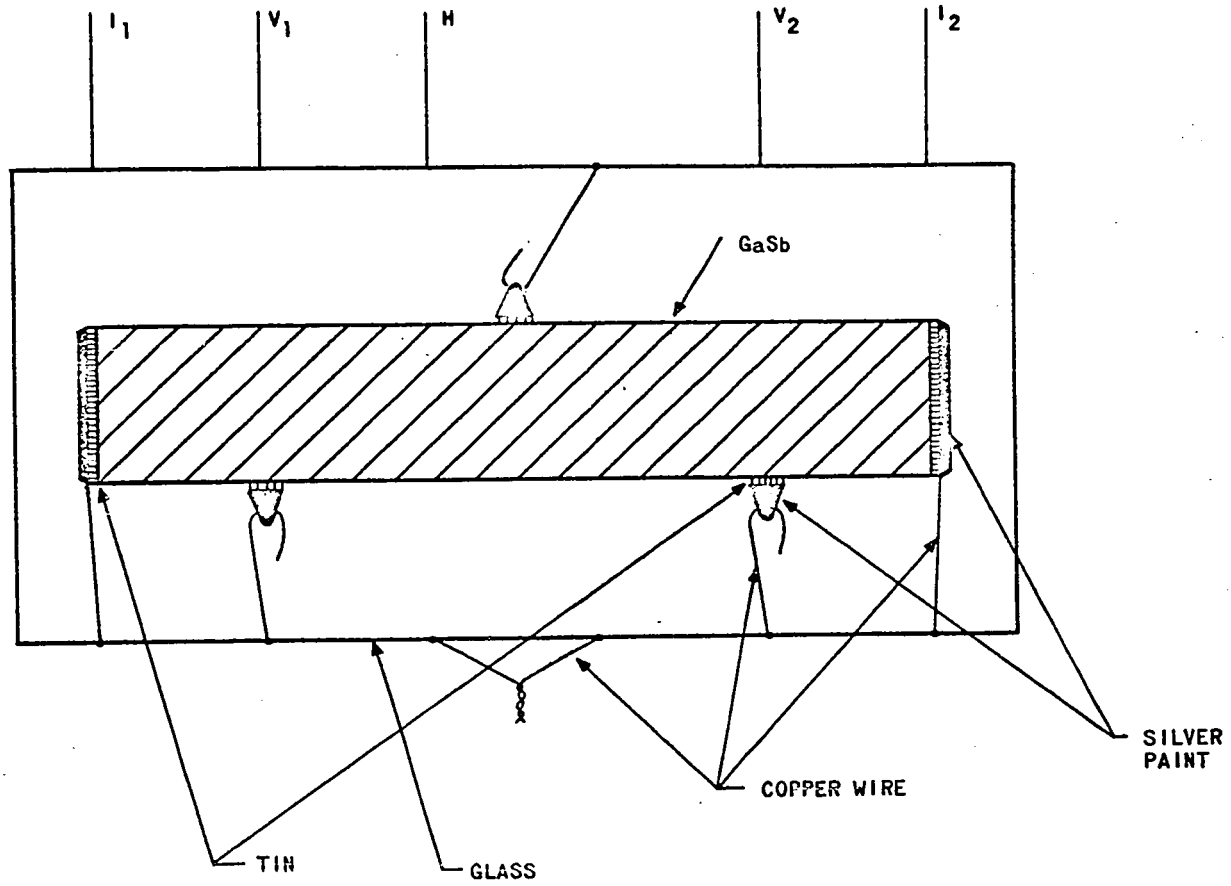

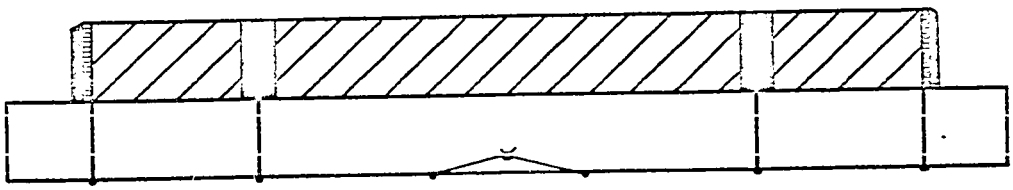

SIDE VIEW

FIGURE F3:10 - MOUNTED SPECIMEN

baking varnish. Conducting silver paint was used to connect the copper wires to the tin contacts. The mounted specimen was aligned perpendicular to the axis of the specimen holder, by means of a precision T-square, prior to clamping it in place. Soldering the copper wires to the five copper pins completed the preparation and mounting of the specimen.

B. MEASUREMENT OF THE TRANSPORT EFFECTS

The specimen holder was inserted into the cryostat, the cryostat head was locked in position and the electrical leads were connected. The batteries were connected and allowed to stabilize for at least 24 hours prior to making any measurements. The specimen was aligned perpendicular to the magnetic field, to an accuracy of 0.5^{o} , by rotating the cryostat head until the maximum Hall voltage was located.

The procedure used to measure the isothermal electron transport effects was as follows:

(a) For measurements requiring the metal cryostat, evacuate the specimen chamber and fill it with He exchange gas to a pressure of approximately 600 mm. of Hg.

(b) Fill the refrigerant tank(s) or glass dewar with the appropriate refrigerant(s).

(c) If using the metal cryostat, adjust the temperature controller to give the required temperature and allow suf-

ficient time for the temperature to stabilize. If using the glass dewar, adjust the manostat to give the required refrigerant vapor pressure.

(d) Adjust the specimen current to the required value and measure the potential drop it produces, across the one ohm standard resistance, by means of the potentiometer.

(e) Disconnect the Hall and magnetoresistance back-off batteries. Measure the resistivity voltage and the fraction of it which appears on the Hall leads by means of the potentiometer.

(f) Connect the back-off batteries, and adjust to zero the voltages appearing on the Hall and the magnetoresistance leads.

(g) Measure the temperature by the method appropriate to the temperature range involved.

(h) Calibrate the chart recorder, select the appropriate chart speed and sensitivity scale, and set the chart recorder selector switch to the Hall position.

(i) Turn on the magnetic field and adjust the magnet current to 225 amperes. Adjust the heater power to the stabilizing bath surrounding the magnet control resistor. The water must be boiling gently.

(j) Commence sweeping the magnetic field towards zero. Preset

on the potentiometer, one at a time, the magnet control resistor calibration voltages. Activate the marker pen each time the galvanometer indicates a null.

(k) Disconnect the magnet current at the end of the sweep. Measure the specimen current and temperature.

(l) Repeat steps (h) to (k) inclusive for the Hall effect in reversed magnetic field and for the magnetoresistance in forward and reversed magnetic fields.

C. INITIAL ANALYSIS OF THE EXPERIMENTAL DATA

(1) TWO-BAND ANALYSIS

T and ρ_0 were measured in zero magnetic field. ρ_1 , ρ_2 , R_0 and R_1 were determined from the chart recorder plots of the Hall and magnetoresistance voltages as functions of the magnetic flux density. An arbitrary reference line was drawn on each of the recorder charts. The distance between the reference line and the recorded curve was measured at each magnetic field calibration mark by means of a travelling microscope. These chart distances were converted into voltages. This technique produces, in general, non-zero readings for the zero-magnetic-field regions at both ends of each magnetic field sweep. The two zero-field error voltages were plotted on the chart, using an amplified scale, and were joined by a straight line. The resulting error voltages at the calibra-

tion points were read from the chart and used to correct the previous set of readings.

For a perfect specimen the magnetoresistance voltage should be constant with respect to reversal of the magnetic field direction, since it is only a function of even powers of B . In practise a term linear in B was superimposed upon the true magnetoresistance voltage. This term was eliminated by averaging each pair of values corresponding to the two field directions. The magnetoresistance voltages, V_M , were converted into resistivities by means of the relation

$\Delta\rho = (V_M/I)(tw/l)$ where: I = specimen current

t = specimen thickness

w = specimen width

l = effective specimen length

The experimental Hall voltage, V_{HE} , was not the true Hall voltage, V_H , because a fraction, X , of the magnetoresistance voltage was superimposed upon the true Hall voltage. The true Hall voltage was given by $V_H = V_{HE} - XV_M$. Let the subscripts + and - refer to the forward and reversed magnetic field directions, respectively.

When $V_{M_+} = V_{M_-}$, $V_{H_+} = -V_{H_-} = (V_{HE_+} - V_{HE_-})/2$.

It was necessary, in general, to compute V_H from

$V_{H_+} = V_{HE_+} - XV_{M_+}$, $V_{H_-} = V_{HE_-} - XV_{M_-}$.

It was found that the magnitudes of V_{H_+} and V_{H_-} were almost identical. Define $V_H = (V_{H_+} - V_{H_-})/2$. Then $RB = tV_H/I$.

$\Delta\rho$ and RB were curve fitted as functions of B, by the method of "least squares", using an I.B.M. 1620 #2 computer. The equations fitted were: $\Delta\rho = \rho_1 B^2 + \rho_2 B^4$ and $RB = R_0 B + R_1 B^3$. The "weighted probable" errors in the four coefficients were also computed.

The values for ρ_0 , ρ_1 , ρ_2 , R_0 and R_1 were inserted into another program which computed two sets of N_0/r_0F_0 , N_1/r_1F_1 , $\mu_0 r_0 F_0$ and $\mu_1 r_1 F_1$. ρ_0 , ρ_1 and R_0 were common to both computations. One set of band parameters was computed using ρ_2 as the forth experimental coefficient, the other set, using R_1 . Theoretically, the two sets of band parameters should be identical. In practise this was not found to be the case. This difference will be discussed in chapter 4.

(2) DE HAAS-SHUBNIKOV OSCILLATIONS

Magneto-oscillations were observed in the Hall effect and magnetoresistance at liquid He temperatures. The oscillations in the Hall effect were too small to measure accurately. The oscillations in the magnetoresistance were only measured for the specimens having the 3 highest carrier concentrations, since the oscillation amplitude decreased very

rapidly with decreasing carrier concentration.

The magneto-oscillation measurements were performed at approximately 2 , 3 and 4°K using the glass dewar. The temperature of the liquid He was regulated by means of the manostat shown in figure F3:04 , and measured by means of mercury and oil manometers. The specimen current and the resistivity voltage were measured by the technique used in the two-band measurements. At each of the 3 temperatures, only one magnetic field sweep was performed due to the high rate of evaporation of the liquid He. Only the magneto-resistance for the "forward" magnetic field was measured.

The oscillation envelopes and the mean position between them were drawn on each recorder chart. A continuous magnetic flux density calibration was plotted on each chart and the flux densities corresponding to the oscillation null points were determined. The travelling microscope was used to measure the oscillation amplitude as a function of the magnetic flux density. These amplitudes were converted to resistivities. The null and amplitude data were curve fitted by the computer in order to determine the carrier concentration, N_0 , and the effective mass, M_0^* , of the (000) band.

CHAPTER 4

EXPERIMENTAL RESULTS AND BAND STRUCTURE ANALYSIS

INTRODUCTION

The purpose of this chapter is to record and analyse the experimental data. An attempt will also be made to estimate the accuracy of the experimental measurements and the values obtained for the band parameters. The analysis of the conduction band structure of GaSb will not be carried out until chapter 5 when the results of the present chapter will be compared with those already available in the scientific literature.

1. EXPERIMENTAL RESULTS

A. SPECIMEN INFORMATION

The six Te-doped, single crystal GaSb samples were supplied by Dr. A. Strauss of the Lincoln Laboratories, M.I.T. The specimen dimensions and the M.I.T. sample numbers are given in Table T4:01 . Each specimen dimension was measured at approximately five different positions on the specimen. The average deviation from the mean value is recorded immediately below the corresponding mean specimen dimension. Since the resistivity contacts did not have an infinitesimal width, there was some doubt about the choice of positions between which to measure the effective specimen length. The lengths

TABLE T4:01 - SPECIMEN DIMENSIONS

SPECIMEN NO.	M.I.T. NO.	LENGTH (l)	WIDTH (w)	THICKNESS (t)	CONTACT WIDTH
5	60-22 #9	0.662 0.001	0.1810 0.0005	0.0698 0.0003	0.036
6	M-45L	0.591 0.001	0.1981 0.0001	0.0643 0.0005	0.042
7	62-63 , B	0.681 0.001	0.1639 0.0001	0.0654 0.0001	0.035
8	60-41 , B+2	0.631 0.001	0.1859 0.0002	0.0656 0.0003	0.040
9	60-52 , T-1	0.619 0.004	0.2035 0.0002	0.0707 0.0001	0.030
10	61-33 , B	0.575 0.001	0.1891 0.0001	0.0760 0.0001	0.036
6A	M-45L	0.636 0.001	0.1987 0.0001	0.0864 0.0001	0.039
7A	62-63 , B	0.628 0.001	0.1327 0.0001	0.0652 0.0001	0.046
8A	60-41, B+2	0.618 0.001	0.1858 0.0001	0.0657 0.0001	0.041

ALL DISTANCES IN CM.

quoted in the table are for the center-to-center distance between the contacts. The resistivity contact widths are given in the last column of the table.

B. TWO-BAND DATA

Typical curves for R and $\Delta\rho$ as functions of B^2 are shown in figure F4:01 . The experimental voltages were proportional to $\Delta\rho$ and RB . Therefore, the curve for R shows increased scatter as B tends to zero. R is plotted on a magnified scale in order to show its dependence on B^2 . A plot of R versus B^2 should be linear. R_0 and R_1 are respectively equal to the intercept and slope at $B^2 = 0$. Deviations from a linear dependence on B^2 and the scatter of the experimental points give an estimate of the relative accuracy of measurement. The plot of $\Delta\rho$ versus B^2 should be a smooth curve passing through the origin. ρ_1 is the slope of this curve at the origin. A plot of $\Delta\rho/B^2$ versus B^2 should be linear. ρ_1 and ρ_2 would be given, respectively, by the intercept and slope at $B^2 = 0$.

The two-band coefficients ρ_0 , ρ_1 , ρ_2 , R_0 and R_1 , which were obtained by "least squares" curve fitting of the experimental data, are tabulated in tables T4:02 to T4:07 , and graphically represented in figures F4:02 to F4:06 . The specimen which had the highest carrier density, #7 , was

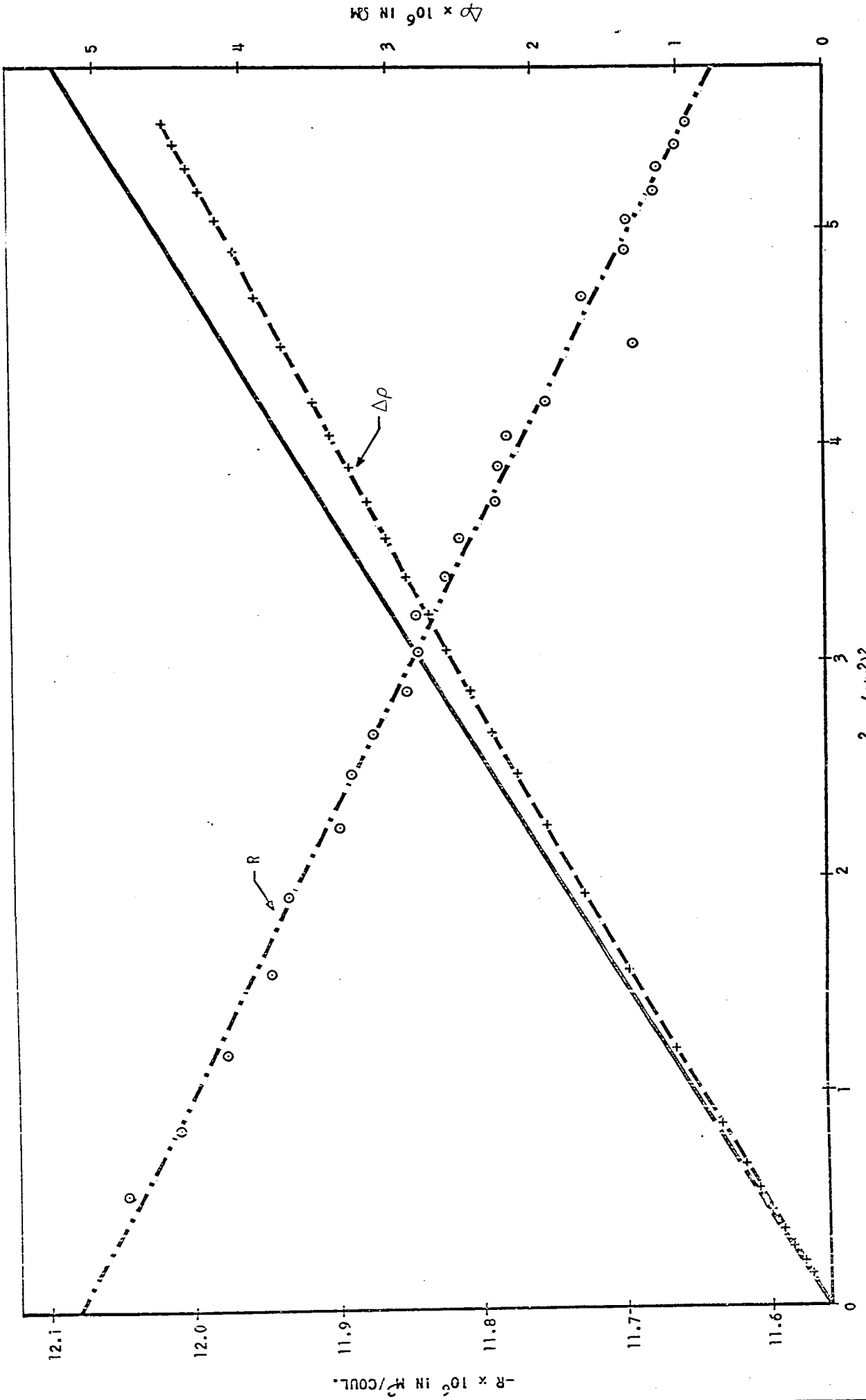

FIGURE F4:01 - R AND $\Delta\rho$ AS FUNCTIONS OF B^2 - SPECIMEN #8 FOR T = 297.8°K

TABLE T4:02 - SPECIMEN #5

T in ^{o}K	4.21	23.62	30.32	40.00	78.47 .21	152.71 .02	204.54 .02	250.04 .23	283.81 .01
$\rho_0 \times 10^6$	14.58	14.55	14.53	14.54	15.15	20.26	27.34	35.86	43.63
$\rho_1 \times 10^8$					4.38 .01	21.99 .02	46.01 .05	70.79 .02	88.82 .03
$-\rho_2 \times 10^{10}$					14.96 .19	32.36 .64	59.30 1.34	94.12 .65	124.3 .8
$-R_0 \times 10^6$	7.607	7.682	7.720	7.817	8.319 .001	10.259 .002	11.682 .002	12.824 .002	13.428 .003
$R_1 \times 10^8$					-.087 .039	2.215 .071	3.933 .075	6.668 .056	9.105 .097
$-\frac{N_0}{r_0 F_0} \times 10^{-24}$	.8205	.8125	.8085	.7985	.7503 .7247	.5476 .5435	.4355 .4264	.3502 .3409	.2975 .2891
$-\frac{N_1}{r_1 F_1} \times 10^{-24}$					.0476	.2253 .1956	.5554 .3917	.8256 .5928	1.0128 .7653
$-\mu_0 r_0 F_0$	.5217	.5280	.5313	.5376	.5491 .5569	.5316 .5327	.4709 .4740	.4185 .4220	.3809 .3843
$-\mu_1 r_1 F_1$					.1770	.0755 .0949	.0418 .0668	.0333 .0509	.0294 .0418
DATE	May 22	May 22	May 22	May 22	May 5	May 7	Apr.30	May 12	May 4

ALL VALUES IN RATIONALIZED M.K.S. UNITS

TABLE T4:03 - SPECIMEN #6

T in ^{o}K	4.21	79.96 .04	152.17 .19	203.70 .01	248.60 .05	289.56 .08
$\rho_0 x10^6$	4.756	6.587	9.226	12.262	15.512	19.118
$\rho_1 x10^8$	15.972 .009	21.065 .016	32.326 .018	40.700 .023	46.727 .025	50.238 .027
$-\rho_2 x10^{10}$	23.28 .24	34.06 .45	52.99 .50	77.32 .61	94.82 .67	107.3 .7
$-R_0 x10^6$	4.4050 .0024	4.6982 .0013	5.1816 .0011	5.3166 .0030	5.5410 .0012	5.4550 .0018
$R_1 x10^8$	1.333 .069	2.222 .041	3.350 .033	4.178 .092	5.541 .036	5.859 .055
$-\frac{N_0}{r_0 F_0} x10^{-24}$	1.3045 1.2976	1.1577 1.1502	.9551 .9415	.8277 .7974	.7027 .6764	.6218 .5805
$-\frac{N_1}{r_1 F_1} x10^{-24}$	1.2010 .7275	1.1530 .9019	2.0715 1.4079	3.7896 1.8432	3.1971 2.0844	4.8184 2.5134
$-\mu_0 r_0 F_0$	.9643 .9659	.7620 .7635	.6284 .6313	.5142 .5204	.4485 .4539	.3837 .3922
$-\mu_1 r_1 F_1$	.0453 .0810	.0568 .0769	.0369 .0584	.0220 .0511	.0273 .0457	.0182 .0393
DATE	July 8	May 26	June 18	May 27	June 23	May 29

ALL VALUES IN RATIONALIZED M.K.S. UNITS

TABLE T4:04 - SPECIMENS #7 & #7A FOR T = 4.21°K

SPECIMEN	7	7A
$\rho_0 \times 10^6$	3.848	3.824
$\rho_1 \times 10^8$	37.24 .01	36.45 .01
$-\rho_2 \times 10^{10}$	117.5 .3	121.9 .3
$-R_0 \times 10^6$	2.5710 .0035	2.4122 .0006
$R_1 \times 10^8$	5.694 .095	5.199 .015
$-\frac{N_0}{r_0 F_0} \times 10^{-24}$	1.6309 1.6033	1.6968 1.6432
$-\frac{N_1}{r_1 F_1} \times 10^{-24}$	44.460 11.551	13.267
$-\mu_0 r_0 F_0$	.8144 .8190	.7799 .7882
$-\mu_1 r_1 F_1$	.0066 .0267	.0254
DATE	Aug. 6/64	Jan.26/65

ALL VALUES IN RATIONALIZED M.K.S. UNITS

TABLE T4:05 - SPECIMEN #8

T in ^{o}K	4.203 .001	79.95 .01	100.04 .01	125.32 .01	149.52 .49	175.64 .18	200.25 .25	252.17 .15	297.80 .20
$\rho_0 x10^6$	12.50	15.09	16.13	18.06	20.18	23.42	26.88	36.01	45.56
$\rho_1 x10^8$					24.25 .01	34.45 .01	43.96 .01	70.70 .02	89.35 .01
$-\rho_2 x10^{10}$					35.76 .29	44.23 .34	37.96 .26	104.20 .58	124.00 .30
$-R_0 x10^6$	6.819	7.843	8.285	8.890	9.290 .001	10.036 .001	10.495 .001	11.660 .001	12.080 .002
$R_1 x10^8$					-.386 .026	.970 .033	1.951 .026	5.216 .023	7.768 .044
$-\frac{N_0}{r_0 F_0} x10^{-24}$	.9154	.7958	.7534	.7021	.6719 .5774	.5067	.4843 .4662	.3735 .3475	.3078 .2871
$-\frac{N_1}{r_1 F_1} x10^{-24}$					.2784	.4029	10.10 .6166	2.632 .7220	3.155 1.1014
$-\mu_0 r_0 F_0$	.5455	.5197	.5136	.4922	.4604 .4927	.4707	.4326 .4379	.3866 .3954	.3420 .3497
$-\mu_1 r_1 F_1$					.0891	.0695	.0023 .0455	.0110 .0498	.0101 .0332
DATE	Sept.11	Sept.25	Sept.25	Sept.21	Sept.16	Sept.22	Sept.15	Sept.23	Sept.10

ALL VALUES IN RATIONALIZED M.K.S. UNITS

TABLE T4:06 - SPECIMEN #9

T in ^{o}K	4.21 .01	79.80 .06	98.49 1.70	126.00 .01	151.77 .21	176.16 .01	199.91 .31	248.11 .43	296.41 .01
$\rho_0 x10^6$	66.52	64.46	62.89	62.37	65.20	70.94	79.34	104.40	138.66
$\rho_1 x10^8$								235.47 .17	355.25 .06
$-\rho_2 x10^{10}$								530.0 4.3	789.2 1.6
$-R_0 x10^6$	24.124	24.814	25.291	26.724	28.545	30.642	32.953	40.047 .022	45.508 .003
$R_1 x10^8$								41.461 .572	36.443 .087
$\frac{N_0}{r_0 F_0} x10^{-24}$	.2587	.2515	.2468	.2336	.2187	.2037	.1894	.10140 .10555	.08627 .07937
$\frac{N_1}{r_1 F_1} x10^{-24}$								.13260 .15076	.48750 .20860
$-\mu_0 r_0 F_0$	.3627	.3850	.4021	.4285	.4378	.4319	.4153	.4624 .4571	.4112 .4220
$-\mu_1 r_1 F_1$								.0973 .0766	.0196 .0552
DATE	Oct.27	Oct.27	Oct.27	Oct.27	Oct.27	Oct.27	Oct.27	Oct.28	Oct.26

ALL VALUES IN RATIONALIZED M.K.S. UNITS

TABLE T4:07 - SPECIMEN #10

T in ^{o}K	4.21	81.76	100.80	124.87	150.84	176.48	200.56	226.30	200.20 .04	251.45 .02	296.90 .05
$\rho_0 \times 10^6$	28.340	27.584	28.058	29.591	32.541	36.854	42.124	49.075	42.032	57.030	74.132
$\rho_1 \times 10^8$									64.57 .01	111.47 .02	160.04 .02
$-\rho_2 \times 10^{10}$									129.4 .3	177.8 .4	277.7 .5
$-R_0 \times 10^6$	11.880	12.592	13.077	13.863	14.912	16.201	17.290	18.431	17.532 .004	19.991 .004	21.898 .002
$R_1 \times 10^8$									5.03 .28	10.29 .22	15.67 .05
$-\frac{N_0}{r_0 F_0} \times 10^{-24}$	.5254	.4957	.4773	.4502	.4186	.3853	.3610	.3387	.2933 .2786	.2231 .2130	.1755 .1639
$-\frac{N_1}{r_1 F_1} \times 10^{-24}$									.3820 .2026	.5650 .3460	.9485 .4763
$-\mu_0 r_0 F_0$	.4192	.4564	.4661	.4685	.4583	.4396	.4105	.3756	.4576 .4647	.4117 .4176	.3737 .3817
$-\mu_1 r_1 F_1$									.0374 .0940	.0311 .0592	.0196 .0454
DATE	Nov.12	Nov.13	Nov.13	Nov.16	Nov.16	Nov.16	Nov.16	Nov.16	Nov.17	Nov.17	Nov.12

ALL VALUES IN RATIONALIZED M.K.S. UNITS

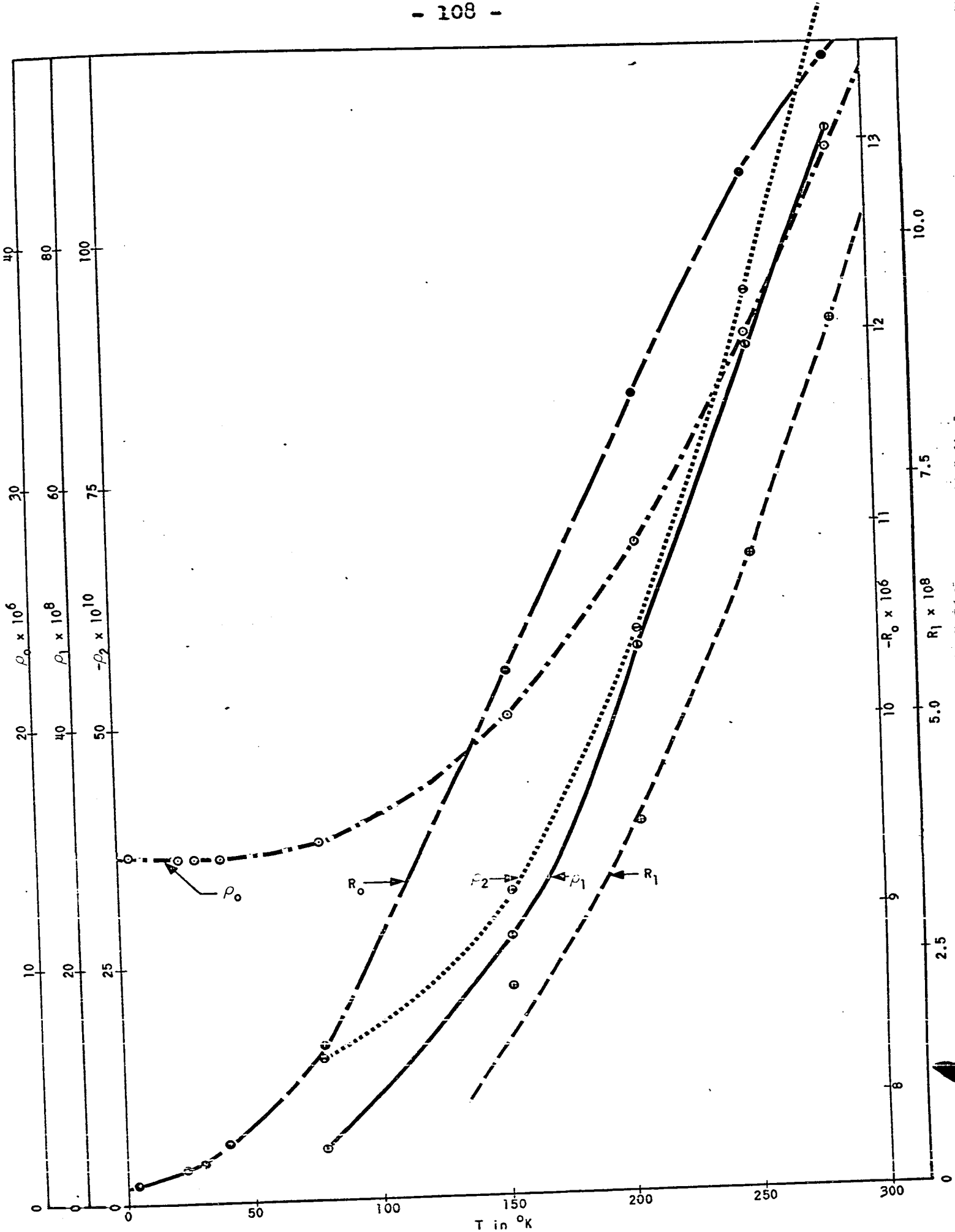

FIGURE F4:02 – SPECIMEN #5: TWO BAND COEFFICIENTS IN M.K.S. UNITS

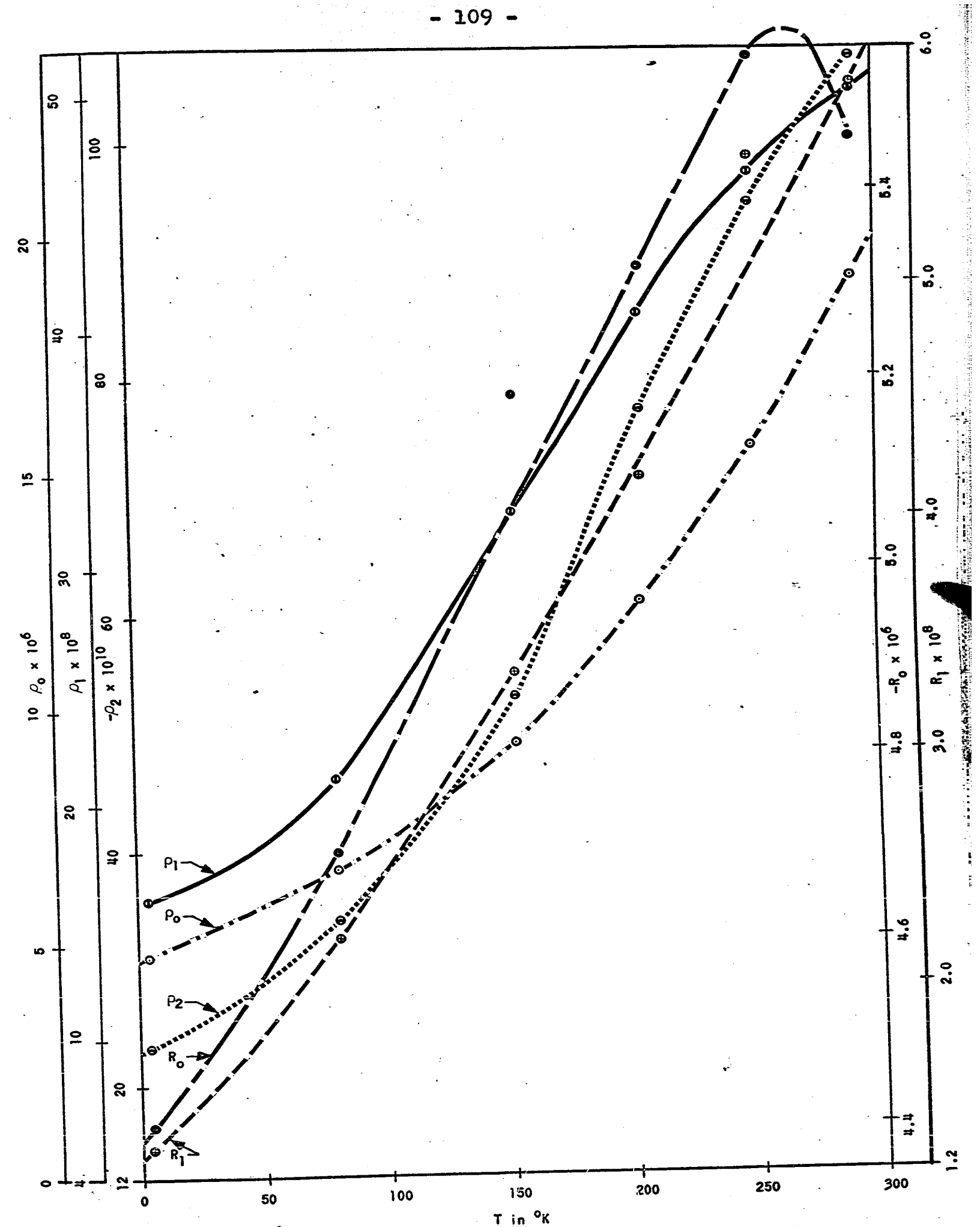

FIGURE F4:03 - SPECIMEN #6: TWO BAND COEFFICIENTS IN M.K.S. UNITS

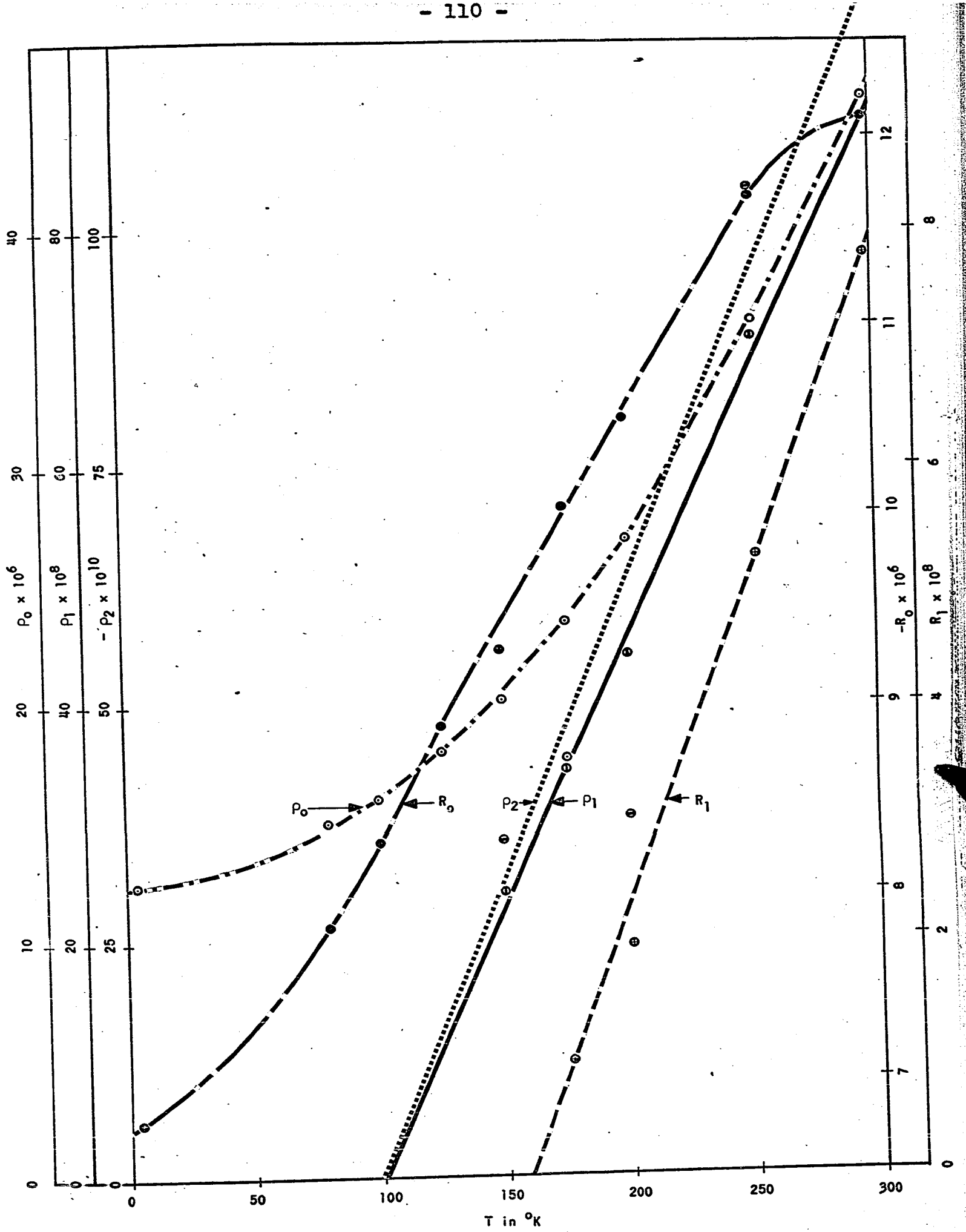

FIGURE F4:04 - SPECIMEN #8: TWO BAND COEFFICIENTS IN M.K.S. UNITS

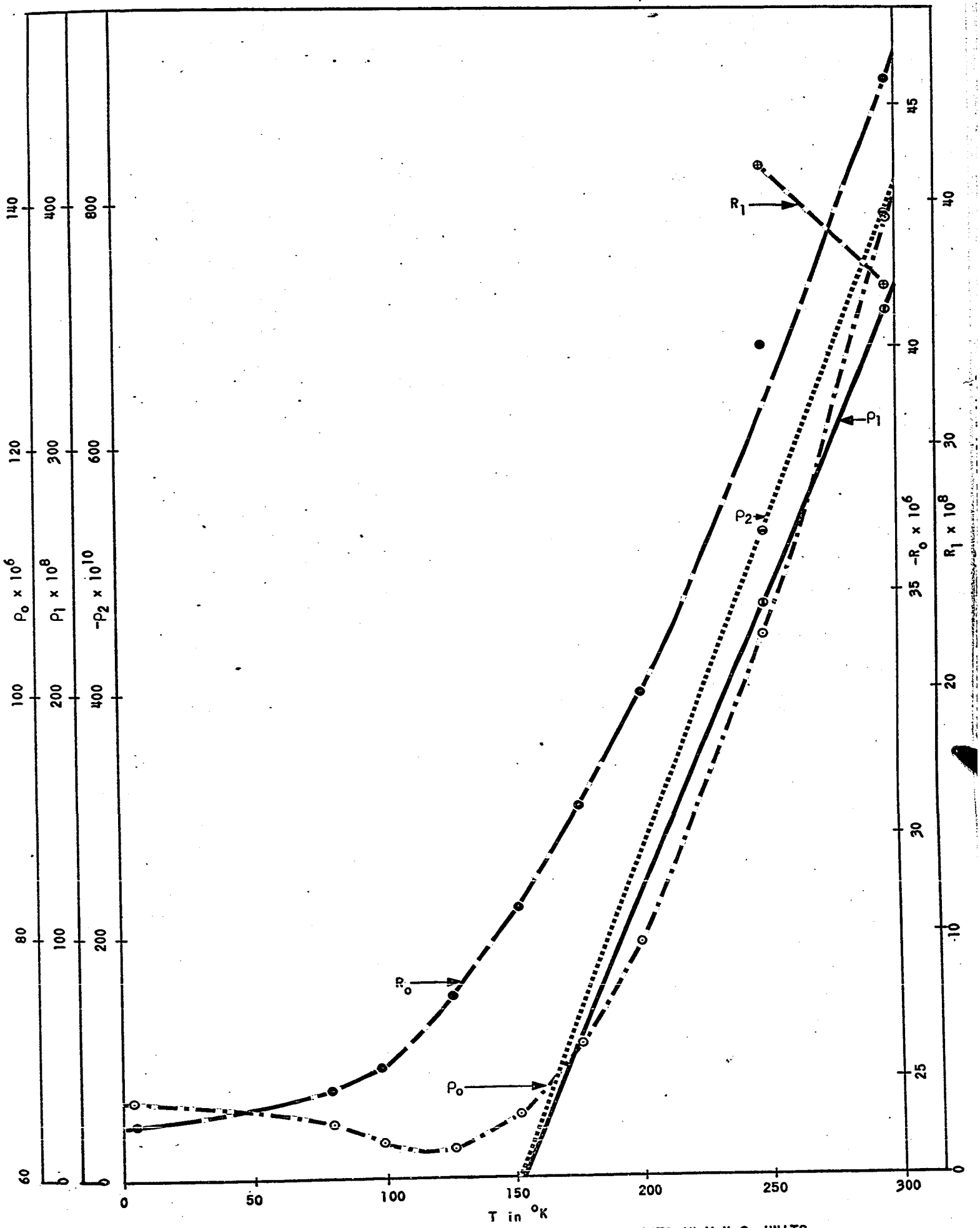

FIGURE F4:05 - SPECIMEN #9: TWO BAND COEFFICIENTS IN M.K.S. UNITS

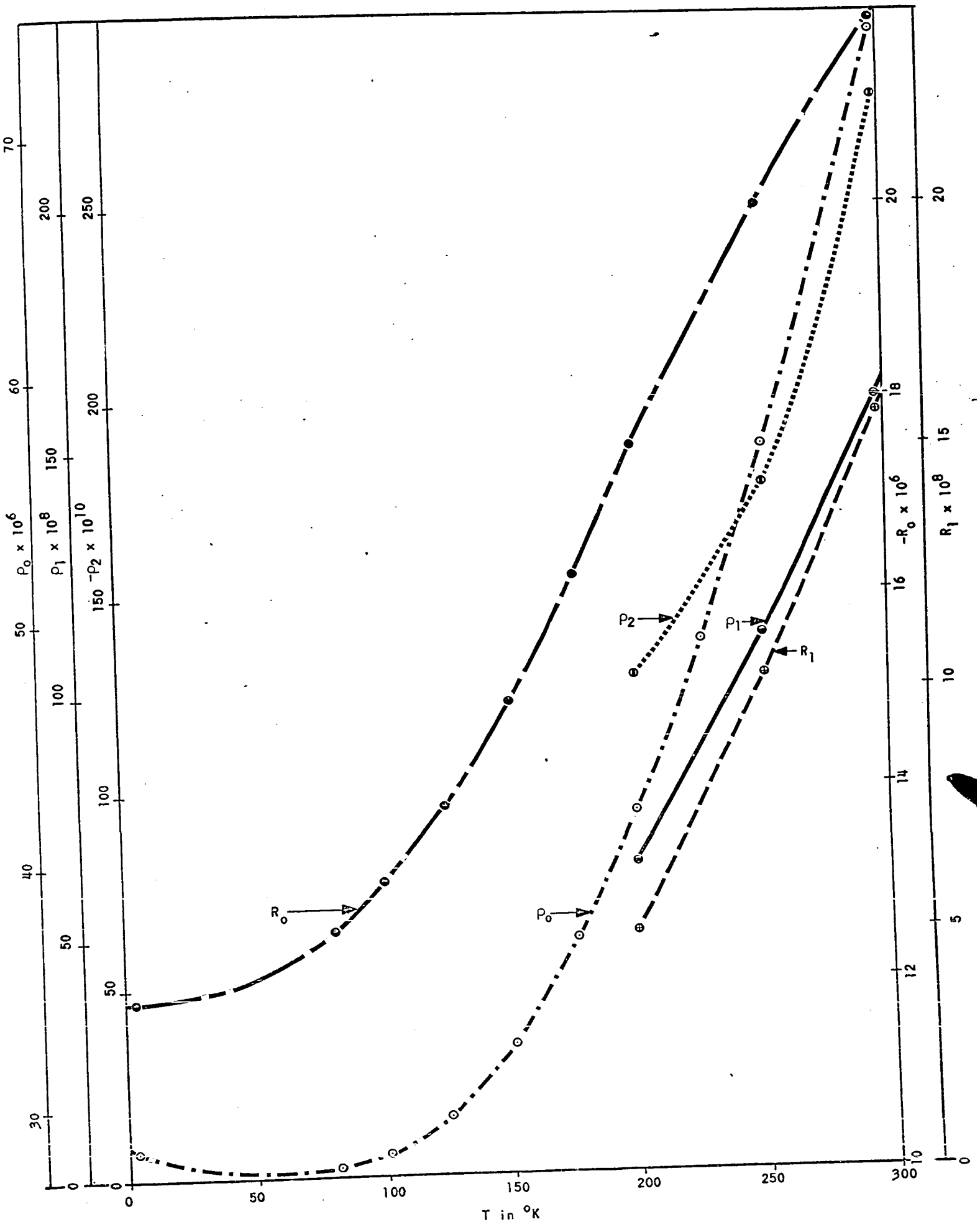

FIGURE F4:06 - SPECIMEN #10: TWO BAND COEFFICIENTS IN M.K.S. UNITS

measured at eleven temperatures. However, the data for $T > 78^{\circ}K$ showed considerable scatter and produced inconsistent results. Therefore, this data was set aside and is neither tabulated nor plotted. This will be discussed later in more detail.

Two types of error estimation are included in these tables. The maximum observed temperature drift, that occurred during a set of experimental measurements, is recorded immediately below the corresponding temperature. Also, the "weighted probable errors" in ρ_1 , ρ_2 , R_0 and R_1 , resulting from scatter in the experimental data, are recorded immediately below the corresponding coefficients.

Certain general trends may be observed from figures F4:02 to F4:06 . The five coefficients increase in magnitude with increasing temperature for all specimens. An increase in the temperature of a specimen produces an increase in the total thermal energy possessed by the conduction electrons. This allows a larger fraction of the conduction electrons to occupy the $\langle 111 \rangle$ band which lies approximately 0.08 ev. above the minimum of the (000) band. The $\langle 111 \rangle$ band has a much larger density-of-states effective mass, and therefore a much smaller mobility. The increase in the number of low mobility electrons causes increases in the magnitudes of ρ_0 and R_0 . The three

remaining coefficients are identically zero when conduction takes place in one degenerate, isotropic band. A change from one-band to two-band conduction or an increase in the number of carriers in the higher band produces an increase in the magnitude of each of these three coefficients.

A two-band analysis was performed for each set of coefficients. The results are tabulated in tables T4:02 to T4:07 . When only the (000) band contributed to the conduction processes, $\rho_1 = \rho_2 = R_1 = 0$ and N_0/r_0 and $\mu_0 r_0$ were determined from ρ_0 and R_0 . In the case of two-band conduction, the four two-band parameters were determined by two methods which should produce identical results. Unfortunately, this was not the case. Each parameter, which was calculated using ρ_2 as the fourth experimental coefficient is recorded immediately below the corresponding parameter calculated using R_1 .

The band parameters, which were calculated using R_1 as the fourth experimental coefficient, showed considerable scatter when plotted as functions of T . In most cases, the magnitude of $\mu_1 r_1 F_1$ was much lower than the value for Ge , under similar conditions of temperature and carrier concentration in the <111> conduction band. The band parameters which were calculated using ρ_2 as the fourth coefficient produced relat-

ively smooth curves when plotted as functions of T . In most cases, the magnitude of $\mu_1 r_1 F_1$ was in good agreement with that of Ge under similar conditions. Therefore, the band structure analysis was based upon the four coefficients, ρ_0 , ρ_1 , ρ_2 and R_0 .

C. DE HAAS-SHUBNIKOV DATA

Attempts were made to measure the periodicity and the amplitude of the magneto-oscillation, for specimens 5 to 10 , as functions of B and T . The measurements were neither sufficiently accurate nor sufficiently complete to produce a useful contribution to the band structure analysis. A new set of specimens, 5A to 10A , were prepared from what remained of the GaSb single crystal samples. Only three of these specimens, 6A , 7A and 8A , produced sufficiently large magneto-oscillations at 4.2°K to permit measurement to the required degree of accuracy. Magneto-oscillation was not observed for the three specimens having the lowest carrier concentrations, because the fractional change in the resistivity due to the oscillatory behavior decreased very rapidly with decreasing carrier concentration. Also, these relatively small magneto-oscillations were masked by the Hall-type voltage which appeared superimposed upon the magnetoresistance voltages.

Figure F4:07 is a plot of the magnetoresistance, including the oscillatory behavior, as a function of B for specimen #6 at 4.21°K . This was the first specimen for which oscillatory behavior was observed. Since the oscillation amplitude was a relatively small fraction of the total magnetoresistance, it was very difficult to measure this amplitude to a sufficiently high relative accuracy.

The magneto-oscillation amplitudes for specimens 6A , 7A and 8A are tabulated as functions of B and T in tables T4:08 , T4:09 and T4:10 . The oscillation periodicities, as given by the oscillation null points, are tabulated as functions of B and T in tables T4:11 , T4:12 and T4:13 . The experimental points were tabulated because it may be possible to improve the analysis used for the interpretation of this data.

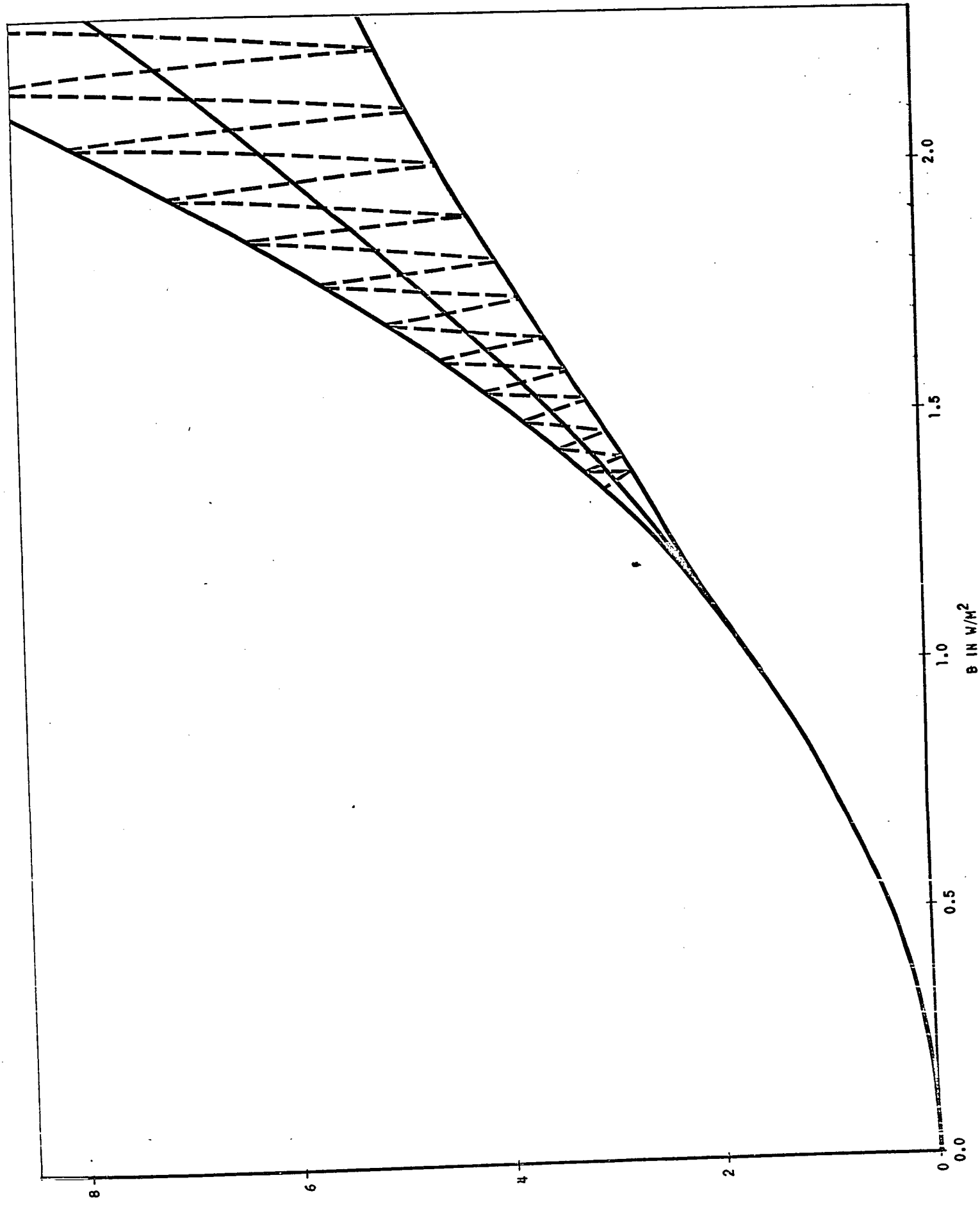
Δρ x 10⁷ in Ωm
8
6
4
2
0
0.0
0.5
1.0
1.5
2.0
B IN W/M²

TABLE T4:08

MAGNETORESISTANCE OSCILLATION AMPLITUDE - SPECIMEN #6A

B	$\Delta\rho_{osc.} \times 10^8$	B	$\Delta\rho_{osc.} \times 10^8$	B	$\Delta\rho_{osc.} \times 10^8$
2.335	25.84	2.339	30.77	2.327	32.92
2.303	25.27	2.307	29.50	2.293	31.51
2.273	24.40	2.275	28.19	2.259	30.17
2.242	23.46	2.242	26.89	2.225	28.84
2.211	22.35	2.210	25.64	2.192	27.57
2.175	21.06	2.175	24.53	2.157	26.31
2.139	19.74	2.140	23.43	2.119	24.80
2.102	18.45	2.105	22.32	2.082	23.27
2.065	17.22	2.069	20.93	2.044	21.81
2.028	16.17	2.033	19.56	2.007	20.63
1.991	15.18	1.997	18.16	1.969	19.37
1.955	13.96	1.962	16.86	1.933	18.06
1.920	12.98	1.926	15.80	1.898	16.98
1.886	12.11	1.890	14.85	1.865	15.78
1.853	11.14	1.857	13.81	1.832	14.77
1.822	10.38	1.825	12.86	1.801	13.95
1.791	9.57	1.793	11.97	1.772	13.06
1.763	8.75	1.766	11.01	1.745	12.36
1.735	8.19	1.738	10.28	1.717	11.69
1.707	7.56	1.709	9.70	1.688	10.88
1.679	6.92	1.681	9.10	1.661	10.14
1.651	6.43	1.653	8.51	1.633	9.45
1.624	5.93	1.625	7.79	1.606	8.71
1.597	5.40	1.598	7.13	1.579	7.99
1.569	4.91	1.571	6.55	1.549	7.35
1.539	4.45	1.540	6.03	1.518	6.52
1.506	3.92	1.508	5.37	1.483	5.85
1.471	3.38	1.473	4.63	1.443	5.07
1.430	2.88	1.433	3.92	1.398	4.25

$T = 4.201 \pm 0.001^{\circ}K$ $T = 3.060 \pm 0.001^{\circ}K$ $T = 2.130 \pm 0.003^{\circ}K$

$\rho_0 = 4.847 \times 10^{-6}$

ρ_0 , B AND $\Delta\rho$ IN M.K.S. UNITS

TABLE T4:09

MAGNETORESISTANCE OSCILLATION AMPLITUDE - SPECIMEN #7A

B	$\Delta\rho_{osc.} \times 10^8$	B	$\Delta\rho_{osc.} \times 10^8$	B	$\Delta\rho_{osc.} \times 10^8$
2.335	15.22	2.345	18.36	2.338	19.34
2.302	14.11	2.313	17.06	2.305	18.51
2.270	13.33	2.282	16.07	2.273	17.78
2.238	12.68	2.250	15.29	2.240	17.01
2.206	12.27	2.216	14.77	2.207	16.20
2.169	12.00	2.182	14.44	2.170	15.92
2.132	11.75	2.144	14.25	2.130	15.51
2.093	11.28	2.105	13.67	2.093	14.86
2.055	10.56	2.068	12.98	2.054	14.24
2.017	10.05	2.031	12.36	2.016	13.82
1.979	9.56	1.993	11.94	1.978	13.19
1.942	9.00	1.956	11.31	1.941	12.47
1.906	8.55	1.920	10.92	1.906	12.15
1.872	7.97	1.884	10.29	1.872	11.46
1.839	7.52	1.852	9.76	1.838	11.05
1.808	7.25	1.820	9.46	1.807	10.60
1.778	6.78	1.790	9.01	1.778	10.12
1.749	6.42	1.762	8.73	1.749	9.95
1.721	5.99	1.734	8.37	1.720	9.33
1.693	5.70	1.705	7.83	1.692	8.91
1.664	5.48	1.677	7.76	1.663	8.54
1.636	5.24	1.649	6.81	1.635	8.16
1.608	4.81	1.620	6.48	1.608	7.75
1.581	4.47	1.594	6.23	1.581	7.24
1.551	4.19	1.566	5.85	1.550	6.64
1.518	4.01	1.535	5.39	1.518	6.23
1.483	3.46	1.501	4.73	1.482	5.65
1.442	2.95	1.465	4.60	1.442	5.03
1.397	2.50	1.421	4.07	1.396	4.49

$T = 4.204 \pm 0.001^{\circ}K$ $T = 2.972 \pm 0.004^{\circ}K$ $T = 2.077 \pm 0.005^{\circ}K$

$\rho_0 = 3.824 \times 10^{-6}$

ρ_0, B AND $\Delta\rho$ IN M.K.S. UNITS

TABLE T4:10

MAGNETORESISTANCE OSCILLATION AMPLITUDE - SPECIMEN #8A

B	$\Delta\rho_{osc.} \times 10^8$	B	$\Delta\rho_{osc.} \times 10^8$	B	$\Delta\rho_{osc.} \times 10^8$
2.329	2.003	2.317	2.324	2.348	2.685
2.298	1.877	2.284	2.197	2.316	2.553
2.266	1.755	2.252	2.067	2.285	2.422
2.236	1.636	2.220	1.940	2.254	2.292
2.202	1.512	2.184	1.807	2.223	2.161
2.165	1.391	2.145	1.670	2.186	2.029
2.127	1.270	2.107	1.523	2.147	1.878
2.088	1.160	2.069	1.378	2.110	1.724
2.050	1.053	2.030	1.248	2.071	1.561
2.013	0.945	1.993	1.139	2.034	1.422
1.975	0.862	1.956	1.050	1.995	1.292
1.940	0.778	1.920	0.951	1.958	1.174
1.904	0.695	1.886	0.852	1.923	1.054
1.871	0.633	1.853	0.764	1.887	0.969
1.838	0.571	1.823	0.676	1.855	0.907
1.807	0.508	1.794	0.600	1.823	0.829
1.777	0.458	1.765	0.530	1.793	0.750
1.748	0.406	1.736	0.485	1.764	0.681
1.720	0.356	1.706	0.466	1.736	0.610
1.692	0.331	1.678	0.462	1.707	0.550
1.663	0.299	1.650	0.428	1.679	0.503
1.635	0.261	1.623	0.362	1.650	0.462
1.608	0.230	1.596	0.298	1.623	0.417
1.581	0.194	1.568	0.254	1.596	0.371
1.551	0.174	1.537	0.248	1.568	0.327
1.518	0.152	1.504	0.197	1.538	0.291
1.484	0.123	1.467	0.154	1.505	0.241
1.446	0.094	1.425	0.133	1.469	0.218
1.400	0.083			1.428	0.172

$T = 4.203 \pm 0.001^{\circ}K$ $T = 3.040 \pm 0.002^{\circ}K$ $T = 2.077 \pm 0.003^{\circ}K$

$\rho_0 = 12.305 \times 10^{-6}$

ρ_0, B AND $\Delta\rho$ IN M.K.S. UNITS

TABLE T4:11 - SPECIMEN #6A

PERIODICITY OF THE MAGNETO-OSCILLATION WITH RESPECT TO THE MAGNETIC FLUX DENSITY

PERIOD	B IN w/M^2	B IN w/M^2	B IN w/M^2
1	2.333	2.330	2.333
1.5	2.262	2.260	2.258
2	2.196	2.195	2.192
2.5	2.136	2.137	2.133
3	2.078	2.082	2.077
3.5	2.022	2.018	2.022
4	1.968	1.968	1.968
4.5	1.918	1.918	1.918
5	1.870	1.870	1.870
5.5	1.826	1.825	1.825
6	1.783	1.782	1.783
6.5	1.744	1.744	1.745
7	1.705	1.705	1.706
7.5	1.667	1.666	1.668
8	1.630	1.630	1.630
8.5	1.597	1.597	1.598
9	1.565	1.565	1.566
9.5	1.532	1.532	1.533
10	1.503	1.503	1.503
10.5	1.473	1.475	1.475
11	1.447	1.449	1.448
11.5	1.420	1.420	1.420
12		1.393	1.393
T IN ^{o}K	4.201±0.001	3.060±0.001	2.130±0.003

TABLE T4:12 - SPECIMEN #7A

PERIODICITY OF THE MAGNETO-OSCILLATION WITH RESPECT TO THE MAGNETIC FLUX DENSITY

PERIOD	B IN w/M^2	B IN w/M^2	B IN w/M^2
.5	2.364	2.362	2.361
1	2.298	2.297	2.297
1.5	2.234	2.234	2.234
2	2.179	2.177	2.177
2.5	2.123	2.122	2.124
3	2.070	2.070	2.072
3.5	2.022	2.022	2.023
4	1.971	1.971	1.972
4.5	1.927	1.927	1.927
5	1.883	1.881	1.882
5.5	1.842	1.842	1.842
6	1.803	1.802	1.802
6.5	1.767	1.767	1.767
7	1.730	1.730	1.731
7.5	1.696	1.696	1.696
8	1.661	1.662	1.662
8.5	1.627	1.628	1.628
9	1.598	1.598	1.598
9.5	1.569	1.568	1.569
10	1.540	1.540	1.540
10.5	1.511	1.512	1.512
11	1.485	1.485	1.486
11.5	1.460	1.460	1.460
12	1.435	1.435	1.436
12.5	1.412	1.411	1.411
T IN ^{o}K	4.204±0.001	2.972±0.004	2.077±0.005

TABLE T4:13 - SPECIMEN #8A

PERIODICITY OF THE MAGNETO-OSCILLATION WITH RESPECT TO THE MAGNETIC FLUX DENSITY

PERIOD	B IN w/M^2	B IN w/M^2	B IN w/M^2
.5	2.372		
1	2.300	2.307	2.307
1.5	2.227	2.231	2.234
2	2.160	2.165	2.166
2.5	2.097	2.103	2.104
3	2.037	2.041	2.044
3.5	1.978	1.985	1.985
4	1.925	1.930	1.932
4.5	1.874	1.878	1.881
5	1.826	1.833	1.833
5.5	1.782	1.789	1.788
6	1.739	1.744	1.745
6.5	1.698	1.703	1.703
7	1.657	1.662	1.662
7.5	1.620	1.624	1.624
8	1.585	1.588	1.588
8.5	1.550	1.555	1.556
9	1.516	1.520	1.522
9.5	1.486	1.490	1.490
10	1.455	1.461	1.460
10.5	1.429	1.432	1.431
11	1.400	1.402	1.399
T IN ^{o}K	4.203±0.001	3.040±0.002	2.077±0.003

2. ANALYSIS OF THE DATA

A. TWO-BAND ANALYSIS

1. EFFECTIVE MASS CALCULATIONS

The band structure analysis could not be completed until the effective masses for the (000) and ⟨111⟩ conduction bands were determined. The object of the magneto-oscillation measurements was to determine the effective mass of the (000) conduction band, M_0^* , as a function of the density of electrons in this band, N_0 . This object was not achieved. It was therefore necessary to obtain a value for M_0^* from the scientific literature. The accepted value for the ratio of the (000) electron effective mass to the free electron rest mass, M_0^*/M , at the bottom of the band, is 0.047 . It is well known that plots of E versus k are parabolic only in the immediate vicinity of an extremum. Therefore, M_0^* is a function of the occupied electron energies above the minimum of the (000) band.

Cardona (65:2) used the following relation to predict the effective masses of carriers in a number of semiconductors.

$$M/M_i^* = 1/G_i = 1 + p_i^2/(E_{g_i} + E_i) \qquad \ldots.(4:01)$$

where: E_{g_i} = the energy separation between the conduction and valence bands for the appropriate direction

in k-space.

E_i = the electron energy measured above the minimum of the appropriate conduction band.

p_i^2 = an energy which is determined by the periodic potential of the crystal lattice.

$= E_{g_i}(1/G_{i_0} - 1)$

$G_{i_0} = M_i^*/M$ at the minimum of the band.

Upon rearranging equation (4:01) one obtains:

$$G_i = G_{i_0}(1 + E_i/E_{g_i})/(1 + G_{i_0}E_i/E_{g_i})$$

$$G_0 \simeq G_{0_0}(1 + (1 - G_{0_0})E_0/E_{g_0}) \quad \text{for the (000) band} \quad \ldots.(4:02)$$

since $G_{0_0} \ll 1$ and $E_0/E_{g_0} \ll 1$.

This relation predicts the density-of-states effective mass at any particular energy in the band, E_0 . However, the effective mass which is required for the interpretation of the experimental measurements is the density-of-states effective mass averaged over all the occupied states.

Since G_0 is only a few percent larger than G_{0_0}, the averaging process may be performed with the aid of an approximation without introducing a significant error into the results for G_0 . Consider the ideal case of a perfectly parabolic band at 0^oK . The Fermi energy is given by:

$E_{F_0} = C_0 N_0^{2/3} / \langle G_0 \rangle$ where: $C_0 = h^2 (3\pi^2)^{2/3} / 8\pi^2 M$

$= 3.63 \times 10^{-19}$ ev.m.^{2} ....(4:03)

It may also be shown that:

$N_0 \propto E_0^{3/2}$ and $dN_0 \propto E_0^{1/2} dE_0$ . ....(4:04)

At $T = 0^oK$, only those states satisfying $E_0 \leq E_{F_0}$ can be occupied.

Therefore: $\langle G_0 \rangle = \int_0^{E_{F_0}} G_0 dN_0 \Big/ \int_0^{E_{F_0}} dN_0$ ....(4:05)

Substitute equations (4:02) and (4:04) into equation (4:05).

Then: $\langle G_0 \rangle \simeq G_{0_0} (1 + 0.6(1 - G_{0_0}) E_{F_0} / E_{g_0})$ ....(4:06)

Substitute equation (4:03) into equation (4:06).

Then: $\langle G_0 \rangle \simeq G_{0_0} (1 + 0.6(1 - G_{0_0}) C_0 N_0^{2/3} / E_{g_0} \langle G_0 \rangle)$ ....(4:07)

Define: $X = 0.6(1 - G_{0_0}) C_0 / E_{g_0} G_{0_0}$ ....(4:08)

Substitute equation (4:08) into equation (4:07) and solve for $\langle G_0 \rangle$. Then: $\langle G_0 \rangle \simeq G_{0_0} (1 + XN_0^{2/3} - (XN_0^{2/3})^2)$ ....(4:09)

For the (000) conduction band of GaSb at 0^oK :

$G_{0_0} = 0.047$

$E_{g_0} = 0.0813$ ev.

$X = 5.45 \times 10^{-18}$ m.^{2}

The effective mass of the ⟨111⟩ conduction band, M_1^*, may be determined by the simultaneous solution of the two-band Fermi energy equations for two specimens showing two-band conduction at liquid He temperatures. Consider the following identity.

$$E_{F_0} = E_{F_1} + \Delta E \qquad \ldots.(4:10)$$

where: E_{F_0} = the Fermi energy of the (000) conduction band, taking the zero of energy at the (000) band minimum.

E_{F_1} = the Fermi energy of the ⟨111⟩ conduction band, taking the zero of energy at the ⟨111⟩ band minima.

ΔE = the energy separation of the ⟨111⟩ and (000) conduction band minima.

ΔE is a function of the temperature, but not of the electron concentrations, for the concentrations of Te which were used in this investigation.

Consider two specimens, designated by subscripts 1 and 2, having different carrier concentrations at $4.2^{\circ}K$. Then $\Delta E_1 = \Delta E_2$ and on substitution into equation (4:10) one obtains: $(E_{F_0} - E_{F_1})_1 = (E_{F_0} - E_{F_1})_2 \qquad \ldots.(4:11)$

Substitute equation (4:03) into equation (4:11). For purposes of notation replace ⟨G_i⟩ by G_{i_j} and N_i by N_{i_j}, where

i designates the band and j designates the specimen.

Then: $N_{0_1}{}^{2/3}/G_{0_1} - N_{1_1}{}^{2/3}/G_{1_1} = N_{0_2}{}^{2/3}/G_{0_2} - N_{1_2}{}^{2/3}/G_{1_2}$ ....(4:12)

Since the ⟨111⟩ band has a relatively large effective mass, any change in its value, due to the presence of even a relatively large electron concentration, is negligible. Therefore

$G_{1_1} = G_{1_2} = G_1$.

Equation (4:12) reduces to:

$$G_1 = (N_{1_2}{}^{2/3} - N_{1_1}{}^{2/3})/(N_{0_2}{}^{2/3}/G_{0_2} - N_{0_1}{}^{2/3}/G_{0_1}) \qquad \ldots.(4:13)$$

Only the two samples from which specimens 6 and 7 were obtained showed two-band conduction at $4.2^{\circ}K$. The experimental data for #6 is probably the most accurate and reliable of all the data obtained. The results for #7 at $4.2^{\circ}K$ should be reasonably accurate. Two-band measurements were performed on #7A at $4.2^{\circ}K$ in order to obtain another set of data for the calculation of M_1^* .

Equations (2:27) show that the initial two-band calculations evaluate N_i/r_iF_i , and not N_i . When the F_i are known, the N_i can be evaluated by means of an approximation program which will be discussed in the next section of this chapter.

$F_i(K_i)$ was defined in equations (2:26):

$F_i(K_i) = 3K_i(K_i + 2)/(2K_i + 1)^2$ where $K_i = (M_L^*/M_T^*)_i$.

Since the constant energy surfaces for the (000) band are approximately spheres in k-space, $K_0 = 1$ and $F_0 = 1$. Very little is known about the ⟨111⟩ conduction band of GaSb . The value of K_1 , and therefore F_1 , has not been accurately established. However, it is possible to establish limits for the values of K_1 and F_1 . Experiments have shown that $K_i \geq 1$ for most, if not all, semiconductors. Therefore $1 \leq K_i < \infty$. Equation (2:26) shows that F_i is a monotonic decreasing function of K_i and $1 \geq F_i > 0.75$. The only available value for K_1 was determined by Piller (64:6), $K_1 = 8.6$. Therefore $F_1 \simeq 0.8256$.

Although it is necessary to know the value of F_1 in order to explicitly determine M_1^*/M , it is possible to evaluate the effective mass ratio as a simple function of F_1 . This is possible because the r_1 , which corresponds to the experimentally determined N_1/r_1F_1 , is not a function of F_1 . Smith, page 79 equation (19) , shows that for an approximately parabolic band the carrier density is given by:

$$N_i = 4\pi(2MkT/h^2)^{3/2}(M_i^*/M)^{3/2}F_{1/2}(\eta_i^*) \qquad \ldots.(4:14)$$

where: $$F_n(\eta^*) = \int_0^\infty (X^n/(1 + \exp(X - \eta^*)))dX \qquad \ldots.(4:15)$$

$= n^{\underline{th}}$ Fermi integral for a degeneracy of η^*

$$\eta^* = E_F/kT \qquad \ldots.(4:16)$$

It may also be shown that $r_i = \langle \tau_i^2 \rangle / \langle \tau_i \rangle^2$ is a function of only η_i^* and S , when $\tau_i \propto E_i^S$. r_i and η_i^* were evaluated by a self-consistent, successive approximation calculation which will be discussed in the next section of this chapter.

Equation (4:14) may be written in the form:

$$F_{1/2}(\eta_i^*) = C(T) \cdot N_i / (M_i^*/M)^{3/2}$$
$$= C(T) \cdot (N_i/F_i) / ((M_i^*/M)/F_i^{2/3})^{3/2} \quad \ldots.(4:17)$$

The approximation calculation eliminates r_i from N_i/r_iF_i by means of a loop calculation involving equation (4:17) . Now equation (4:13) may be written in the form:

$$G_1/F_1^{2/3} = ((N_{1_2}/F_1)^{2/3} - (N_{1_1}/F_1)^{2/3}) / (N_{0_2}^{2/3}/G_{0_2} - N_{0_1}^{2/3}/G_{0_1}) \quad \ldots.(4:18)$$

Since N_{1_i} and G_1 appear in equations (4:17) and (4:18) in the same forms, N_{1_i}/F_1 and $G_1/F_1^{2/3}$, $G_1/F_1^{2/3}$ can be evaluated as follows without first evaluating N_{1_i} and F_1 . Since $r_i \simeq 1$, the values for N_0/r_0F_0 and N_1/r_1F_1 for specimens 6 , 7 and 7A were substituted into equation (4:18) , using the assumption that $r_1 = 1$. The resulting approximate value for $G_1/F_1^{2/3}$ and the values for N_i/r_iF_i were inserted into the complete two-band analysis, which will be discussed later. The approximate values computed for N_0 and N_1/F_1 , for specimens 6 , 7 and 7A at 4.2^oK , were substituted into equation (4:18). The improved value for $G_1/F_1^{2/3}$ was inserted into

the complete two-band analysis. This approximation process was repeated until the change in the value of $G_1/F_1^{2/3}$, between two successive passes through the loop, was less than 1 part in 5000. The values for N_i/r_iF_i, N_i/F_i and $G_i/F_i^{2/3}$ are recorded in table T4:14. The value of $(M_1^*/M)/F_1^{2/3} = 1.244$, which was obtained from specimens 6 and 7A, is probably the more reliable of the two values. It may be noted that specimens 7 and 7A, which had different carrier concentrations, produced values for M_1^* which were different by less than one percent.

According to M. Cardona, in a private communication, the <111> conduction band edge in GaSb is not split, or at worst the linear term produced by splitting would not be observed for the <111> band electron concentrations in specimens 6, 7 and 7A. Therefore, the <111> conduction band minima must be centered on the Brillouin zone boundary and the band must consist of four equivalent minima. Each minimum would then have an effective mass ratio of $G_1/4^{2/3} = 0.494 \times F_1^{2/3}$. Each <111> conduction band minimum in Ge has an effective mass ratio of 0.22.

The only available value for K_1, for the conduction band of GaSb, was determined by H. Pillar (64:6) by free carrier Faraday rotation measurements. He obtained the

TABLE T4:14

DATA AND RESULTS FOR THE CALCULATION OF THE ⟨111⟩ CONDUCTION BAND DENSITY-OF-STATES EFFECTIVE MASS

NOTE: $F_0 = 1$

SPECIMEN NUMBER	7	6	7A
N_0/r_0F_0 IN $m.^{-3}$	1.6033×10^{24}	1.2976×10^{24}	1.6432×10^{24}
N_1/r_1F_1 IN $m.^{-3}$	11.551×10^{24}	0.7275×10^{24}	13.267×10^{24}
N_0/F_0 IN $m.^{-3}$	1.6033×10^{24}	1.2976×10^{24}	1.6432×10^{24}
N_1/F_1 IN $m.^{-3}$	11.599×10^{24}	0.8156×10^{24}	13.313×10^{24}
$G_0 = M_0^*/M$	0.05025	0.04985	0.05030
$G_1/F_1^{2/3} = (M_1^*/M)/F_1^{2/3}$	1.254		1.244
$(M_1^*/M)/(4F_1)^{2/3}$	0.498		0.494

NOTE: $(G_{1_{6,7}} - G_{1_{6,7A}})/G_{1_{6,7A}} = 0.008$

ASSUME: $K_1 = 8.6$

THEN: $F_1 = 0.8256$ $\quad F_1^{2/3} = 0.8801$

$M_1^*/M = 1.095$ $\quad (M_1^*/M)/4^{2/3} = 0.435$

following values:

$M^*_{1_L}/M = 1.2$ $\qquad$ $M^*_{1_T}/M = 0.14$

$K_1 = 8.6$ $\qquad$ $M^*_1/M = 0.73$

When $K_1 = 8.6$, $F_1 = 0.8256$ and $F_1^{2/3} = 0.8801$.

The ⟨111⟩ conduction band effective mass ratios, determined from the data for specimens 6 and 7A , are $M^*_1/M = 1.095$ and $(M^*_1/M)/4^{2/3} = 0.435$.

An attempt was made to determine M^*_1 from the data obtained at temperatures other than 4.2^oK . If a method could be found for solving equation (4:11) at any temperature, all measurements showing two-band behavior could be used for determining M^*_1 . In the classical limit, $E_F/kT \longrightarrow -\infty$, it may be shown that:

$$N = 2(2\pi M^* kT/h^2)^{3/2} \cdot \exp(E_F/kT)$$

$$= C \cdot \exp(E_F/kT) \qquad \ldots\ldots(4:19)$$

$$E_F = kT(\mathrm{LOG}_e N - \mathrm{LOG}_e C)$$

If the ⟨111⟩ band is completely non-degenerate, equation (4:11) reduces to:

$$E_{F_{0_1}} - E_{F_{0_2}} = kT \cdot \mathrm{LOG}_e(N_{1_1}/N_{1_2}) \qquad \ldots\ldots(4:20)$$

Equation (4:20) is independent of the value of M^*_1 . Therefore, M^*_1 can only be determined with reasonable accuracy when the ⟨111⟩ band may be considered to be completely degenerate.

For specimen #6 at 78°K, $E_F/kT < 0$. It was therefore impossible to evaluate M_1^* at any temperature except 4.2°K.

Becker (65:3) stated that it is possible that the K_i, in equations (2:27), should be functions of both the $(\tau_L/\tau_T)_i$ and the $(M_L^*/M_T^*)_i$, such that $K_i \simeq 1$. Assume that $K_1 = 1$ and $F_1 = 1$. The values for M_1^*/M and $(M_1^*/M)/4^{2/3}$ increase by 13.5% to 1.244 and 0.498, respectively. The values for N_1 would be increased, and those for μ_1 decreased, by 21.1%. Although tables T4:15 to T4:19 and figures F4:08 to F4:22 would no longer be correct, there would be no significant change in the temperature dependence of the two-band parameters.

Although the values of M_1^*/M, N_1 and μ_1 are affected by the choice of the value for K_1, it was shown on page 130 that the values obtained for $F_{1/2}(\eta_i^*)$ and η_i^* were not dependent upon the value of K_i. Therefore, the values obtained for ΔE and $d(\Delta E)/dT$ are not affected by a change in the values of K_1 and F_1.

(2) BAND STRUCTURE CALCULATIONS

The two-band analysis of the experimental data did not completely determine the electron densities and mobilities. N_i and μ_i were expressed in the forms N_i/r_iF_i and $\mu_i r_i F_i$, where r_i was a scattering parameter which was a function of the type(s) of scattering process(es) involved and the degeneracy of the band. By definition $r_i = \langle \tau_i^2 \rangle / \langle \tau_i \rangle^2$. A number of authors have shown that when $\tau \propto E^S$,

$$r = \frac{3(2S + 3/2)}{2(S + 3/2)^2} \cdot \frac{F_{1/2}(\eta^*)\, F_{2S + 1/2}(\eta^*)}{(F_{S + 1/2}(\eta^*))^2} \qquad \ldots.(4:21)$$

These Fermi integrals can be directly evaluated only in the extreme limits of degeneracy. In the degenerate limit,

$$\eta^* \longrightarrow \infty \,, \; F_n(\eta^*) = (\eta^{*n+1})/(n + 1) \text{ and } r = 1 \qquad \ldots.(4:22)$$

for any type of scattering mechanism. In the classical limit, $\eta^* \longrightarrow -\infty$, $F_n(\eta^*) = \exp(\eta^*) \cdot \Gamma(n + 1)$ and

$$r = \frac{3(2S + 3/2)}{2(S + 3/2)^2} \cdot \frac{\Gamma(3/2) \cdot \Gamma(2S + 3/2)}{(\Gamma(S + 3/2))^2} \qquad \ldots.(4:23)$$

where Γ is the mathematical Gamma function.

For an intermediate degeneracy, the Fermi integrals must be evaluated by numerical integration. A computer program, using Simpson's Rule, was written to compute $F_n(\eta^*)$

and $r(\eta^*,S)$ for n = -0.5 , 0.0 , 0.5 , 1.0 , 1.5 , 2.0 , 3.5 and S = -0.5 , 0.5 , 1.5 . These functions were evaluated at closely spaced intervals in the range $-10.0 \leq \eta^* \leq 100.0$, and are tabulated in the appendix. Certain of these functions are tabulated in semiconductor books. However, these tabulations did not cover a sufficiently wide range of values for η^* , and the numbers quoted were frequently very inaccurate.

A computer program was written to evaluate r_i and therefore N_i and μ_i . The tables of values, which were computed for $F_{1/2}(\eta^*)$ and $r(\eta^*,S)$, were incorporated into this program. The computation required only two assumptions, namely, the type of scattering mechanism involved and the value of K_1 . Many scientific papers discuss the various types of scattering mechanisms and their mathematical representations. These papers were discussed in Chapter 1.

In this computer program only r_i , which was always of the order of 1 , was a function of the energy dependence of the scattering relaxation time. It was necessary to assume a general form for the relaxation time. The simplest choice was $\tau \propto E^S$. It was shown in chapter 1 that this type of energy dependence is valid for all of the commonly encountered scattering mechanisms in semiconductors. Although tables of

$r(\eta^*, S)$ for $S = -1/2$, $1/2$, $3/2$ were incorporated into the computer program, the results from the program were not very sensitive to the choice of the value for S . It was shown in chapter 1 that ionized impurity scattering will be dominant in n-type GaSb under most, if not all, of the conditions for which data was obtained. Therefore, it was usually assumed that $S = 3/2$.

N_i , μ_i , r_i , E_{F_i} and $(E_{F_0} - E_{F_1})$ for $i = 0,1$ were determined as functions of the temperature, for the six specimens, by means of a computer program. The computer evaluated these band parameters by a process of successive approximations. It was necessary to assume values for F_i , M_i^*/M and S . It was also assumed that the electrons in the (000) and ⟨111⟩ bands were scattered by the same mechanism. This is probably a valid assumption for most of the experimental conditions which were investigated. Although tables of r_i were available for $S = -1/2$, $1/2$, $3/2$, it was usually assumed that $S = 3/2$, the accepted value for ionized impurity scattering. Although this might not be the best choice for every set of conditions encountered, the shapes of the plots of the band parameters as functions of the temperature should not be significantly altered.

The basic steps in the computations were as follows:

(1) Read N_i/r_iF_i , T , F_i , M_i^*/M and S .

(2) Assume that $r_i = 1$. Compute the experimental value of the Fermi integral, $F_{1/2_{exp.}}(\eta^*)$, from equation (4:14).

(3) Using the tables previously computed, curve fit η^* as a function of $F_{1/2}(\eta^*)$, in the vicinity of $F_{1/2_{exp.}}$, and determine the value of $\eta^*_{exp.}$ which corresponds to $F_{1/2_{exp.}}$.

(4) Using the tables previously computed, curve fit r_i as a function of η^* , in the vicinity of $\eta^*_{exp.}$, and determine the value of $r_{i_{exp.}}$ which corresponds to $\eta^*_{exp.}$.

(5) When the (000) band is under consideration, the value of M_0^*/M must be corrected for the variation of the effective mass with filling of the band. Equation (4:06) may be expressed in the following form:

$$M_0^*/M \simeq G_{0_0}(1 + 0.6(1 - G_{0_0})E_{F_0}/E_{g_0}) \qquad \ldots.(4:24)$$

where: $G_{0_0} = M_0^*/M$ at the minimum of the (000) band.

$E_{g_0} = (0.813 - 3.7 \times 10^{-4} \times T)$e.v. for T in ^oK

Equation (4:24) is not strictly valid since the multiplicative factor, 0.6 , was evaluated for the case when $T = 0^oK$. However, the effective mass correction term is only a few percent of the effective mass value at the bottom of the band, so a small error in the value of this

correction term is insignificant.

(6) Repeat steps (2) to (5) inclusive, using the corrected values for M_0^*/M and r_i . Continue this approximation process until the fractional change in $\eta^*_{exp.}$, between two successive passes through the loop, is less than 1 part in 10,000.

(7) The values for N_i , r_i and E_{F_i} have now been determined. The energy separation between the minima of the (000) and ⟨111⟩ bands, ΔE , is determined by the difference in the Fermi energies for the two bands at the same temperature, $\Delta E = E_{F_0} - E_{F_1}$.

The results of these calculations are recorded in tables T4:15 to T4:19 and figures F4:08 to F4:22 . These results will be discussed and interpreted in Chapter 5.

TABLE T4:15 - SPECIMEN #5

TWO-BAND PARAMETERS, FERMI ENERGIES AND ENERGY SEPARATION OF THE (000) AND ⟨111⟩

CONDUCTION BANDS

T in ^{o}K	4.21	23.62	30.32	40.00	78.47	152.71	204.54	250.04	283.81
$N_0 \times 10^{-24}$	.8205	.8183	.8179	.8146	.7793	.6775	.5900	.5104	.4543
$N_1 \times 10^{-24}$					.0757	.3108	.6215	.9399	1.2130
$(N_0+N_1) \times 10^{-24}$					.8550	.9883	1.2115	1.4503	1.6673
μ_0	.5217	.5242	.5252	.5270	.5179	.4273	.3425	.2818	.2445
μ_1					.1112	.0597	.0421	.0321	.0264
μ_0/μ_1					4.66	7.16	8.13	8.78	9.26
E_{F_0} in e.v.	.0650	.0648	.0648	.0645	.0622	.0547	.0470	.0383	.0309
E_{F_1} in e.v.					-.0265	-.0461	-.0573	-.0675	-.0750
ΔE in e.v.					.0888	.1009	.1042	.1058	.1059

THE VALUES OF N_i AND μ_i ARE GIVEN IN M.K.S. UNITS

TABLE T4:16 - SPECIMEN #6

TWO-BAND PARAMETERS, FERMI ENERGIES AND ENERGY SEPARATION OF THE (000) AND ⟨111⟩ CONDUCTION BANDS

T in ^{o}K	4.21	79.96	152.17	203.70	248.60	289.56
$N_0 \times 10^{-24}$	1.2976	1.2044	1.0912	1.0040	.9143	.8321
$N_1 \times 10^{-24}$	.6734	1.3713	2.1804	2.8670	3.2551	3.9284
$(N_0+N_1) \times 10^{-24}$	1.9710	2.5757	3.2716	3.8710	4.1694	4.7605
μ_0	.9659	.7291	.5446	.4133	.3357	.2736
μ_1	.0875	.0505	.0377	.0328	.0292	.0251
μ_0/μ_1	11.04	14.44	14.45	12.60	11.50	10.90
E_{F_0} in e.v.	.0870	.0824	.0759	.0700	.0633	.0563
E_{F_1} in e.v.	.0025	-.0065	-.0195	-.0292	-.0395	-.0471
ΔE in e.v.	.0845	.0888	.0954	.0992	.1029	.1034

THE VALUES OF N_i AND μ_i ARE GIVEN IN M.K.S. UNITS

TABLE T4:17 - SPECIMEN #8

TWO-BAND PARAMETERS, FERMI ENERGIES AND ENERGY SEPARATION OF THE (000) AND ⟨111⟩

CONDUCTION BANDS

T in ^{o}K	4.21	79.95	100.04	125.32	149.52	175.64	200.25	252.17	297.80
$N_0 \times 10^{-24}$	.9154	.8519	.8336	.8125	.7103	.6589	.6333	.5198	.4558
$N_1 \times 10^{-24}$					.4414	.6383	.9750	1.1434	1.7419
$(N_0+N_1) \times 10^{-24}$					1.1517	1.2972	1.6083	1.6632	2.1977
μ_0	.5455	.4855	.4642	.4253	.4005	.3619	.3223	.2643	.2202
μ_1					.0561	.0438	.0287	.0314	.0209
μ_0/μ_1					7.13	8.26	11.22	8.41	10.53
E_{F_0} in e.v.	.0697	.0659	.0646	.0630	.0567	.0527	.0499	.0388	.0296
E_{F_1} in e.v.					-.0402	-.0453	-.0476	-.0641	-.0712
ΔE in e.v.					.0969	.0980	.0975	.1029	.1008

THE VALUES OF N_i AND μ_i ARE GIVEN IN M.K.S. UNITS

TABLE T4:18 - SPECIMEN #9

TWO-BAND PARAMETERS, FERMI ENERGIES AND ENERGY SEPARATION OF THE (000) AND ⟨111⟩ CONDUCTION BANDS

T in ^{o}K	4.21	79.80	98.49	126.00	151.77	176.16	199.91	248.11	296.41
$N_0 \times 10^{-24}$	.2590	.3034	.3126	.3160	.3122	.3039	.2932	.1811	.1421
$N_1 \times 10^{-24}$								.2402	.3323
$(N_0+N_1) \times 10^{-24}$								.4213	.4744
μ_0	.3623	.3191	.3174	.3167	.3066	.2895	.2682	.2665	.2358
μ_1								.0480	.0346
μ_0/μ_1								5.55	6.81
E_{F_0} in e.v.	.0308	.0330	.0330	.0320	.0301	.0276	.0245	.0056	-.0091
E_{F_1} in e.v.								-.0962	-.1134
ΔE in e.v.								.1018	.1043

THE VALUES OF N_i AND μ_i ARE GIVEN IN M.K.S. UNITS

TABLE T4:19 - SPECIMEN #10

TWO-BAND PARAMETERS, FERMI ENERGIES AND ENERGY SEPARATION OF THE (000) AND ⟨111⟩ CONDUCTION BANDS

T in ^{o}K	4.21	81.76	100.80	124.87	150.84	176.48	200.56	200.20	251.45	296.90
$N_0 x10^{-24}$	.5254	.5540	.5554	.5514	.5406	.5229	.5099	.4087	.3397	.2766
$N_1 x10^{-24}$								.3223	.5501	.7570
$(N_0+N_1) x10^{-24}$								.7310	.8898	1.0336
μ_0	.4192	.4083	.4005	.3825	.3548	.3239	.2906	.3167	.2618	.2261
μ_1								.0590	.0372	.0285
μ_0/μ_1								5.36	7.03	7.93
E_{F_0} in e.v.	.0488	.0497	.0493	.0483	.0466	.0442	.0419	.0345	.0239	.0117
E_{F_1} in e.v.								-.0669	-.0798	-.0924
ΔE in e.v.								.1014	.1038	.1042

THE VALUES OF N_i AND μ_i ARE GIVEN IN M.K.S. UNITS

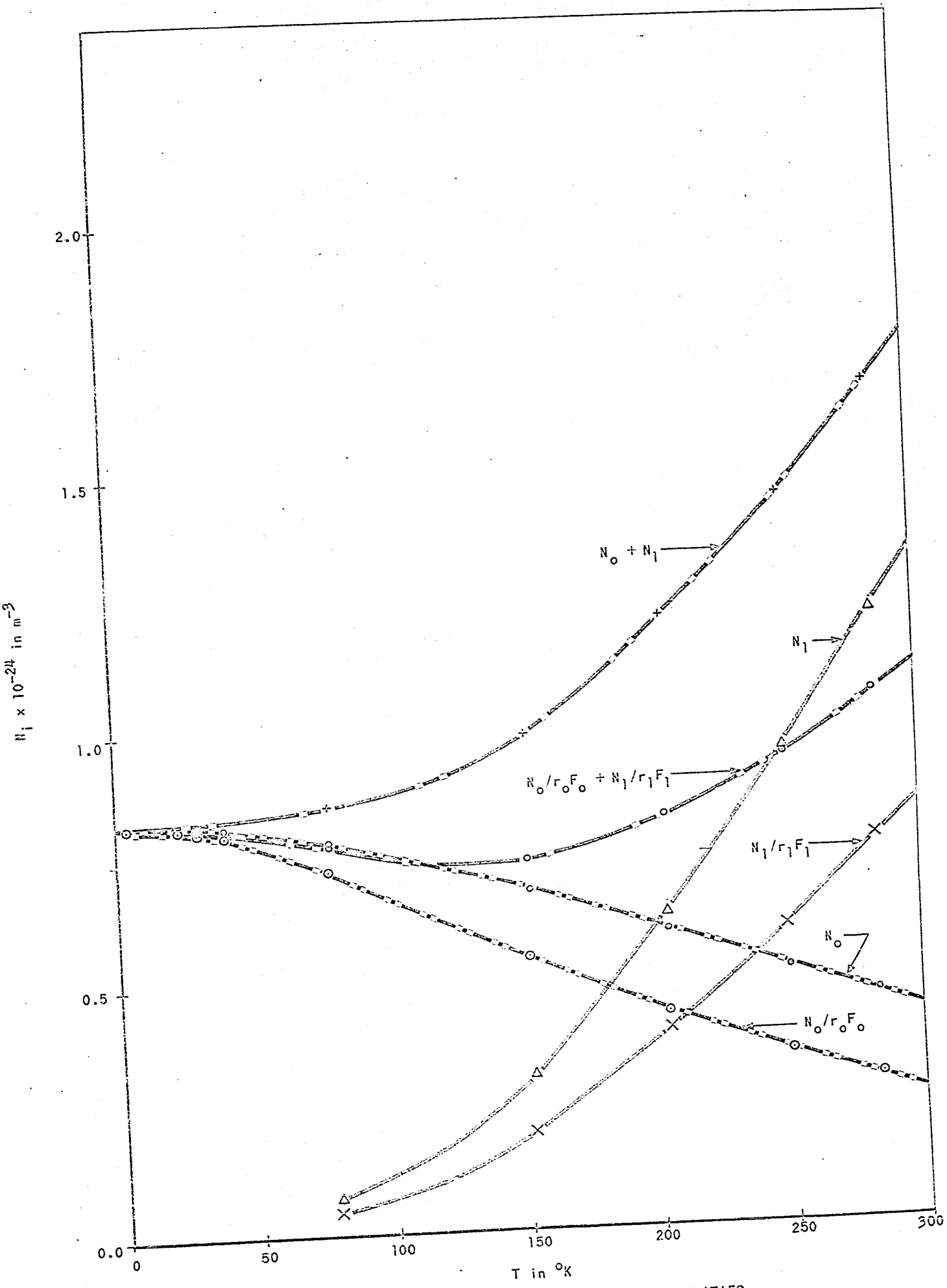

FIGURE F4:08 – SPECIMEN #5: CARRIER DENSITIES

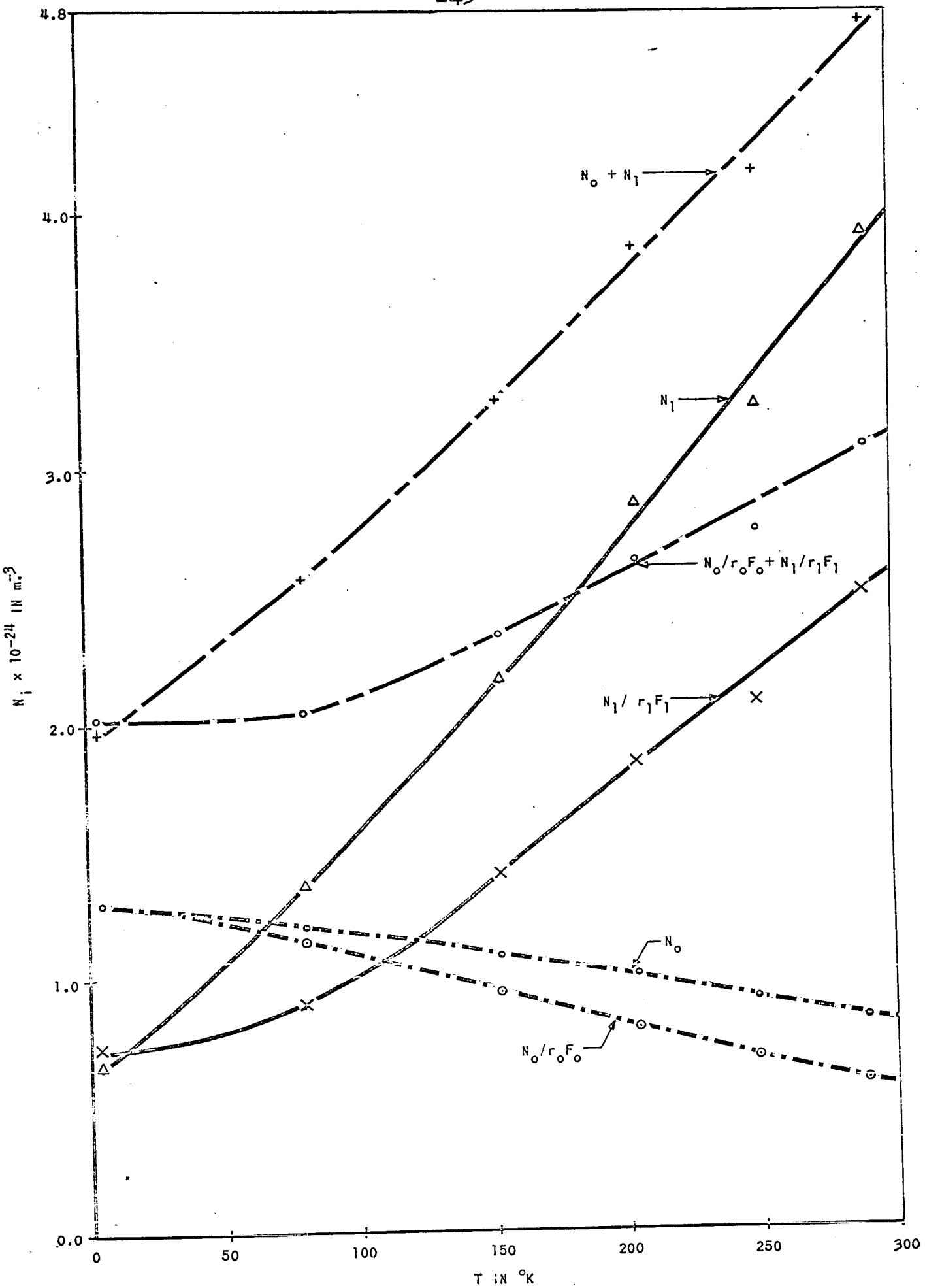

FIGURE F4:09 - SPECIMEN #6: CARRIER DENSITIES

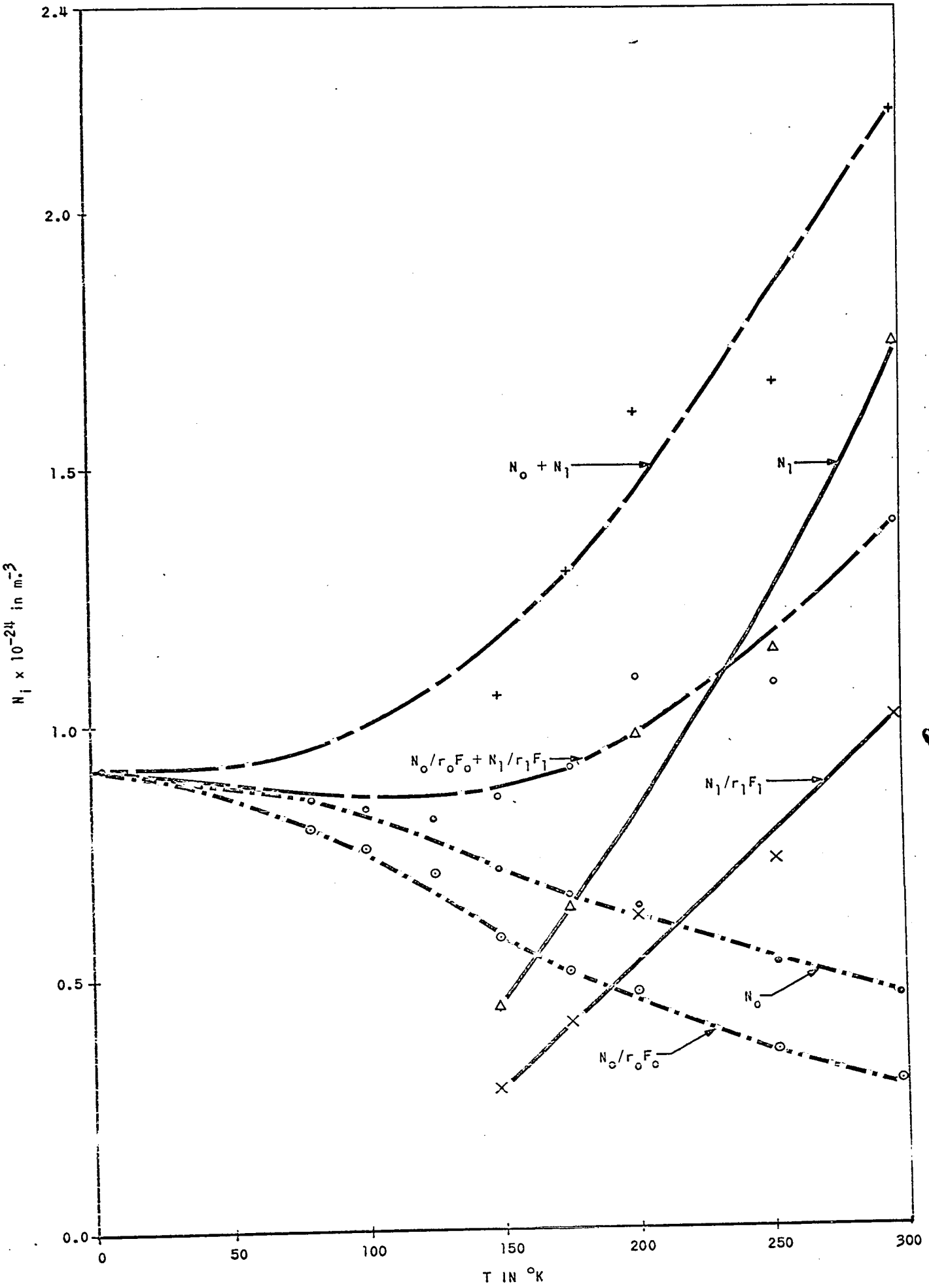

FIGURE F4:10 - SPECIMEN #8: CARRIER DENSITIES

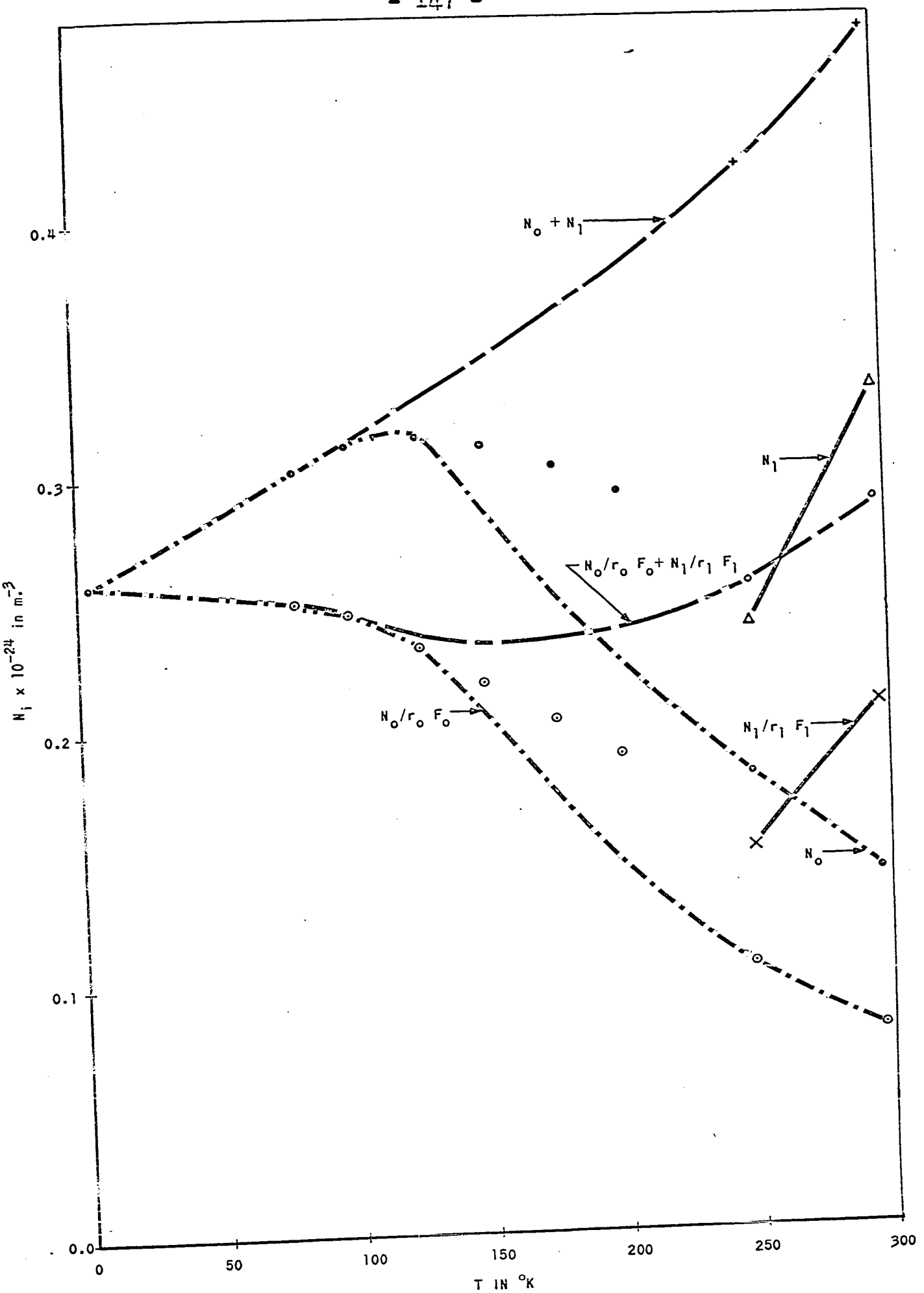

FIGURE F4:11 - SPECIMEN #9: CARRIER DENSITIES

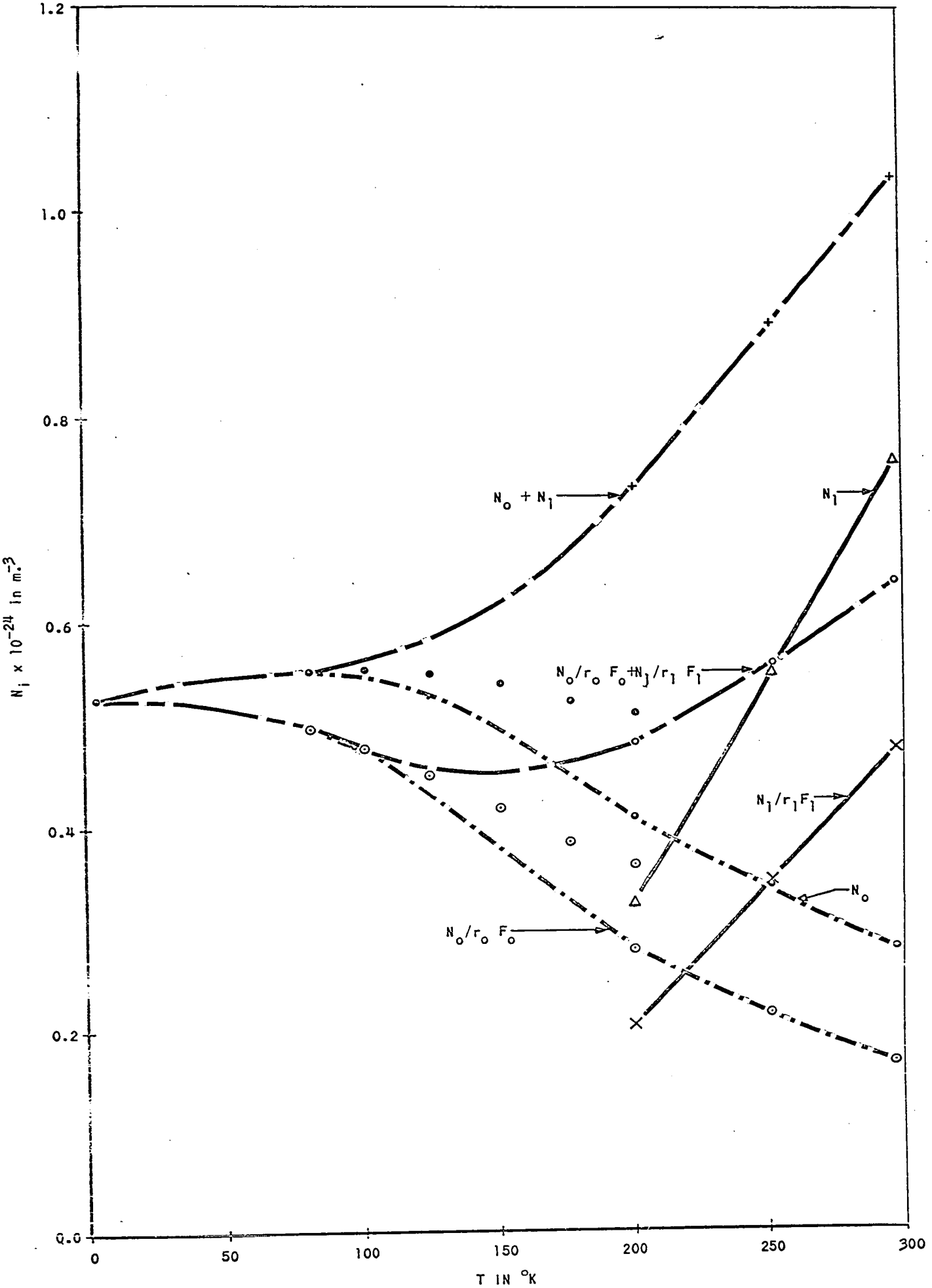

FIGURE F4:12 - SPECIMEN #10: CARRIER DENSITIES

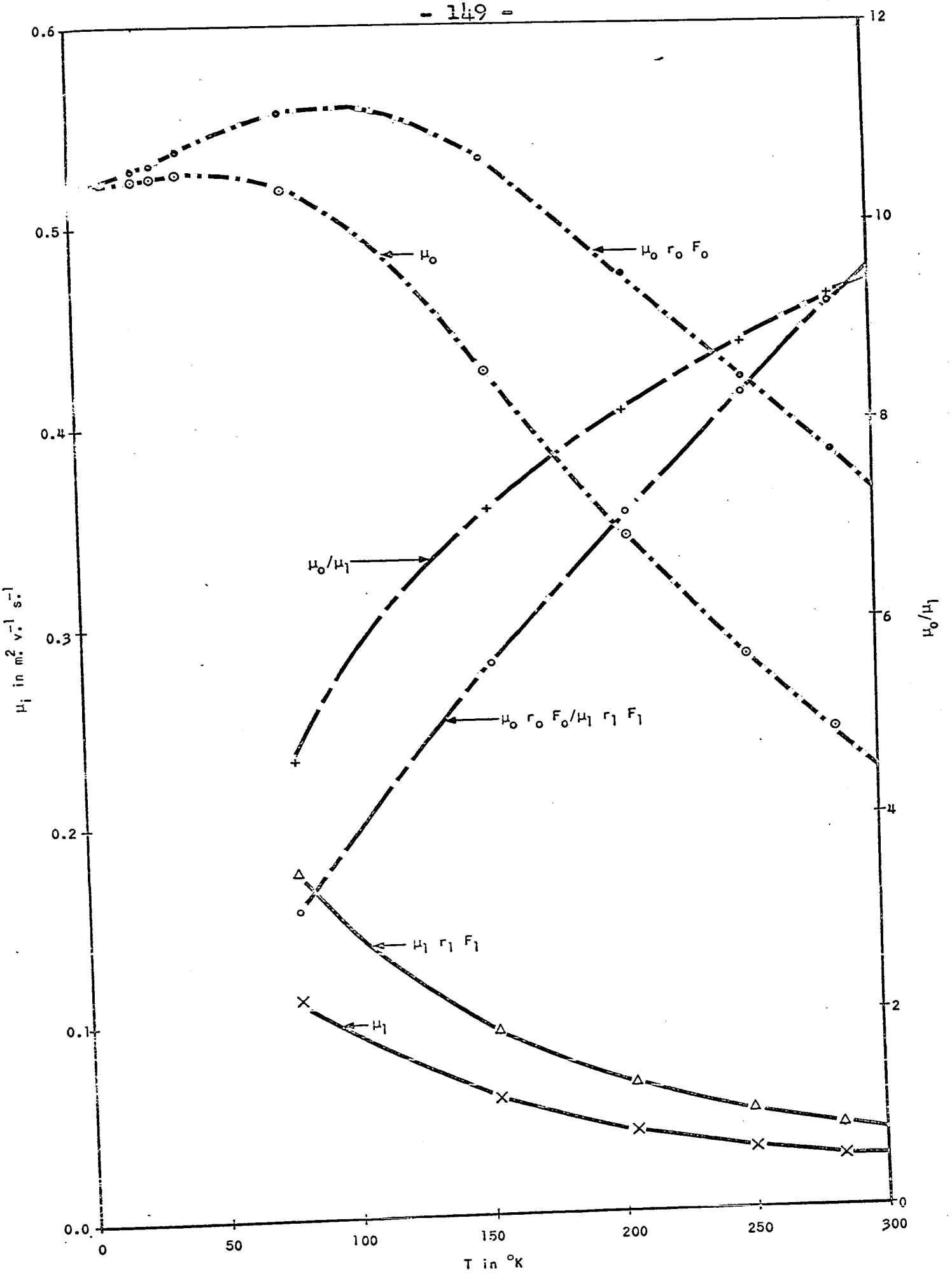

FIGURE F4:13 - SPECIMEN #5: CARRIER MOBILITIES

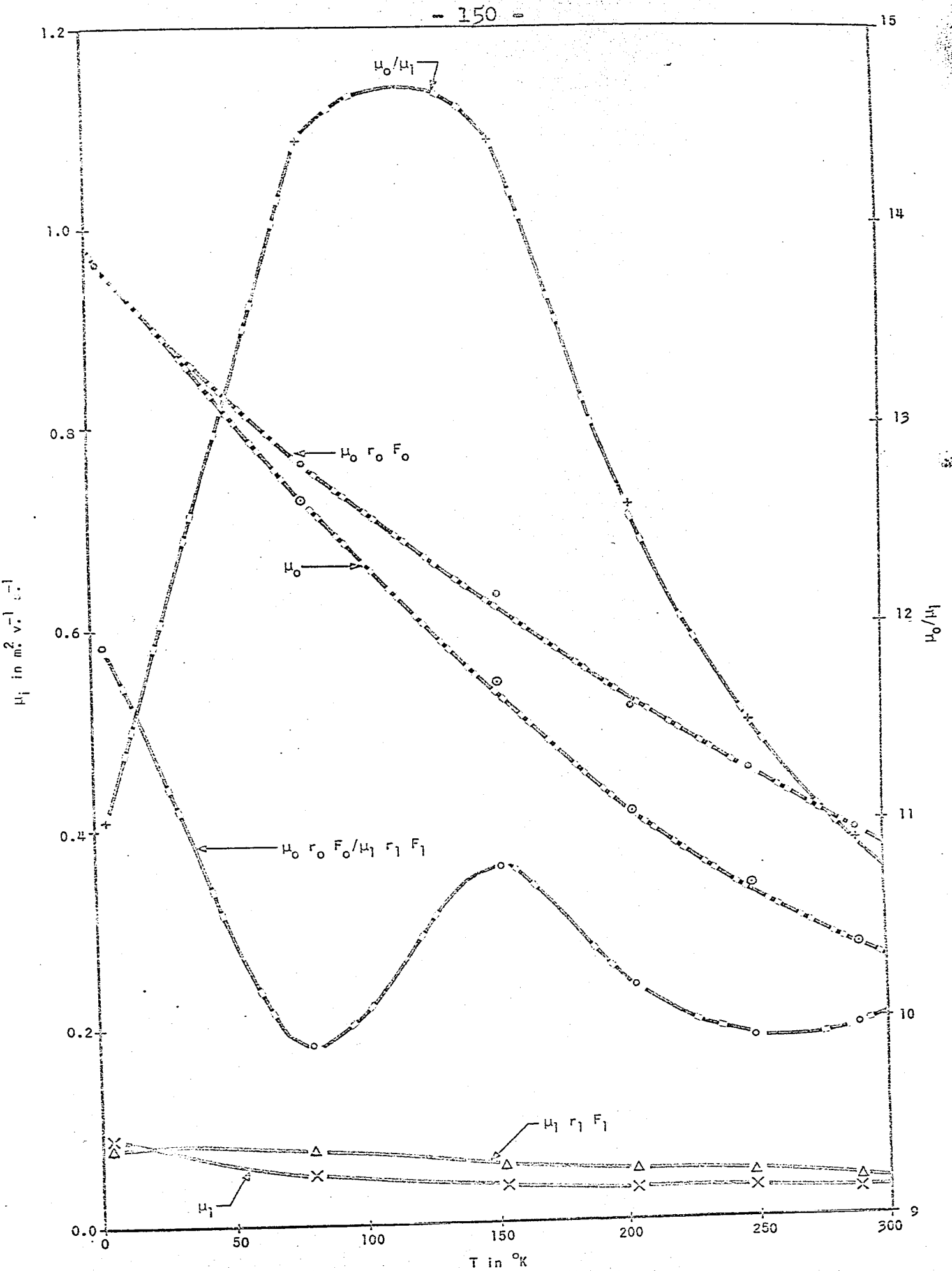

FIGURE F4:14 – SPECIMEN #6: CARRIER MOBILITIES

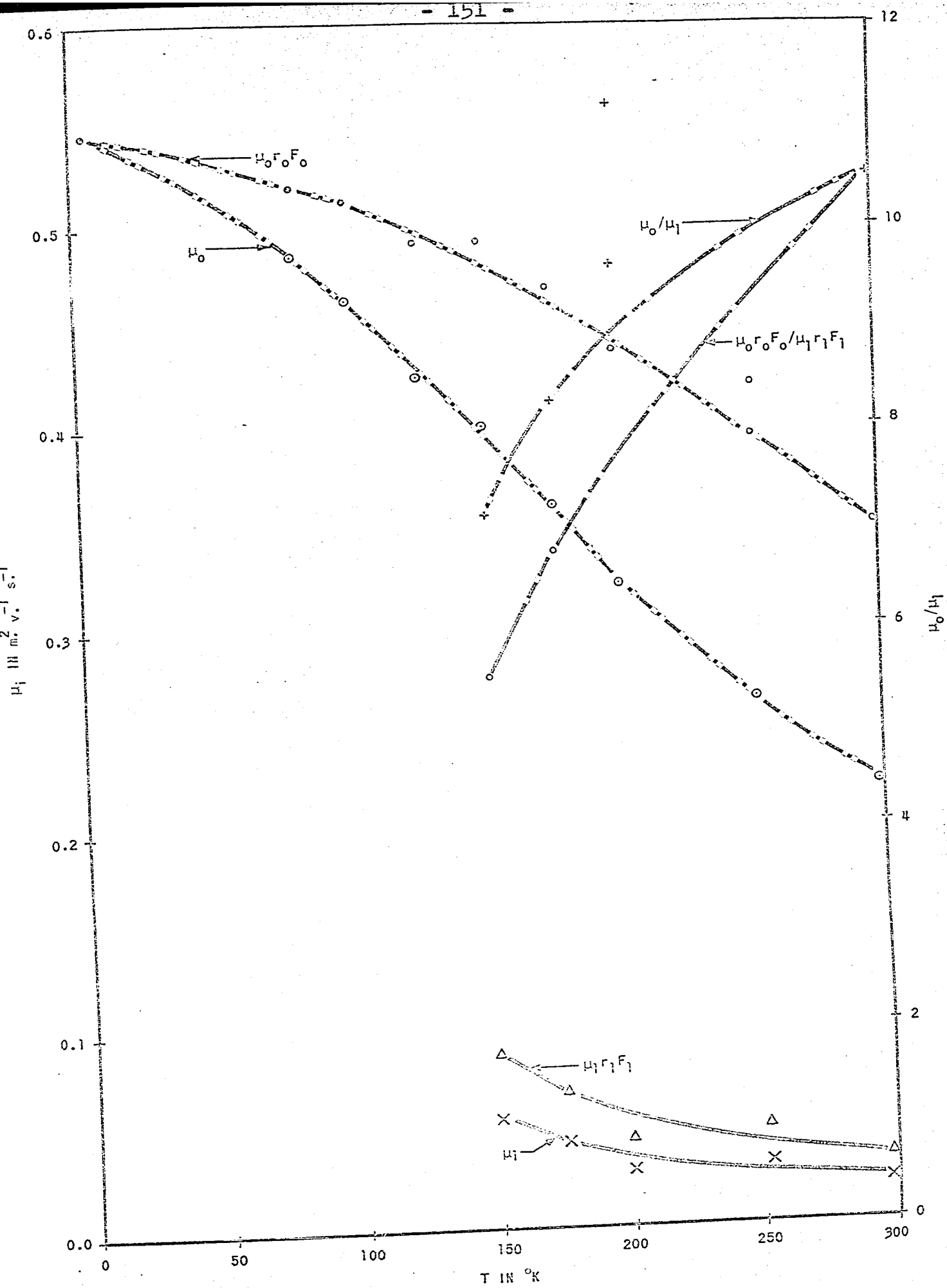

FIGURE F4:15 - SPECIMEN #8: CARRIER MOBILITIES

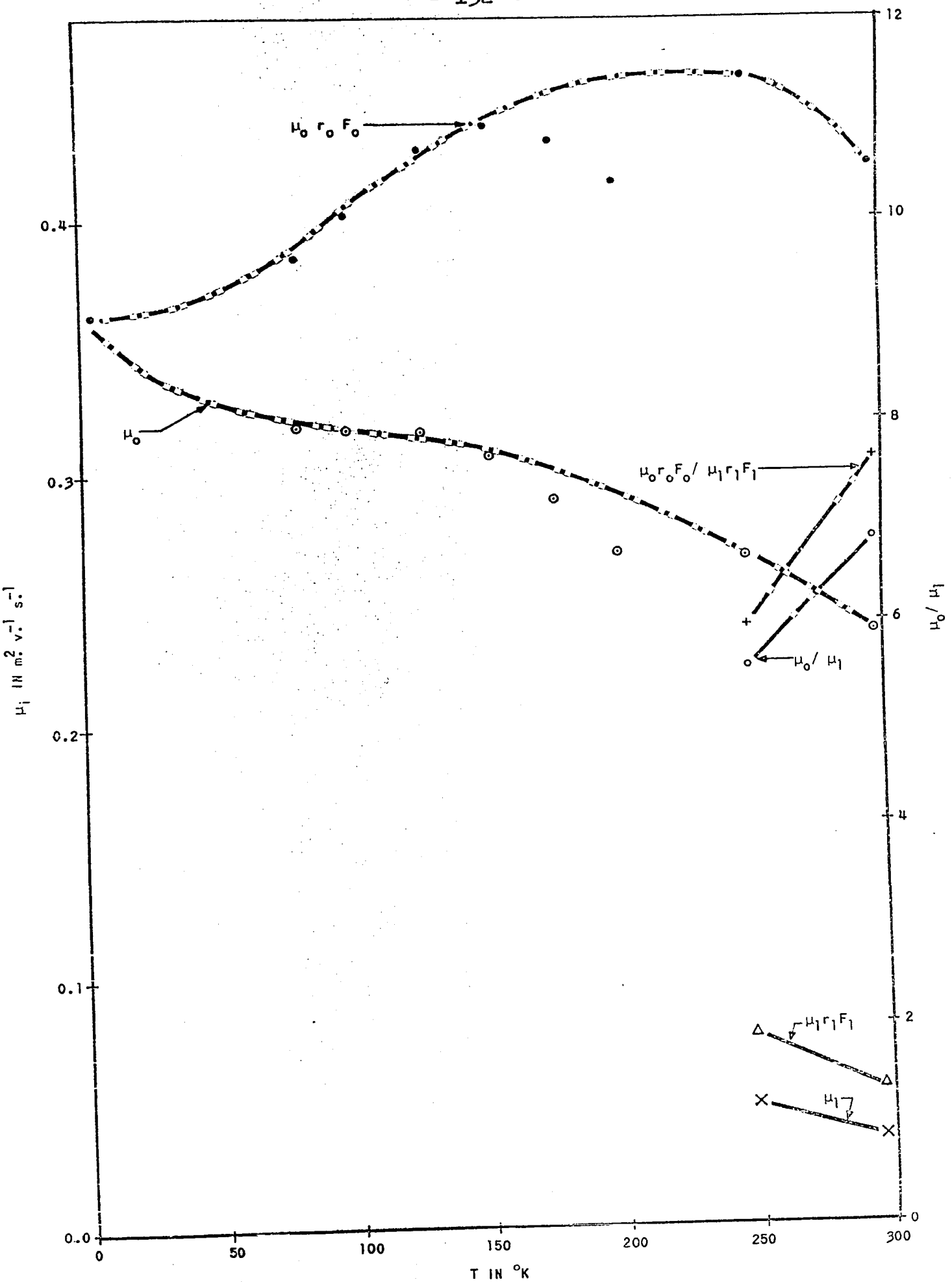

FIGURE F4:16 – SPECIMEN #9: CARRIER MOBILITIES

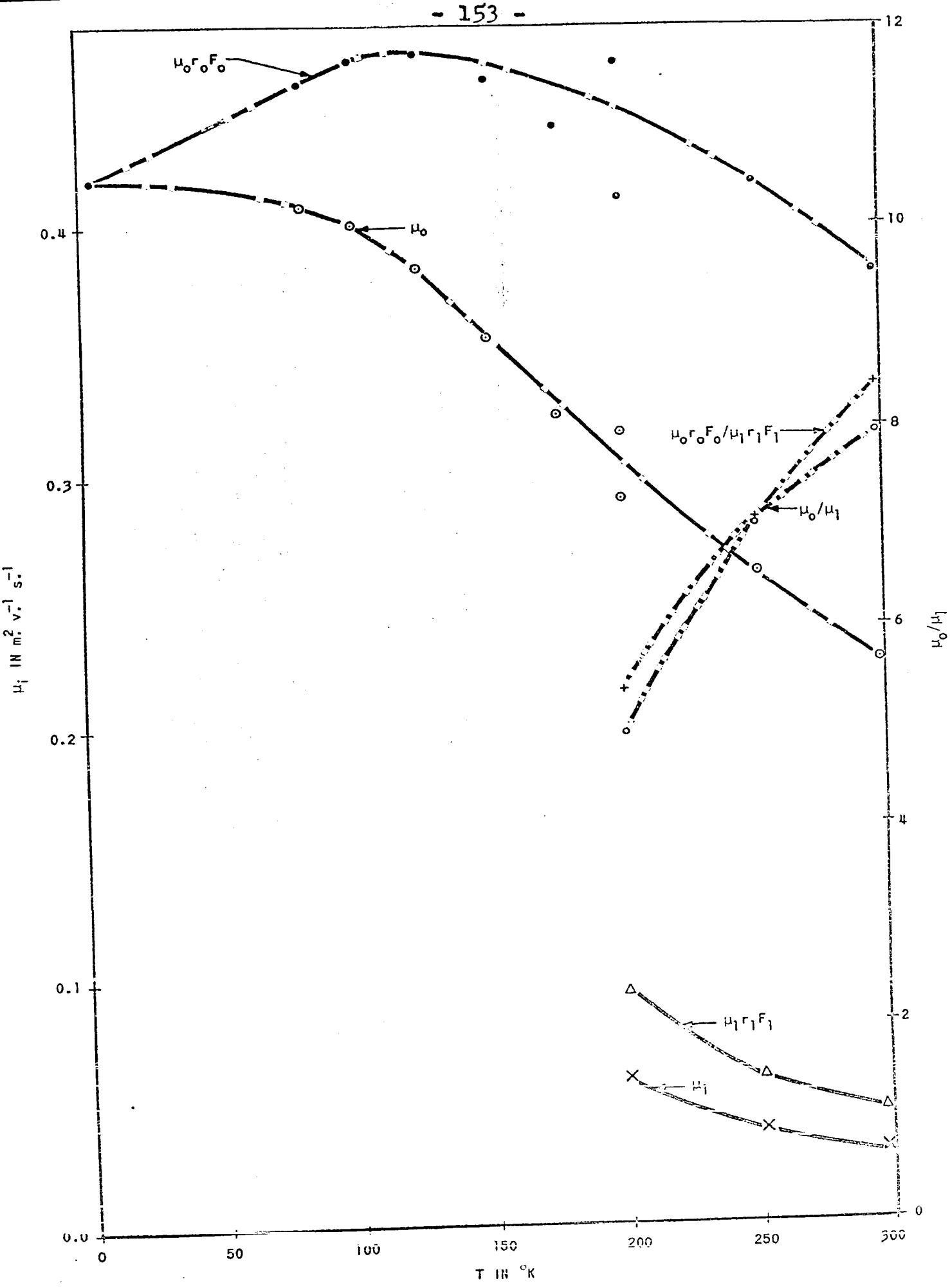

FIGURE F4:17 – SPECIMEN #10: CARRIER MOBILITIES

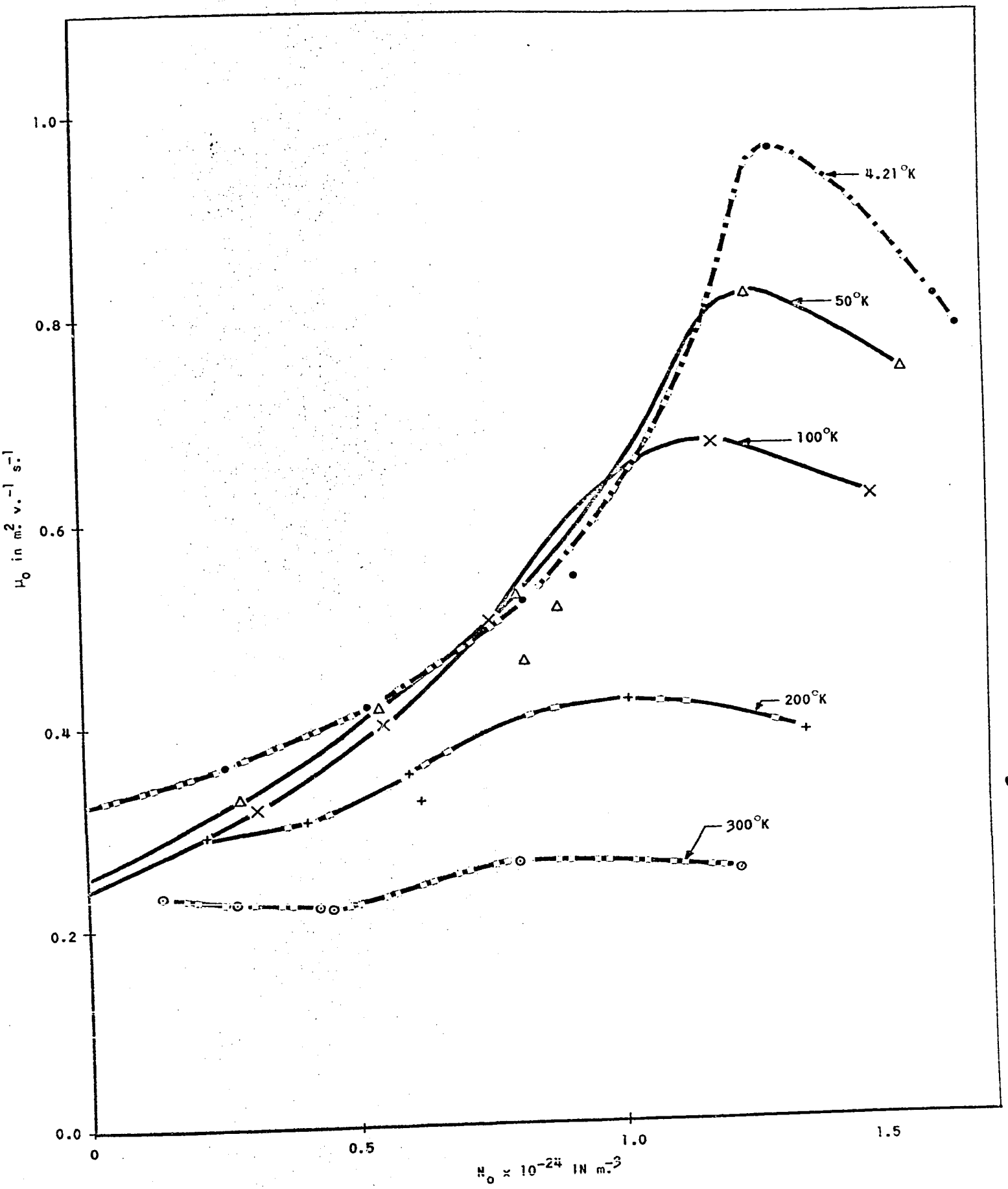

FIGURE F4:18 - DEPENDENCE OF μ_o UPON N_o AND T

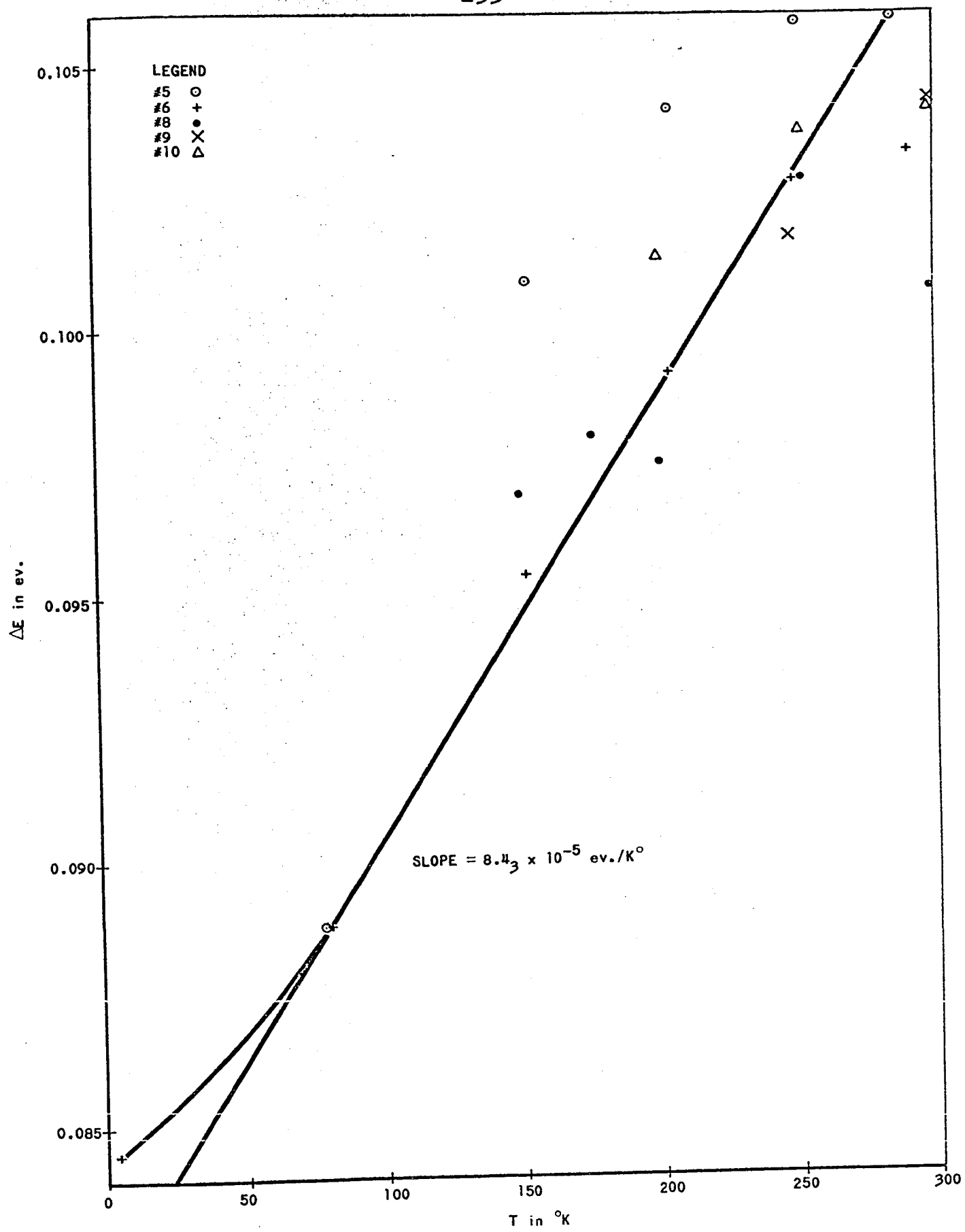

FIGURE F4:19 – TEMPERATURE DEPENDENCE OF THE ENERGY SEPARATION BETWEEN THE (000) AND <111> CONDUCTION BAND MINIMA

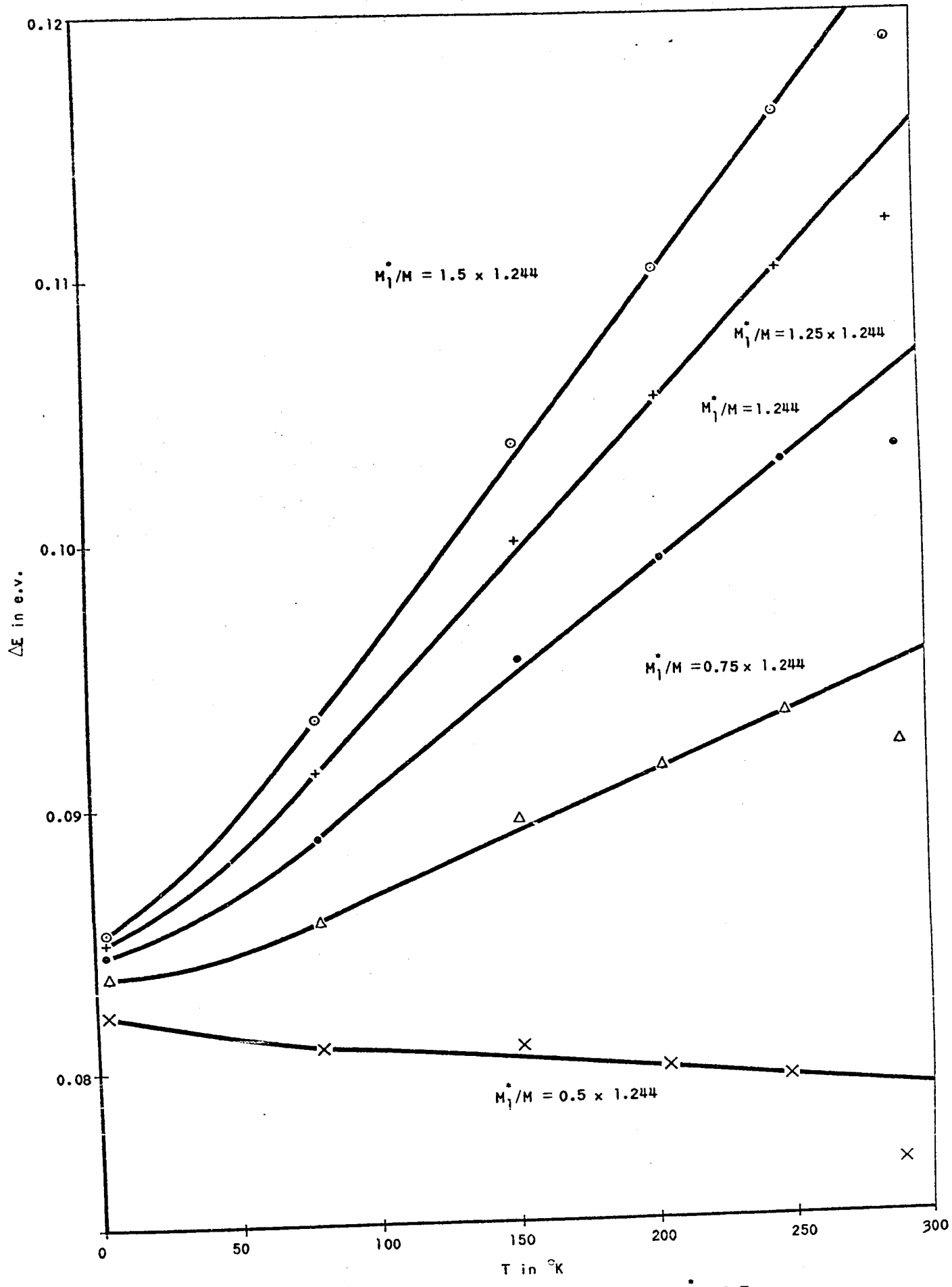

FIGURE F4:20 - SPECIMEN #6: DEPENDENCE OF ΔE UPON M_1^* AND T

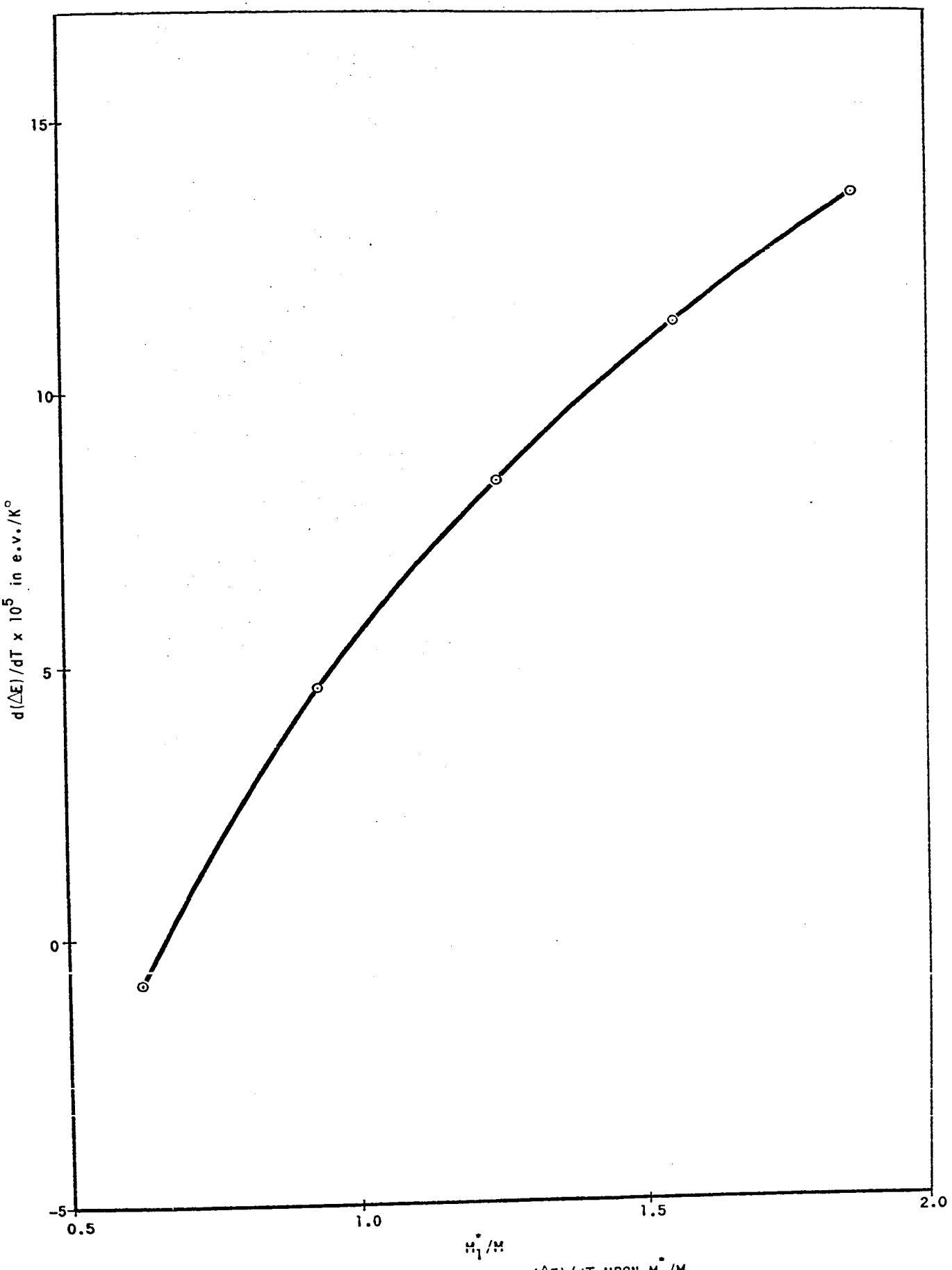

FIGURE F4:21 - SPECIMEN #6: DEPENDENCE OF $d(\Delta E)/dT$ UPON M_1^*/M

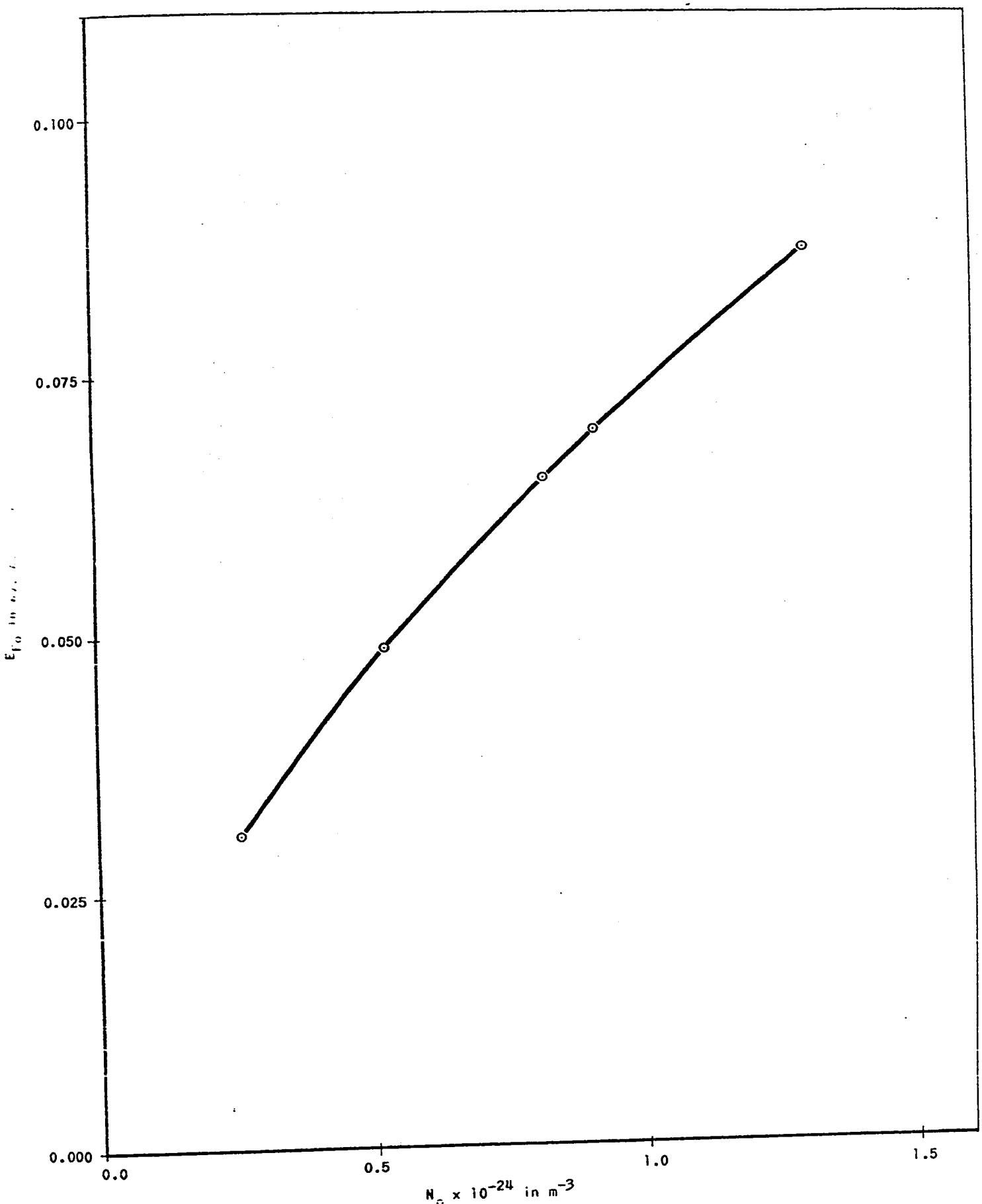

FIGURE F4:22 – DEPENDENCE OF E_{Fo} AT 4.2°K UPON N_0

B. ANALYSIS OF THE DE HAAS-SHUBNIKOV OSCILLATION DATA

(1) ANALYSIS OF THE MAGNETIC FLUX DENSITY DEPENDENCE OF THE PERIODICITY OF THE MAGNETORESISTANCE OSCILLATIONS

The electron density in the (000) conduction band of GaSb may be determined from the oscillatory magnetoresistance data. Equation (2:41) expressed N_0 as a function of $d(1/B)/dn$, where "n" is one of a set of sequential integers which are used to number the oscillation periods.

$$N_0 \simeq (4e\pi(M^*_{D_0}/M^*_{E_{F_0}})/(d(1/B)/dn))^{3/2}/3\pi^2 \qquad \ldots.(2:41)$$

$M^*_{D_0}/M^*_{E_{F_0}} \leq 1$ is the ratio of the density-of-states effective mass to the effective mass at the Fermi surface. It may be evaluated by manipulation of equations (4:02) , (4:03) and (4:06) .

$$G_{0_{E_F}} \simeq G_{0_0}(1 + (1 - G_{0_0})E_{F_0}/E_{g_0}) \qquad \ldots.(4:02)$$

$$\langle G_0 \rangle \simeq G_{0_0}(1 + 0.6(1 - G_{0_0})E_{F_0}/E_{g_0}) \qquad \ldots.(4:06)$$

$$E_{F_0} = C_0 N_0^{2/3}/\langle G_0 \rangle \quad , \; C_0 = 3.63 \times 10^{-19} \text{ev.m.}^2 \qquad \ldots.(4:03)$$

Now: $M^*_{D_0}/M^*_{E_{F_0}} = G_0 / G_{0_{E_F}}$

$$\simeq 1 - 0.4Y(1 - Y) \qquad \ldots.(4:25)$$

where: $Y = (1 - G_{0_0})E_{F_0}/E_{g_0}$

$= (1 - G_{0_0})C_0N_0^{2/3}/\langle G_0\rangle E_{g_0}$

$\simeq (1 - G_{0_0})C_0N_0^{2/3}/G_{0_0}E_{g_0}$

This approximation will introduce a negligible error into equation (4:25) since $Y \ll 1$ and $\langle G_0\rangle$ is only a few percent larger than G_{0_0} .

A computer program was written to determine $d(1/B)/dn$, and therefore $N_0/(M^*_{D_0}/M^*_{E_{F_0}})^{3/2}$, for each set of oscillation data. In the process of developing equation (2:41) , it was shown that the magnetic flux densities which correspond to the oscillation null points must satisfy the following equation: $1/B_i = I_0 + I_1N_i$ where I_0 and I_1 are constants for any particular specimen at a fixed temperature. The N_i are integers so introduce no error. However, since the accuracy of the values measured for B_i was approximately proportional to B , the equation which was fitted was:

$$B_i = I_0B_i^2 + I_1N_iB_i^2 \qquad \ldots.(4:26)$$

The unweighted "probable error" for the "least mean squares" curve fit was determined by means of the following relation:

$$P.E.(I_1) = 0.6745\left(\left(\sum_i (I_1 - (1/B_i - I_0))^2/(n(n-1))\right)^{1/2}\right) \qquad \ldots.(4:27)$$

This relation overestimates the error since it assumes that every value of B_i has the same fractional error.

The values obtained for $N_0/(M^*_{D_0}/M^*_{E_{F_0}})^{3/2}$, N_0 and P.E.(N_0) are recorded in table T4:20 . The corresponding values for N_0 , determined by the two-band analysis, are also recorded for those specimens for which they were determined. It will be noted that the values obtained for N_0 from the oscillatory magnetoresistance data and the two-band measurements are not in good agreement. It will be shown later that the values for N_0 , which were determined by the two-band measurements are probably accurate to better than one percent. Therefore, the electron concentrations, which were determined from the oscillatory magnetoresistance data may contain large errors. This could be due to scatter in the data, as indicated by the relatively large probable errors, or to breakdown of the theory due to interband scattering between the (000) and ⟨111⟩ bands.

(2) ANALYSIS OF THE MAGNETIC FLUX DENSITY DEPENDENCE OF THE AMPLITUDE OF THE MAGNETORESISTANCE OSCILLATIONS

It is theoretically possible to determine the value of M^*_0/M by analysis of the magnetic flux density dependence of the amplitude of the magnetoresistance oscillations at low

TABLE T4:20

THE (000) BAND ELECTRON CONCENTRATIONS, DETERMINED FROM THE PERIODICITIES OF THE MAGNETO-OSCILLATIONS.

SPECIMEN NUMBER	T in ^{o}K	$N_0/(M_{D_0}/M_{E_{F_0}})^{3/2}$	N_0 Mag.Osc.	ΔN_0	N_0 Two-Band
6A	4.201	1.327	1.363	.647	
6A	3.060	1.331	1.367	.621	
6A	2.130	1.335	1.371	.624	
7A	4.204	1.541	1.644	.723	1.643
7A	2.972	1.543	1.647	.725	
7A	2.077	1.545	1.649	.726	
8A	4.203	1.209	1.279	.546	
8A	3.040	1.213	1.284	.0002	
8A	2.077	1.210	1.280	.0002	
6	4.210	1.314	1.350	.431	1.298
6	2.207	1.319	1.355	.304	
7	4.210	1.527	1.631	.003	1.603
7	2.268	1.527	1.631	.003	

ALL ELECTRON CONCENTRATIONS IN $m^{-3} \times 10^{-24}$

temperatures. The amplitude data should obey the following relation:

$$\Delta\rho_{osc.} = J_0 B^{J_1} \exp(-J_2/B) \qquad \ldots.(4:28)$$

where $J_2 = 4\pi^3 k M_0^* (T + T')/eh$

and T' = the collision broadening temperature

This equation may be written in the following form:

$$LOG_e(\Delta\rho_{osc.}) = LOG_e(J_0) + J_1 \cdot LOG_e(B) - J_2/B \qquad \ldots.(4:29)$$

Since the relative accuracy of measurement was proportional to $\Delta\rho_{osc.}$, equation (4:29) was weighted by means of the multiplicative factor $\Delta\rho_{osc.}/LOG_e(\Delta\rho_{osc.})$. The resulting equation was "least mean squares" curve fitted and the values for J_0, J_1 and J_2 and their unweighted probable errors were determined. The results of these calculations are recorded in table T4:21. Although the predicted probable errors were very small, plots of J_2 versus T did not produce straight lines. Therefore M_0^* and T' could not be determined.

It may be seen from table T4:21 that J_1 is not a constant with respect to T. Although it is difficult to predict the value of J_1 from the theory, it should at least be a constant with respect to T. Therefore, the data was analysed

TABLE T4:21

MAGNETIC INDUCTION DEPENDENCE OF THE AMPLITUDE OF THE MAGNETORESISTANCE OSCILLATIONS

SPECIMEN NUMBER	T in ^{o}K	$J_0 \times 10^5$	$-J_1$	J_2
6A	4.201	17.379	1.829	11.530
	.001	.018	.002	.002
6A	3.060	5.014	1.159	9.614
	.001	.007	.003	.002
6A	2.130	3.273	.972	8.801
	.003	.004	.003	.002
7A	4.204	1.078	1.104	7.875
	.001	.003	.007	.005
7A	2.972	.599	.823	6.672
	.004	.002	.006	.006
7A	2.077	.988	1.180	6.938
	.005	.002	.005	.004
8A	4.203	2.077	1.277	13.673
	.001	.006	.008	.005
8A	3.040	.980	.907	12.218
	.002	.006	.012	.010
8A	2.077	.926	.957	11.780
	.003	.002	.004	.003

ALL VALUES QUOTED IN M.K.S. UNITS

by a technique which eliminated J_1 . Consider equation (4:28) at two temperatures, T_1 and T_2 , but for the same value of B .

Then: $\Delta\rho_{osc._1}/\Delta\rho_{osc._2} = (J_{0_1}/J_{0_2})\exp(-(J_{2_1} - J_{2_2})/B)$ ....(4:30)

This equation may be written in the form:

$$LOG_e(\Delta\rho_{osc._1}/\Delta\rho_{osc._2}) = LOG_e(J_{0_1}/J_{0_2}) - (J_{2_1} - J_{2_2})/B \quad ....(4:31)$$

This equation was "least mean squares" curve fitted, using $(\Delta\rho_{osc._1}/\Delta\rho_{osc._2})/LOG_e(\Delta\rho_{osc._1}/\Delta\rho_{osc._2})$ as the multiplicative weighting function, and the unweighted probable error for $(J_{2_1} - J_{2_2})$ was computed. If T' is constant with respect to temperature, it then follows that:

$$J_{2_1} - J_{2_2} = 4\pi^3 kM_0^*(T_1 - T_2)/eh \quad ....(4:32)$$

The values obtained for J_{0_1}/J_{0_2} , $J_{2_1} - J_{2_2}$, $P.E.(J_{2_1} - J_{2_2})$ and M_0^*/M are tabulated in table T4:22 . The values obtained for M_0^*/M are not in good agreement. It also appears that M_0^*/M decreases with increasing electron concentration in the (000) band. This is contrary to existing beliefs, and suggests that it may be necessary to take account of the ⟨111⟩ band.

TABLE T4:22

CALCULATION OF THE VALUE OF M_0^*/M FROM THE MAGNETIC INDUCTION DEPENDENCE OF THE AMPLITUDE OF THE MAGNETORESISTANCE OSCILLATIONS

SPECIMEN NUMBER	T_1 in ^oK	T_2 in ^oK	J_{0_1}/J_{0_2}	$-(J_{2_1} - J_{2_2})$ in w/m^2	M_0^*/M
6A	4.201	3.060	.1619	.691 .002	.0413
6A	3.060	2.130	.1216	.463 .001	.0339
6A	4.201	2.130	.2835	1.154 .002	.0380
7A	4.204	2.972	.1178	.650 .003	.0360
7A	2.972	2.077	.0800	.399 .002	.0303
7A	4.204	2.077	.1978	1.049 .002	.0336
8A	4.203	3.040	.1294	.731 .003	.0428
8A	3.040	2.077	.1451	.548 .004	.0387
8A	4.203	2.077	.2745	1.278 .002	.0410

3. DISCUSSION AND CALCULATION OF EXPERIMENTAL ERRORS

A. DISCUSSION OF ERRORS

The errors which affected the results of this investigation may be divided into two categories, systematic errors and random errors. Both types of errors can affect the values which were determined for the effective mass ratio of the ⟨111⟩ conduction band and the temperature dependence of the energy separation between the (000) and ⟨111⟩ minima. The random errors also produce scatter of the points on plots of the two-band coefficients and parameters as functions of the temperature.

(1) SYSTEMATIC ERRORS

The main sources of systematic errors were errors in the specimen dimensions and miscalibration of the equipment used to measure the experimental signals. The equipment and techniques which were employed in this investigation were discussed in detail in chapter 3. Only the resulting possible errors will be discussed here.

The specimen dimensions and the mean deviations in these dimensions are recorded in table T4:01 . It may be observed that the mean deviations in l , w and t , for most of the specimens, were less than 0.2% of the respective dimensions. However, the widths of the resistivity contacts were approx-

imately 6% of the center-to-center distance between the contacts. It is therefore conceivable, but highly improbable, that the values quoted for the effective specimen lengths could be too large by up to 6% .

The specimen current, resistivity voltage and temperature and the magnetic flux density were determined by means of two potentiometers. The errors introduced by the potentiometers were negligible compared to the errors from other sources. In this investigation it was much more important to control the temperature accurately than to measure it accurately. According to White (59:13), the absolute accuracy of a copper resistance thermometer should be better than 0.1 K^o . The temperature could be controlled and resolved to 0.02 K^o for $T > 60^oK$ and 0.002 K^o for $2^oK \leq T \leq 4.2^oK$.

The magnetic flux density was calibrated to better than 0.25% $\pm$ 10 gauss. The 0.25% was a constant multiplicative error, whereas the $\pm$ 10 gauss produced scatter of the experimental data. The dependencies of ρ and R upon the magnetic induction were determined by means of a recording potentiometer which was calibrated to an absolute accuracy of 0.25%. The galvanometer amplifier, when used, introduced a multiplicative error of less than 1%.

It was mentioned earlier in this chapter that the results

for specimen #7 were scattered and inconsistent and therefore had to be set aside. This "ageing" of the specimen was probably due to repeated thermal cycling. The permanent change in its electron transport properties resulted in non-reproducil le results. Only #7 shows this "ageing" effect. It is desireable to obtain all the required data for a specimen during a single temperature cycle. This was not possible since adjusting the experimental conditions and collecting the data required approximately eight hours.

(2) RANDOM ERRORS

Random errors were generated by "short term" fluctuations in the specimen current and temperature, backlash in the recording potentiometer, variations in the room temperature, electrical noise and reading errors in measuring the recorder graphs. These random errors produced scatter of the points on plots of ρ and R as functions of B . The two-band coefficients and their weighted probable errors were determined by means of a "root mean square" curve fitting computer program. These weighted probable errors are recorded with their respective two-band coefficients in tables T4:02 to T4:07.

It may be seen from these tables that the maximum weighted probable errors in ρ_1 , ρ_2 , R_0 and R_1 were less than 0.17 , 2.3 , 0.59 and 6.0 percent, respectively. If 3 of the 23 sets

of data were set aside, these maximum percentage errors would be reduced by a factor of approximately 3 . The results for R_1 , which had the largest weighted probable errors, showed the greatest scatter when plotted as a function of T . Since R_1 , when combined with ρ_0 , ρ_1 and R_0 , produced inconsistent results for the two-band parameters, these results were set aside.

The five two-band coefficients are plotted as functions of the temperature in figures F4:02 to F4:06. It may be observed that most of the points lie on smooth curves. The absence of serious scatter suggests that the calculated probable errors take account of all the important types of random errors.

B. CALCULATION OF ERRORS

It is very difficult to express algebraically the errors in the two-band parameters as functions of the errors in the two-band coefficients. Tables were prepared which allow rapid estimation of the errors in the two-band parameters. The two-band coefficients and the specimen dimensions were individually increased in magnitude by one percent, for ten representative sets of two-band coefficients. The resulting percentage errors in the two-band parameters are recorded in tables T4:23 to T4:26.

TABLE T4:23

PERCENTAGE ERRORS WHICH RESULT IN N_0 AS A RESULT OF POSITIVE ONE PERCENT ERRORS IN THE MAGNITUDES OF THE EXPERIMENTAL DATA

SPECIMEN NUMBER	T IN ^{o}K	$d\rho_0$	$d\rho_1$	$d\rho_2$	dR_0	d1	dw	dt
5	78.47	-.06	-.02	-.01	-.90	.09	-.09	-.99
5	283.81	-.50	-.17	-.11	-.22	.78	-.78	-.99
6	4.21	-.10	-.07	-.01	-.82	.18	-.18	-.99
6	152.17	-.27	-.15	-.04	-.52	.46	-.46	-.99
6	289.56	-.67	-.13	-.18	-.02	.98	-.98	-.99
7	4.21	-.39	-.20	-.06	-.34	.66	-.66	-.99
7A	4.21	-.43	-.21	-.07	-.30	.70	-.70	-.99
8	297.80	-.59	-.16	-.14	-.11	.89	-.89	-.99
9	296.41	-.59	-.14	-.15	-.12	.88	-.88	-.99
10	296.90	-.58	-.15	-.14	-.13	.87	-.87	-.99

TABLE T4:24

PERCENTAGE ERRORS WHICH RESULT IN N_1 AS A RESULT OF POSITIVE ONE PERCENT ERRORS IN THE MAGNITUDES OF THE EXPERIMENTAL DATA

SPECIMEN NUMBER	T IN ^{o}K	$d\rho_0$	$d\rho_1$	$d\rho_2$	dR_0	d1	dw	dt
5	78.47	.92	1.02	- .03	- .03	-1.91	1.91	-.99
5	283.81	.19	2.74	- .82	-2.97	-2.06	2.06	-.99
6	4.21	.17	1.94	- .58	-2.47	-1.52	1.52	-.99
6	152.17	.18	2.52	- .76	-2.83	-1.91	1.91	-.99
6	289.56	.15	3.27	- .99	-3.24	-2.36	2.36	-.99
7	4.21	.05	8.13	-2.43	-5.81	-5.36	5.36	-.99
7A	4.21	.05	8.69	-2.58	-6.08	-5.70	5.70	-.99
8	297.80	.15	3.32	-1.01	-3.27	-2.39	2.39	-.99
9	296.41	.22	2.38	- .69	-2.79	-1.87	1.87	-.99
10	296.90	.20	2.62	- .78	-2.91	-2.00	2.00	-.99

TABLE T4:25

PERCENTAGE ERRORS WHICH RESULT IN μ_0 AS A RESULT OF POSITIVE ONE PERCENT ERRORS IN THE MAGNITUDES OF THE EXPERIMENTAL DATA

SPECIMEN NUMBER	T IN ^oK	$d\rho_0$	$d\rho_1$	$d\rho_2$	dR_0	dl	dw	dt
5	78.47	-.97	.01	.00	.97	.96	-.96	-.00
5	283.81	-.77	.12	.03	.62	.61	-.61	-.00
6	4.21	-.95	.04	.00	.92	.91	-.91	.00
6	152.17	-.87	.08	.01	.78	.77	-.77	-.00
6	289.56	-.69	.13	.06	.51	.50	-.50	-.00
7	4.21	-.80	.13	.02	.66	.65	-.65	-.00
7A	4.21	-.79	.13	.02	.64	.63	-.63	-.00
8	297.80	-.73	.13	.04	.56	.55	-.55	-.00
9	296.41	-.74	.12	.05	.58	.57	-.57	-.00
10	296.90	-.74	.12	.04	.58	.57	-.57	.00

TABLE T4:26

PERCENTAGE ERRORS WHICH RESULT IN μ_1 AS A RESULT OF POSITIVE ONE PERCENT ERRORS IN THE MAGNITUDES OF THE EXPERIMENTAL DATA

SPECIMEN NUMBER	T IN ^{o}K	$d\rho_0$	$d\rho_1$	$d\rho_2$	dR_0	dl	dw	dt
5	78.47	-.02	- .55	.51	.06	.06	- .06	.00
5	283.81	-.22	-2.51	1.10	1.63	1.64	-1.64	.00
6	4.21	-.04	-1.17	.71	.51	.51	- .51	-.00
6	152.17	-.12	-2.00	.96	1.16	1.17	-1.17	.00
6	289.56	-.30	-3.18	1.29	2.18	2.19	-2.19	.00
7	4.21	-.19	-7.23	2.68	4.73	4.74	-4.74	.00
7A	4.21	-.21	-7.74	2.85	5.09	5.11	-5.11	.00
8	297.80	-.27	-3.15	1.29	2.12	2.12	-2.12	.00
9	296.41	-.26	-2.26	1.00	1.51	1.52	-1.52	.00
10	296.90	-.26	-2.48	1.08	1.66	1.67	-1.67	-.00

It may be observed that N_0 and μ_0 change by less than one percent when any one of the experimental quantities is changed by one percent. However, N_1 and μ_1 are much more sensitive to experimental errors than are N_0 and μ_0 .

(1) TWO-BAND PARAMETERS

The electron densities and mobilities are plotted as functions of the temperature in figures F4:08 to F4:17. The curves of N_1 and μ_1 show more scatter than those of N_0 and μ_0 . However, none of these curves show excessive scatter. It is not important to know the maximum possible error for every value of N_i and μ_i . The maximum possible errors in the two-band parameters will be calculated for specimen #7A , since it is more sensitive to errors than any other specimen. This calculation should establish the upper limits for the errors in the two-band parameters.

If one assumed non-cancelling errors of 0.2% for each of l , w and t , and used the error calculations for specimen #7A from tables T4:23 to T4:26, the maximum possible errors in N_0 , N_1 , μ_0 and μ_1 would be less than 0.5% , 3% , 0.3% and 2% , respectively. It was mentioned earlier in this chapter that the resistivity contact widths were approximately 6% of the center-to-center distance between these contacts. It is probable that the metallic contacts electrically short-circuit

the surface layer immediately beneath them. If the semiconductor-metal interface were uniform, the potential at the contact would be the same as that which would exist for a point contact positioned at the center of the real contact. The alloyed contacts which were used should produce a reasonably uniform semiconductor-metal interface. Therefore, the error introduced into the value for 1 by the finite contact widths should be less than 1% . If a one percent error did exist, the resulting errors in N_0 , N_1 , μ_0 and μ_1 would be less than 0.7% , 6% , 0.6% and 5% , respectively.

The weighted probable errors in ρ_1 , ρ_2 and R_0 for #7A , 0.038% , 0.28% and 0.024% , were obtained from table T4:04 . If one assumed that these errors were non-cancelling, the errors which would result in the values for N_0 , N_1 , μ_0 and μ_1 would be 0.025% , 1.2% , 0.026% and 1.2% , respectively. The magnetic flux density and the recording potentiometer were calibrated to an absolute accuracy of 0.25% . Errors of 0.25% in these calibrations would produce errors of less than 0.4% , 0.2% , 0.4% and 0.3% in the two-band parameters. The maximum possible errors in N_0 , N_1 , μ_0 and μ_1 , resulting from errors of 0.2% in l , w and t , 0.25% in the magnetic field and recorder calibrations, and the weighted probable errors in ρ_1 , ρ_2 and R_0 , would be less than 1% , 5% , .8% and 4%, respect-

ively.

(2) <111> CONDUCTION BAND EFFECTIVE MASS RATIO

The value for $(M_1^*/M)/F_1^{2/3}$ was determined by substitution of the values for N_0 and N_1/F_1 , for specimens 6 , 7 and 7A , into equation (4:18) . The error in the value determined for this effective mass ratio may be calculated when the errors in the electron densities are known. The maximum possible errors in N_0 and N_1 , which result from the possible errors in the specimen dimensions, the two-band coefficients, the magnetic flux density calibration and the recording potentiometer calibration, were calculated for specimens 6 and 7A . With the exception of the magnetic flux density calibration, which had the same multiplicative error for all measurements, the errors were assumed to be non-cancelling. The maximum possible error in $(M_1^*/M)/F_1^{2/3}$ was found to be less than 10% .

Approximately one-half of this error was due to the uncertainty in the thickness of specimen 6 . This contribution to the error was probably overestimated since the uncertainty in the thickness was due to a taper in this thickness. The Hall coefficient which is the two-band coefficient most severely affected by an error in t , is unaffected by a uniform taper. Therefore, the maximum probable error in the value which was determined for $(M_1^*/M)/F_1^{2/3}$ should be approximately

5% .

The three sets of values for N_0 and N_1/F_1 at 4.21°K allowed two independent determinations of $(M_1^*/M)/F_1^{2/3}$. These values were different by less than 1% . This suggests that the actual error is probably less than 10% . The accuracy of the value determined for M_1^*/M depends upon the accuracy of the value assumed for $F_1(K_1)$. If K_1 were in error by 10% , $F_1^{2/3}$ would be in error by 0.9% . Therefore, the value determined for M_1^*/M is probably accurate to approximately 5% .

(3) ENERGY SEPARATION BETWEEN THE (000) AND <111> CONDUCTION BAND MINIMA

This energy gap, ΔE , is plotted as a function of the temperature in figure F4:19 . The values for ΔE from specimens 6 , 7 and 7A at 4.21°K and specimens 5 and 6 at 78°K , agree very well. The maximum spread of the values for ΔE at any particular temperature is less than 7% . The values for ΔE from specimen 6 , for $T \geq 78^\circ K$, form a reasonably good straight line. The values determined from the other specimens are distributed about those from #6 .

Figures F4:20 and F4:21 were plotted to show the dependencies of ΔE and $d(\Delta E)/dT_{T \geq 78^\circ K}$ upon the value chosen for M_1^*/M . It may be shown that an error of 10% in the value of M_1^*/M would produce errors of less than 0.4% in the value for

ΔE at $4.21^{\circ}K$, and 20% in the value for $d(\Delta E)/dT$ for $T \geq 78^{\circ}K$. If the error in M_1^*/M is only 5% , these errors would be reduced to 0.2% and 10% respectively. Since the values for ΔE from #6 did not form a perfect straight line for $T \geq 78^{\circ}K$, $d(\Delta E)/dT$ may contain an additional error of approximately 3% .

CHAPTER 5

DISCUSSION OF RESULTS AND CONCLUSIONS

INTRODUCTION

The purpose of this chapter is to discuss and interpret the results of the experimental measurements and calculations. The information which is obtained will be compared with that already available in the literature. The interpretation of the results will not require modifications of the currently accepted band structure of GaSb.

1. DISCUSSION AND INTERPRETATION OF RESULTS

A. CONDUCTION BAND EFFECTIVE MASSES

(1) (000) CONDUCTION BAND EFFECTIVE MASS

An attempt was made to determine the value of M_0^*/M from de Haas-Shubnikov oscillation data for liquid He temperatures. This attempt was not successful. The magneto-oscillation was investigated for three specimens, 6A , 7A and 8A . 6A and 7A showed two-band conduction and 8A , one-band conduction, at liquid He temperatures. The results of the analysis of the magnetic induction dependence of the oscillation amplitude are recorded in tables T4:21 and T4:22 . The values obtained for M_0^*/M are not in good agreement with each other or the values quoted in the literature.

It is possible that for 6A and 7A the magnetic induction

dependence of the oscillation amplitude may have been influenced by inter-band scattering between the two conduction bands. Two-band conduction has a very marked effect upon the magnitude of the resistivity oscillation amplitude. It may be seen from tables T4:08 to T4:10 that both the fractional and absolute oscillation amplitudes of 8A were smaller than those of 6A by more than an order of magnitude.

Becker and Fan (63:1) , (64:1) observed a marked increase in the oscillation amplitude for GaSb specimens which showed two-band conduction. This behavior was explained by Robinson and Rodriguez (64:7) , (65:1) . They showed that the relatively slowly moving electrons in the ⟨111⟩ band screen the electric field of the ionized impurities. This produces an increase in both the relaxation time and mobility of the (000) band electrons, and therefore an increase in the amplitude of oscillation.

Since the values for M_0^*/M from 6A and 7A are not reliable, only the value from 8A is usable, namely, $M_0^*/M = 0.041$. Unfortunately, the oscillation amplitude for 8A was very small, so the accuracy of the above result is not very good. The accepted value of M_0^*/M for the minimum of the band is 0.047 (61:1) , (59:13) , (62:2) , (61:3). Values as high as 0.052 (64:1) have been obtained when the Fermi level is above the

<111> minima at 4.2°K .

(2) <111> CONDUCTION BAND DENSITY-OF-STATES EFFECTIVE MASS

One of the most important results of this investigation was the determination of the value of the density-of-states effective mass for the <111> conduction band in GaSb. The literature contains several attempts to estimate the value of M_1^*/M for GaSb . Almost all of these estimates were obtained with the aid of assumptions and approximations which reduced the reliability of the results. This investigation constitutes, to the best of the author's knowledge, the first direct determination of the value of M_1^*/M for GaSb .

Sagar (60:11) was the first to explain the behavior of n-type GaSb by means of conduction in two different conduction bands. His piezoresistance measurements showed that the subsidiary minima had <111> symmetry, and so assumed that M_1^*/M for GaSb would have the same value as M_1^*/M for Ge , namely, 0.55 . Keyes and Pollack (60:8) continued Sagar's piezoresistance measurements on GaSb . By extrapolation of their piezoresistance measurements and Sagar's Hall measurements, they deduced that $M_1^*/M = 0.4$. Their analysis required too many approximations to produce a reliable result.

Becker, Ramdas and Fan (61:1) combined magnetoresistance, Hall and optical absorption measurements in order to deduce

the value of 0.90 for M_1^*/M in GaSb . Although they were unable to directly determine the electron densities in the two bands and the energy separation of the minima of these bands, their result for M_1^*/M is probably the most reliable of the values available in the literature. Piller (63:3) measured the Faraday rotations and Hall coefficients for n- and p-type GaSb. He deduced the value of 0.70 for M_1^*/M by assuming that the ratio of the conduction band mobilities, $\mu_0/\mu_1 = 6$. The results of Becker, Ramdas and Fan (61:1) and this investigation indicate that $\mu_0/\mu_1 = 6$ is probably not a very good assumption. Piller (64:6) measured the free-carrier and interband Faraday rotation in n-type GaSb. By assuming his earlier value for M_1^*/M (63:3) he was able to predict the magnitude of the anisotropy for the <111> conduction band, namely, $K_1 = M_{1_L}^*/M_{1_T}^* = 8.6$. This is the only reasonably reliable value for K_1 in the literature.

In the present investigation, M_1^*/M was determined directly from the electron densities in the two conduction bands, N_0 and N_1 . The procedure, which was employed to determine the value of M_1^*/M , was discussed in detail in chapter 4. Only the results of the calculations, which are recorded in table T4:14 , and their reliability will be discussed here. The calculations required only two assumptions, the value of M_0^*/M

at the minimum of the (000) band and the value of K_1 . The two values, which were deduced for M_1^*/M , were different by only 0.8 percent. This is extremely good agreement. The maximum possible error was shown to be less than 10% . The value determined for M_1^*/M is probably accurate to 5% . Therefore, $M_1^*/M = 1.10 \pm 0.06$ and $(M_1^*/M)/4^{2/3} = 0.44 \pm 0.03$. These values are 20% larger than those determined by Becker, Ramdas and Fan [61:1].

B. ENERGY SEPARATION BETWEEN THE MINIMA OF THE (000) AND ⟨111⟩ CONDUCTION BANDS

This investigation was part of the research program, directed by Dr. J. C. Woolley, which investigates the properties of GaSb and its alloys in the temperature range $2^oK \leq T \leq 900^oK$. The ⟨100⟩ conduction band minima in GaSb lie approximately 0.55 ev. above the (000) minimum at 300^oK . This energy separation has a negative temperature coefficient, whereas the energy separation of the (000) and ⟨111⟩ minima has a positive temperature coefficient. At sufficiently high temperatures the ⟨100⟩ minima lie below the ⟨111⟩ minima. It is necessary to know the value of the temperature coefficient of the energy separation between the (000) and ⟨111⟩ minima in order to be able to analyse the three-band behavior of GaSb for $T > 300^oK$.

The values which were determined for $\Delta E_{4.21^{\circ}K}$ and $d(\Delta E)/dT_T \geq 78^{\circ}K$ are directly related to the value which was determined for M_1^*/M , since $\Delta E_{4.21^{\circ}K}$ and M_1^*/M were determined by simultaneous solution of equation (4:10) for two different specimens at $4.21^{\circ}K$. ΔE was computed for various temperatures and electron densities assuming $M_1^*/M = 1.095$ and $S = 3/2$. The results are plotted as a function of T in figure F4:19 . The points for specimen 6 for $T \geq 78^{\circ}K$ lie on a reasonably good straight line. The points at $4.21^{\circ}K$ do not lie on this straight line because, according to the theory, $d(\Delta E)/dT \equiv 0$ at $0^{\circ}K$. The results for specimens 6 , 7 and 7A at $4.21^{\circ}K$, and specimens 5 and 6 at $78^{\circ}K$, are in very good agreement. The results at higher temperatures show more scatter.

Figure F4:20 shows the dependencies of ΔE , for specimen 6 , upon T and M_1^*/M . The resulting values for $d(\Delta E)/dT_T \geq 78^{\circ}K$ are plotted as a function of M_1^*/M in figure F4:21 . It was shown that a 10% error in the value of M_1^*/M would produce errors of less than 0.4% and 20% in $\Delta E_{4.21^{\circ}K}$ and $d(\Delta E)/dT_T \geq 78^{\circ}K$ respectively. Therefore, $\Delta E_{4.21^{\circ}K} = 0.0845 \pm 0.0003$ ev. and $d(\Delta E)/dT_T \geq 78^{\circ}K = (8.4 \pm 1.7) \times 10^{-5}$ ev./K° . The errors quoted are possibly too large by a factor of 2 .

The most reliable available value for M_1^*/M (61:1) is 0.90 . If one assumes this value for M_1^*/M , figures F4:20 and F4:21 predict that $\Delta E_{4.21^oK} = 0.0841$ ev. and $d(\Delta E)/dT_{T \geq 78^oK} = 4.1 \times 10^{-5}$ ev./K^o . The most reliable available values for $d(\Delta E)/dT$, 10^{-4} ev./K^o (61:3) and 1.1×10^{-4} ev./K^o (63:3), correspond to $M_1^*/M \simeq 1.46$. These predictions for $d(\Delta E)/dT$ and M_1^*/M are not reasonable. However, the value determined for $d(\Delta E)/dT$ from this investigation is in reasonable agreement with the values available from the literature. The available value for $\Delta E_{4.2^oK}$, 0.08 ev. (61:1) , (61:10), is in reasonable agreement with 0.0845 ± 0.0003 ev.

C. ELECTRON DENSITIES AND MOBILITIES IN THE (000) AND ⟨111⟩ CONDUCTION BANDS

(1) ELECTRON DENSITIES

N_0 and N_1 are plotted as functions of T in figures F4:08 to F4:12 . N_0/r_0F_0 and N_1/r_1F_1 are compared with N_0 and N_1 in order to show the change produced by correcting for r_i and F_i . Certain general features may be observed from these figures. N_1 and $N_0 + N_1$ increase monotonically with increasing temperature. N_0 decreases monotonically with increasing temperature except for the specimen which has the lowest electron densities, #9 . In this case N_0 passes through a maximum

at approximately $120^{\circ}K$.

This behavior of Te-doped GaSb can be explained by postulating a set of impurity levels or an impurity band which lie(s) "above" the minimum of the (000) conduction band. If an impurity band exists, and if one assumes that there are two impurity states for every Te atom, the center of this band must lie above the (000) minimum. The electrons which occupied impurity states were not observed experimentally because their mobilities, if the term be applicable, were much smaller than those of the electrons in the (000) and ⟨111⟩ conduction bands.

The Fermi energies of the (000) and ⟨111⟩ bands, measured from the minimum/minima of their respective bands, are recorded in tables T4:15 to T4:19 . It may be observed that these Fermi energies increase with increasing impurity concentration and decrease with increasing temperature. E_{F_0} at $4.21^{\circ}K$, which is plotted as a function of N_0 in figure F4:22 , will "lie below" the center of the impurity band or the highest impurity level. If the impurity states consist of a set of impurity levels, these levels must be distributed over a relatively broad range of energies in order to be able to explain the temperature dependencies of the electron densities in the two conduction bands. Since the variation in the values for E_{F_0} at $4.21^{\circ}K$ was relatively large, approximately 0.07 ev. ,

it was necessary to assume that either the density of the impurity levels with respect to the energy, or the energy of the highest impurity level, increases with increasing impurity concentration. Neither possibility conflicts with the existing theory.

For a sufficiently "low" concentration of Te , the impurity states consist of a set of impurity levels. However, when the impurity concentration is sufficiently "high" to produce an appreciable overlap of the impurity wave functions, an impurity band will be formed. For an impurity concentration greater than approximately 0.1 atomic percent, a semiconducting alloy is formed. Its band structure may be calculated by means of the "virtual crystal model". The electron densities in specimens 6 and 7 correspond to impurity concentrations of approximately 0.01 and 0.02 atomic percent. The impurity concentrations in these specimens are probably too high for the impurity states to consist of a set of impurity levels, and too low to be analysed by means of the virtual crystal model.

Bate (62:1) explained certain experimental results for GaSb by postulating a set of Se impurity states which were "split-off" from the ⟨111⟩ minima. An impurity band having ⟨111⟩ symmetry should be produced for a sufficiently "high"

concentration of Te in GaSb . Such a band would not directly interact with the (000) minimum, and therefore would not appear as a distortion of the (000) band. These concepts explain the experimental results for all the Te-doped GaSb specimens which do not show two-band conduction at 4.21°K .

Two-band conduction at 4.21°K requires impurity states which lie above the ⟨111⟩ minima. Therefore, some of the impurity levels or a portion of the impurity band must lie above the ⟨111⟩ minima. If a ⟨111⟩ impurity band overlapped the ⟨111⟩ minima, the two bands should interact to produce a single distorted band. One should then be able to observe all of the quasi-free electrons at any temperature, and $N_0 + N_1$ should be constant with respect to the temperature. However, $N_0 + N_1$ increased monotonically with increasing temperature for specimen #6 , which showed two-band conduction at 4.21°K . This suggests that the impurity states consist of either a set of impurity levels or an impurity band which does not directly interact with the (000) and ⟨111⟩ bands.

(2) ELECTRON MOBILITIES

The drift mobilities, μ_i , the Hall mobilities, $\mu_i r_i F_i$, and the mobility ratios are plotted as functions of T in figures F4:13 to F4:17 . Certain trends may be observed from these figures. The drift mobilities decrease monotonically

with increasing temperature. μ_0 for specimen #5 appears to exhibit a slight maximum at approximately $40^{o}K$. This was probably caused by the assumption that $N_1 = 0$ for $T < 78^{o}K$. The mobility ratio, μ_0/μ_1 , increases with increasing temperature, except for specimen #6 which exhibits a maximum at approximately $120^{o}K$.

This investigation appears to be the first to directly determine the value(s) of μ_0/μ_1 . Sagar (60:11) assumed that $\mu_0/\mu_1 = 6$, independent of N_i and T . He postulated that the $\langle 111 \rangle$ minima had the same density of states as the $\langle 111 \rangle$ minima in Ge . This allowed him to estimate the above value for the mobility ratio. Cardona (60:3), Strauss (61:11) and Piller (63:3) also assumed this value when analysing their experimental data. The only available experimentally determined value was deduced by Becker, Ramdas and Fan (61:1). They used resistivity, Hall, magnetoresistance and infrared absorption measurements in order to extimate the value $\mu_0/\mu_1 = 1/0.06$. The present investigation shows that the mobility ratio is dependent upon T and N_i . The values obtained covered the range from 5 to 21 .

Robinson and Rodriguez (64:7),(65:1) predicted that the values for μ_0 would increase rapidly with increasing N_1 at the onset of two-band conduction. They predicted that the

relatively slowly moving electrons in the ⟨111⟩ minima would screen the potential of the ionized impurities, resulting in increases in the relaxation time and mobility of the (000) electrons. μ_0 is plotted as a function of N_0, for several temperatures, in figure F4:18. It may be observed that for T = 4.21°K, μ_0 increases rapidly with increasing N_0, and exhibits a maximum in the vicinity of 1.3×10^{24} m.$^{-3}$. The decrease in μ_0 beyond the maximum is probably due to the large increase in the number of ionized impurities when the relatively "high" density-of-states ⟨111⟩ minima become populated. As one would expect, the increase in μ_0 is less at the higher temperatures.

These results agree reasonably well with the theory of Robinson and Rodriguez. They predicted that μ_0 would decrease with increasing N_0, in the absence of two-band conduction, because of the increasing number of ionized impurities. This dependence of μ_0 upon N_0 was not observed. They also predicted that μ_0 would rapidly increase with increasing N_0, at the onset of two-band conduction. This behaviour was observed.

2. CONCLUSIONS

The conduction band structure of GaSb , for temperatures below $300^{\circ}K$, was analysed by means of the two-band model. The simple two-band equations were modified in an attempt to take into account the effects produced by variable degeneracy and an energy-dependent relaxation time. The results obtained, using this modified theory, were consistent and reasonable.

The density-of-states effective mass for the $\langle 111 \rangle$ minima, the energy separation between the (000) and $\langle 111 \rangle$ minima at $4.21^{\circ}K$, and the temperature coefficient of this energy separation, were determined. The values determined for these parameters, which are given below, are probably more accurate than the values available in the literature.

$$M_1^*/M = 1.10 \pm 0.06 \qquad (M_1^*/M)/4^{2/3} = 0.44 \pm 0.03$$

$$\Delta E_{4.21^{\circ}K} = 0.0845 \pm 0.0003 \text{ ev.}$$

$$d(\Delta E)/dT_{T \geq 78^{\circ}K} = (8.4 \pm 1.7) \times 10^{-5} \text{ ev./K}^{\circ}$$

Much of the available information about GaSb was deduced using incorrect assumptions. Certain authors assumed that $N_0 + N_1$ was independent of the temperature, for any particular specimen. The present investigation shows that $N_0 + N_1$ increases monotonically with increasing temperature for the temperature range investigated, $T \leq 300^{\circ}K$. The mobility ratio, μ_0/μ_1 , has frequently been assumed to be independent

of the temperature and the electron densities. The present investigation shows that the mobility ratio is a function of T and N_i. The values obtained varied from 5 to 21.

The dependence of μ_0 upon the electron density in the ⟨111⟩ minima and the temperature agreed reasonably well with the theoretical predictions of Robinson and Rodriguez[64:7), (65:1)].

VITA

NAME:	Hartley Bruce Harland
BORN:	Swan River, Manitoba, Canada, 1935
EDUCATED:	
Primary	Strathclair Public School, 1941-49
Secondary	Strathclair High School, 1949-53
University	University of Manitoba, 1953-59
	University of Ottawa, 1959-65
Courses	General Science, Physics
Degrees	B.Sc. 1956, M.Sc. 1959

REFERENCES

49:1 BARDEEN J., PEARSON G.L.
PHYS. REV. - 75 , 865 (1949)

50:1 BARDEEN J., SHOCKLEY W.
PHYS. REV. - 80 , 72 (1950)

50:2 CONWELL E.M., WEISSKOPF V.F.
PHYS. REV. - 77 , 388 (1950)

50:3 ERGINSOY C.
PHYS. REV. - 79 , 1013 (1950)

50:4 FRÖHLICH H., PELZER H., ZIENAU S.
PHIL. MAG. - 41 , 221 (1950)

52:1 CHAMBERS R.G.
PROC. PHYS. SOC. (LOND.) - 65A , 903 (1952)

52:2 DEXTER D.L., SEITZ F.
PHYS. REV. - 86 , 964 (1952)

53:1 HOWARTH D.J., SONDHEIMER E.H.
PROC. ROY. SOC. - 219A , 53 (1953)

53:2 LOW F.E., PINES D.
PHYS. REV. - 91 , 193 (1953)

53:3 PEARSON G.L., TANENBAUM M.
PHYS. REV. - 90 , 153 (1953)

53:4 TANENBAUM M., BRIGGS H.B.
PHYS. REV. - 91 , 1561 (1953)

54:1 ABELES B., MEIBOOM S.
PHYS. REV. - 95 , 31 (1954)

54:2 AUSTIN I.G., McCLYMONT D.R.
PHYSICA - 20 , 1077 (1954)

54:3 BARRIE R., CUNNELL F.A., EDMOND J.T., ROSS I.M.
PHYSICA - 20 , 1087 (1954)

54:4 DEBYE P.P., CONWELL E.M.
PHYS. REV. - 93 , 693 (1954)

54:5 DEXTER R.N., ZEIGER H.J., LAX B.
PHYS. REV. - 95B , 557 (1954)

54:6 HERMAN F.
PHYS. REV. - 93 , 1214 (1954)

54:7 HROSTOWSKI H.J., TANENBAUM M.
PHYSICA - 20 , 1064 (1954)

54:8 [illegible]ER H.N., DUNLAP W.C. JR.
PHYS. REV. - 95 , 51 (1954)

54:9 MORIN F.J., MAITA J.P.
PHYS. REV. - 94A , 1525 (1954)

54:10 READ W.T.
PHIL. MAG. - 45 , 775 , 1119 (1954)

54:11 TAUC J.
CZECH. J. PHYS. - 4 , 311 (1954)

55:1 BENEDEK G.B., PAUL W., BROOKS H.
PHYS. REV. - 100 , 1129 (1955)

55:2 BROOKS H.
ADV. ELECTRONICS & ELECTRON PHYS. - 8 , 85 (1955)

55:3 CONWELL E.M.
PHYS. REV. - 99 , 1195 (1955)

55:4 CRAWFORD J.H., SCHWEINLER H.C., STEVENS D.K.
PHYS. REV. - 99 , 1330 (1955)

55:5 DASH W.C., NEWMAN R.
PHYS. REV. - 99 , 1151 (1955)

55:6 DINGLE R.B.
PHIL. MAG. - 46 , 831 (1955)

55:7 DRESSELHAUS G., KIP A.F., KITTEL C.
PHYS. REV. - 98 , 368 (1955)

55:8 DRESSELHAUS G., KIP A.F., KITTEL C., WAGONER G.
IBID. - 98 , 556 (1955)

55:9 ENZ C.
HELV. PHYS. ACTA - 28 , 158 (1955)

55:10 FREDERIKSE H.P.R., MIELCZAREK E.V.
IBID. - 99 , 1889 (1955)

55:11 GOLDBERG C., ADAMS E.N., DAVIS R.E.
IBID. - 100 , 1146 (1955)

55:12 HERRING C.
BELL SYST. TECH. J. - 34 , 237 (1955)

55:13 KAHN A.H.
PHYS. REV. - 97 , 1647 (1955)

55:14 OSWALD F.
Z. NATURF. - 10A , 927 (1955)

55:15 PETRITZ R.L., SCANLON W.W.
PHYS. REV. - 97 , 1620 (1955)

55:16 RICKAYZEN G.
J. ELECTRON. - 1 , 122 (1955)

55:17 ROBERTS V., QUARRINGTON J.E.
J. ELECTRONICS - 1 , 152 (1955)

55:18 STEVENS D.K., CRAWFORD J.H.
PHYS. REV. - 99 , 487 (1955)

56:1 DEXTER R.N., ZEIGER H.J., LAX B.
PHYS. REV. - 104 , 637 (1956)

56:2 EDMOND J.T., BROOM R.F., CUNNELL F.A.
REP. MEET. SEMICOND. -RUGBY (1956)

56:3 FAN H.Y., SHEPHERD M.L., SPITZER W.
PHOTOCONDUCTIVITY CONFERENCE (1956)

56:4 FRÖHLICH H., PARANJAPE B.V.
PROC. PHYS. SOC. - 69B , 21 (1956)

56:5 FRÖHLICH H., PARANJAPE B.V., KUPER C.G., NAKAJIMA S.
IBID. - 69B , 842 (1956)

56:6 MANSFIELD R.
PROC. PHYS. SOC. (LOND.) - 69B , 76 (1956)

56:7 SCLAR N.
PHYS. REV. - 104 , 1548 (1956)

56:8 SCLAR N.
PHYS. REV. - 104 , 1559 (1956)

56:9 WELKER G., WEISS H.
SOLID STATE PHYSICS - 3 (ACAD. PRESS-1956)

56:10 ZWERDLING S., KEYES R.J., FONER S., KOLM H.H., LAX B.
IBID. - 104 , 1805 (1956)

57:1 BOYLE W.S., BRAILSFORD A.D.
PHYS. REV. - 107 , 903 (1957)

57:2 CALLAWAY J.
J. ELECTRONICS - 2 , 330 (1957)

57:3 FREDERIKSE H.P.R., HOSLER W.R.
PHYS. REV. - 108 , 1136 , 1146 (1957)

57:4 KANE E.O.
J. PHYS. CHEM. SOLIDS - 1 , 249 (1957)

57:5 KOHN W.
SOLID STATE PHYSICS - 5 , 257 (ACAD. PRESS-1957)

57:6 MACFARLANE G.G., MCLEAN T.P., QUARRINGTON J.E., ROBERTS V.
PHYS. REV. - 108 , 1377 (1957)

57:7 POTTER R.F.
PHYS. REV. - 108 , 653 (1957)

57:8 SPITZER W.G., FAN H.Y.
PHYS. REV. - 106B , 882 (1957)

57:9 ZWERDLING S., LAX B.
PHYS. REV. - 106 , 51 (1957)

57:10 ZWERDLING S., LAX B., ROTH L.M.
PHYS. REV. - 108 , 1402 (1957)

58:1 BARCUS L.C., PERLMUTTER A., CALLAWAY J.
PHYS. REV. - 111 , 167 (1958)

58:2 EMELJANENKO O.W., NASLEDOV D.N.
J. TECH. PHYS. MOSCOW - 28 , 1177 (1958)

58:3 MACFARLANE G.G., MCLEAN T.P., QUARRINGTON J.E., ROBERTS V.
PROC. PHYS. SOC. (LOND.) - 71 , 863 (1958)

58:4 RAMDAS A., FAN H.Y.
BULL. AMER. PHYS. SOC. - 3 , 121 (1958)

58:5 SAGAR A.
PHYS. REV. - 112 , 1533 (1958)

58:6 SODHA M.S., EASTMAN P.C.
Z. PHYS. - 150 , 242 (1958)

58:7 WEISBERG L.R., WOOLSTON J.R., GLICKSMAN M.
J. APPL. PHYS. - 29 , 1514 (1958)

59:1 BARCUS L.C., PERLMUTTER A., CALLAWAY J.
PHYS. REV. - 115 , 1778 (1959)

59:2 EDWARDS A.L. SLYKHOUSE T.E., DRICKAMER H.G.
J. PHYS. CHEM. SOLIDS - 11 , 140 (1959)

59:3 GLICKSMAN M.
J. PHYS. CHEM. SOLIDS - 8 , 511 (1959)

59:4 HANNAY N.B.
SEMICONDUCTORS (REINHOLD - 1959)

59:5 LAX B., ROTH L.M., ZWERDLING S.
J. PHYS. CHEM. SOLIDS - 8 , 311 (1959)

59:6 LONG D., MYERS J.
PHYS. REV. - 115 , 1107 (1959)

59:7 MOSS T.S.
OPTICAL PROP. SEMICOND. (BUTTERWORTHS - 1959)

59:8 MOSS T.S., SMITH S.D., TAYLOR K.W.
J. PHYS. CHEM. SOLIDS - 8 , 323 (1959)

59:9 MOSS T.S., WALTON A.K.
PROC. PHYS. SOC. (LOND.) - 74 , 131 (1959)

59:10 PUTLEY E.H.
PROC. PHYS. SOC. (LOND.) - 73 , 280 (1959)

59:11 SMITH R.A.
SEMICONDUCTORS (CAMBRIDGE UNIV. PRESS - 1959)

59:12 SPITZER W.G., WHELAN J.M.
PHYS. REV. - 114 , 59 (1959)

59:13 WHITE G.K.
EXP. TECH. LOW-TEMP. PHYS. (CLARENDON PRESS - 1959)

59:14 ZWERDLING S., LAX B., BUTTON K.J., ROTH L.M.
J. PHYS. CHEM. SOLIDS - 9 , 320 (1959)

60:1 AUKERMAN L.W., WILLARDSON R.K.
J. APPL. PHYS. - 31 , 939 (1960)

60:2 BRUST D., PHILLIPS J.C., BASSANI F.
PHYS. REV. LETTERS - 9 , 94 (1960)

60:3 CARDONA M.
PHYS. REV. LETTERS - 9 , 336 (1960)

60:4 EHRENREICH H.
SEMICOND. PHYS. CONF. (PRAGUE) - 67 (1960)

60:5 EHRENREICH H.
PHYS. REV. - 120 , 1951 (1960)

60:6 EHRENREICH H., OLECHNA D.J.
BULL. AM. PHYS. SOC. - 5 , 151 (1960)

60:7 FAN H.Y., GOBELI G.W.
PHYS. REV. LETTERS - 4 , 546 (1960)

60:8 KEYES R.W., POLLACK M.
PHYS. REV. - 118 , 1001 (1960)

60:9 LAX B., MAVROIDES J.G.
SOLID STATE PHYSICS - 11 , 261 (ACAD. PRESS - 1960)

60:10 PUTLEY E.H.
THE HALL EFFECT & RELATED PHENOMENA - BUTTERWORTHS (1960)

60:11 SAGAR A.
PHYS. REV. - 117 , 93 (1960)

60:12 TAUC J., ABRAHAM A.
PROC. INT. CONF. SEMICOND. - PRAGUE (1960)

61:1 BECKER W.M., RAMDAS A.K., FAN H.Y.
J. APPL. PHYS. - 32 , 2094 (1961)

61:2 CARDONA M.
PHYS. REV. - 121 , 752 (1961)

61:3 CARDONA M.
J. PHYS. CHEM. SOLIDS - 17 , 336 (1961)

61:4 EHRENREICH H.
J. APPL. PHYS. SUPPL. - 32 , 2155 (1961)

61:5 EDWARDS A.L., DRICKAMER H.G.
PHYS. REV. - 122 , 1149 (1961)

61:6 HILSUM C., ROSE-INNES A.C.
SEMICOND. 3-5 CPDS. - 47 (PERGAMON PRESS - 1961)

61:7 IVANOV-OMSKII V.I., KOLOMIETS B.T.
FIZ. TVERD. TELA - 3 , 3553 (1961)

61:8 KRAVCHENKO A.F.
IZVERTIJA WUZOW - 3 , 80 (1961)

61:9 PALIK E.D., TEITLER S., WALLIS R.F.
J. APPL. PHYS. SUPPL. - 32 , 2132 (1961)

61:10 SAGAR A., MILLER R.C.
J. APPL. PHYS. - 32 , 2073 (1961)

61:11 STAUSS A.J.
PHYS. REV. - 121 , 1087 (1961)

61:12 ZWERDLING S., KLEINER W.H., THERIAULT J.P.
J. APPL. PHYS. SUPPL. - 32 , 2118 (1961)

62:1 BATE R.T.
J. APPL. PHYS. - 33 , 26 (1962)

62:2 BRAUNSTEIN R., KANE E.O.
J. PHYS. CHEM. SOLIDS - 23 , 1423 (1962)

62:3 CARDONA M., GREENAWAY D.L.
PHYS. REV. - 125 , 1291 (1962)

62:4 GREENAWAY D.L., CARDONA M.
PROC. INT. CONF. PHYS. SEMICOND. - EXETER (1962)

62:5 IVANOV-OMSKII V.I., KOLOMIETS B.T., CHOU-HUANG
SOV. PHYS. - SOLID STATE - 4 , 276 (1962)

62:6 KRAVCHENKO A.F., FAN H.Y.
SEMICOND. PHYS. CONF. - 737 (EXETER - 1962)

62:7 LONG D.
J. APPL PHYS. - 33 , 1682 (1962)

62:8 PILLER H., PATTON V.
BULL. AMER. PHYS. SOC. - 7 , 184 (1962)

62:9 SMITH S.D., PIDGEON C.R., PROSSER V.
PROC. INT. CONF. PHYS. SEMICOND. - 301 (EXETER - 1962)

62:10 STURGE M.
PHYS. REV. - 127 , 768 (1962)

63:1 BECKER W.M., FAN H.Y.
BULL. AM. PHYS. SOC. - 8 , 246 (1963)

63:2 CARDONA M.
J. PHYS. CHEM. SOLIDS - 24 , 1543 (1963)

63:3 PILLER H.
J. PHYS. CHEM. SOLIDS - 24 , 425 (1963)

63:4 PILLER H., PATTON V.A.
PHYS. REV. - 129 , 1169 (1963)

63:5 SILVERMAN S.J., CARLSON R.O., EHRENREICH H.
J. APPL. PHYS. - 34 , 456 (1963)

63:6 UKHANOV Y.I.
FIZ. TVERD. TELA - 5 , 108 (1963)

64:1 BECKER W.M., FAN H.Y.
PROC. 7th INT. CONF. PHYS. SEMICOND. - 663 (PARIS - 1964)

64:2 BERNARD W., ROTH H., STRAUB W.D., MULHERN J.E.
PHYS REV. - 135A , 1386 (1964)

64:3 CARDONA M.
PROC. 7th INT. CONF. PHYS. SEMICOND. - 181 (PARIS - 1964)

64:4 HINKLEY E.D., EWALD A.W.
PHYS. REV. - 134A , 1261 (1964)

64:5 MADELUNG O.
PHYSICS OF 3-5 COMPOUNDS - WILEY (1964)

64:6 PILLER H.
PROC. 7th INT. CONF. PHYS. SEMICOND. -297 (PARIS - 1964)

64:7 ROBINSON J.E., RODRIGUEZ S.
PHYS. REV. - 135A , 779 (1964)

64:8 WOOLLEY J.C., THOMPSON A.G.
CAN. J. PHYS. - 42 , 2030 (1964)

65:1 ROBINSON J.E., RODRIGUEZ S.
PHYS. REV. - 137A , 663 (1965)

65:2 CARDONA M.
PRIVATE COMMUNICATION

65:3 BECKER W.M.
PRIVATE COMMUNICATION

APPENDIX

ETA*	F(-0.5)	F(0.0)	F(0.5)	F(1.0)	F(1.5)	F(2.0)	F(3.5)
0.0	1.0721E+00	6.9314E-01	6.7740E-01	8.2246E-01	1.1528E+00	1.8030E+00	1.1183E+01
-.1	1.0058E+00	6.4439E-01	6.2615E-01	7.5561E-01	1.0550E+00	1.6453E+00	1.0153E+01
-.2	9.4181E-01	5.9813E-01	5.7747E-01	6.9350E-01	9.6479E-01	1.5005E+00	9.2162E+00
-.3	8.8014E-01	5.5435E-01	5.3193E-01	6.3590E-01	8.8162E-01	1.3676E+00	8.3631E+00
-.4	8.2095E-01	5.1301E-01	4.8941E-01	5.8255E-01	8.0506E-01	1.2458E+00	7.5872E+00
-.5	7.6433E-01	4.7407E-01	4.4979E-01	5.3321E-01	7.3465E-01	1.1343E+00	6.8818E+00
-.6	7.1034E-01	4.3748E-01	4.1293E-01	4.8765E-01	6.6998E-01	1.0323E+00	6.2407E+00
-.7	6.5902E-01	4.0318E-01	3.7871E-01	4.4564E-01	6.1064E-01	9.3906E-01	5.6583E+00
-.8	6.1039E-01	3.7110E-01	3.4698E-01	4.0694E-01	5.5624E-01	8.5386E-01	5.1293E+00
-.9	5.6444E-01	3.4115E-01	3.1762E-01	3.7135E-01	5.0643E-01	7.7608E-01	4.6491E+00
-1.0	5.2115E-01	3.1326E-01	2.9050E-01	3.3864E-01	4.6084E-01	7.0512E-01	4.2132E+00
-1.1	4.8047E-01	2.8733E-01	2.6547E-01	3.0863E-01	4.1917E-01	6.4044E-01	3.8177E+00
-1.2	4.4236E-01	2.6328E-01	2.4241E-01	2.8111E-01	3.8110E-01	5.8150E-01	3.4588E+00
-1.3	4.0674E-01	2.4100E-01	2.2119E-01	2.5591E-01	3.4636E-01	5.2784E-01	3.1333E+00
-1.4	3.7352E-01	2.2041E-01	2.0169E-01	2.3286E-01	3.1466E-01	4.7899E-01	2.8382E+00
-1.5	3.4262E-01	2.0141E-01	1.8380E-01	2.1178E-01	2.8577E-01	4.3456E-01	2.5706E+00
-1.6	3.1393E-01	1.8390E-01	1.6739E-01	1.9252E-01	2.5945E-01	3.9416E-01	2.3280E+00
-1.7	2.8736E-01	1.6778E-01	1.5237E-01	1.7495E-01	2.3548E-01	3.5744E-01	2.1082E+00
-1.8	2.6278E-01	1.5297E-01	1.3862E-01	1.5892E-01	2.1367E-01	3.2407E-01	1.9090E+00
-1.9	2.4009E-01	1.3938E-01	1.2606E-01	1.4431E-01	1.9383E-01	2.9377E-01	1.7285E+00
-2.0	2.1919E-01	1.2692E-01	1.1458E-01	1.3101E-01	1.7580E-01	2.6626E-01	1.5649E+00
-2.1	1.9995E-01	1.1551E-01	1.0411E-01	1.1889E-01	1.5941E-01	2.4129E-01	1.4168E+00
-2.2	1.8227E-01	1.0508E-01	9.4566E-02	1.0787E-01	1.4452E-01	2.1863E-01	1.2826E+00
-2.3	1.6605E-01	9.5545E-02	8.5864E-02	9.7851E-02	1.3099E-01	1.9807E-01	1.1610E+00
-2.4	1.5118E-01	8.6836E-02	7.7938E-02	8.8739E-02	1.1872E-01	1.7943E-01	1.0510E+00
-2.5	1.3757E-01	7.8889E-02	7.0724E-02	8.0459E-02	1.0758E-01	1.6252E-01	9.5136E-01
-2.6	1.2512E-01	7.1644E-02	6.4161E-02	7.2938E-02	9.7472E-02	1.4719E-01	8.6112E-01
-2.7	1.1375E-01	6.5043E-02	5.8193E-02	6.6108E-02	8.8302E-02	1.3330E-01	7.7941E-01
-2.8	1.0336E-01	5.9032E-02	5.2769E-02	5.9909E-02	7.9986E-02	1.2071E-01	7.0544E-01
-2.9	9.3894E-02	5.3562E-02	4.7841E-02	5.4284E-02	7.2446E-02	1.0930E-01	6.3847E-01
-3.0	8.5259E-02	4.8587E-02	4.3366E-02	4.9180E-02	6.5611E-02	9.8963E-02	5.7784E-01
-3.1	7.7394E-02	4.4063E-02	3.9303E-02	4.4551E-02	5.9416E-02	8.9597E-02	5.2296E-01
-3.2	7.0233E-02	3.9953E-02	3.5615E-02	4.0354E-02	5.3802E-02	8.1113E-02	4.7328E-01
-3.3	6.3718E-02	3.6219E-02	3.2268E-02	3.6548E-02	4.8714E-02	7.3429E-02	4.2831E-01
-3.4	5.7793E-02	3.2828E-02	2.9233E-02	3.3098E-02	4.4105E-02	6.6470E-02	3.8761E-01
-3.5	5.2408E-02	2.9750E-02	2.6480E-02	2.9972E-02	3.9930E-02	6.0168E-02	3.5078E-01

ETA*	F(-0.5)	F(0.0)	F(0.5)	F(1.0)	F(1.5)	F(2.0)	F(3.5)
-3.6	4.7514E-02	2.6957E-02	2.3984E-02	2.7139E-02	3.6148E-02	5.4462E-02	3.1743E-01
-3.7	4.3070E-02	2.4422E-02	2.1721E-02	2.4572E-02	3.2723E-02	4.9295E-02	2.8726E-01
-3.8	3.9035E-02	2.2124E-02	1.9670E-02	2.2246E-02	2.9621E-02	4.4617E-02	2.5995E-01
-3.9	3.5372E-02	2.0039E-02	1.7811E-02	2.0140E-02	2.6812E-02	4.0382E-02	2.3523E-01
-4.0	3.2049E-02	1.8149E-02	1.6127E-02	1.8232E-02	2.4269E-02	3.6547E-02	2.1287E-01
-4.1	2.9034E-02	1.6436E-02	1.4601E-02	1.6504E-02	2.1966E-02	3.3077E-02	1.9262E-01
-4.2	2.6300E-02	1.4884E-02	1.3219E-02	1.4939E-02	1.9881E-02	2.9935E-02	1.7430E-01
-4.3	2.3821E-02	1.3477E-02	1.1967E-02	1.3522E-02	1.7994E-02	2.7091E-02	1.5773E-01
-4.4	2.1573E-02	1.2202E-02	1.0833E-02	1.2239E-02	1.6285E-02	2.4517E-02	1.4272E-01
-4.5	1.9536E-02	1.1047E-02	9.8066E-03	1.1078E-02	1.4738E-02	2.2187E-02	1.2915E-01
-4.6	1.7690E-02	1.0001E-02	8.8767E-03	1.0026E-02	1.3338E-02	2.0078E-02	1.1686E-01
-4.7	1.6018E-02	9.0541E-03	8.0346E-03	9.0746E-03	1.2071E-02	1.8169E-02	1.0575E-01
-4.8	1.4502E-02	8.1960E-03	7.2722E-03	8.2128E-03	1.0924E-02	1.6442E-02	9.5691E-02
-4.9	1.3129E-02	7.4189E-03	6.5820E-03	7.4327E-03	9.8860E-03	1.4879E-02	8.6587E-02
-5.0	1.1886E-02	6.7153E-03	5.9571E-03	6.7266E-03	8.9463E-03	1.3464E-02	7.8350E-02
-5.1	1.0759E-02	6.0782E-03	5.3914E-03	6.0874E-03	8.0959E-03	1.2184E-02	7.0896E-02
-5.2	9.7398E-03	5.5014E-03	4.8794E-03	5.5089E-03	7.3262E-03	1.1025E-02	6.4151E-02
-5.3	8.8162E-03	4.9791E-03	4.4158E-03	4.9853E-03	6.6296E-03	9.9769E-03	5.8047E-02
-5.4	7.9799E-03	4.5064E-03	3.9963E-03	4.5114E-03	5.9992E-03	9.0280E-03	5.2525E-02
-5.5	7.2227E-03	4.0784E-03	3.6165E-03	4.0826E-03	5.4287E-03	8.1693E-03	4.7527E-02
-5.6	6.5372E-03	3.6910E-03	3.2728E-03	3.6944E-03	4.9125E-03	7.3923E-03	4.3005E-02
-5.7	5.9165E-03	3.3403E-03	2.9617E-03	3.3431E-03	4.4453E-03	6.6891E-03	3.8913E-02
-5.8	5.3547E-03	3.0229E-03	2.6802E-03	3.0252E-03	4.0225E-03	6.0528E-03	3.5210E-02
-5.9	4.8461E-03	2.7356E-03	2.4254E-03	2.7375E-03	3.6398E-03	5.4770E-03	3.1860E-02
-6.0	4.3857E-03	2.4756E-03	2.1948E-03	2.4772E-03	3.2936E-03	4.9559E-03	2.8828E-02
-6.1	3.9690E-03	2.2403E-03	1.9861E-03	2.2416E-03	2.9803E-03	4.4844E-03	2.6085E-02
-6.2	3.5919E-03	2.0273E-03	1.7972E-03	2.0284E-03	2.6968E-03	4.0578E-03	2.3603E-02
-6.3	3.2505E-03	1.8346E-03	1.6263E-03	1.8354E-03	2.4402E-03	3.6717E-03	2.1357E-02
-6.4	2.9415E-03	1.6601E-03	1.4716E-03	1.6608E-03	2.2081E-03	3.3224E-03	1.9325E-02
-6.5	2.6619E-03	1.5023E-03	1.3316E-03	1.5028E-03	1.9980E-03	3.0063E-03	1.7486E-02
-6.6	2.4088E-03	1.3594E-03	1.2050E-03	1.3599E-03	1.8079E-03	2.7202E-03	1.5822E-02
-6.7	2.1798E-03	1.2301E-03	1.0903E-03	1.2305E-03	1.6359E-03	2.4614E-03	1.4316E-02
-6.8	1.9725E-03	1.1131E-03	9.8666E-04	1.1134E-03	1.4802E-03	2.2272E-03	1.2954E-02
-6.9	1.7849E-03	1.0072E-03	8.9280E-04	1.0075E-03	1.3394E-03	2.0153E-03	1.1721E-02
-7.0	1.6152E-03	9.1146E-04	8.0787E-04	9.1167E-04	1.2120E-03	1.8235E-03	1.0606E-02
-7.1	1.4616E-03	8.2476E-04	7.3101E-04	8.2493E-04	1.0966E-03	1.6500E-03	9.5970E-03
-7.2	1.3225E-03	7.4630E-04	6.6146E-04	7.4644E-04	9.9233E-04	1.4930E-03	8.6837E-03
-7.3	1.1967E-03	6.7531E-04	5.9853E-04	6.7542E-04	8.9791E-04	1.3509E-03	7.8574E-03

ETA*	F(-0.5)	F(0.0)	F(0.5)	F(1.0)	F(1.5)	F(2.0)	F(3.5)
-7.4	1.0829E-03	6.1106E-04	5.4159E-04	6.1115E-04	8.1247E-04	1.2224E-03	7.1097E-03
-7.5	9.7993E-04	5.5293E-04	4.9006E-04	5.5300E-04	7.3516E-04	1.1060E-03	6.4331E-03
-7.6	8.8671E-04	5.0032E-04	4.4343E-04	5.0038E-04	6.6521E-04	1.0008E-03	5.8209E-03
-7.7	8.0235E-04	4.5272E-04	4.0124E-04	4.5277E-04	6.0191E-04	9.0560E-04	5.2670E-03
-7.8	7.2602E-04	4.0965E-04	3.6306E-04	4.0969E-04	5.4463E-04	8.1942E-04	4.7658E-03
-7.9	6.5695E-04	3.7067E-04	3.2851E-04	3.7070E-04	4.9281E-04	7.4145E-04	4.3123E-03
-8.0	5.9445E-04	3.3540E-04	2.9726E-04	3.3543E-04	4.4591E-04	6.7089E-04	3.9019E-03
-8.1	5.3789E-04	3.0349E-04	2.6897E-04	3.0351E-04	4.0348E-04	6.0705E-04	3.5306E-03
-8.2	4.8671E-04	2.7461E-04	2.4338E-04	2.7463E-04	3.6509E-04	5.4928E-04	3.1946E-03
-8.3	4.4040E-04	2.4848E-04	2.2022E-04	2.4850E-04	3.3034E-04	4.9701E-04	2.8906E-03
-8.4	3.9850E-04	2.2484E-04	1.9926E-04	2.2485E-04	2.9891E-04	4.4972E-04	2.6155E-03
-8.5	3.6058E-04	2.0344E-04	1.8030E-04	2.0345E-04	2.7046E-04	4.0692E-04	2.3666E-03
-8.6	3.2627E-04	1.8408E-04	1.6314E-04	1.8409E-04	2.4473E-04	3.6820E-04	2.1414E-03
-8.7	2.9523E-04	1.6657E-04	1.4762E-04	1.6657E-04	2.2144E-04	3.3316E-04	1.9376E-03
-8.8	2.6713E-04	1.5072E-04	1.3357E-04	1.5072E-04	2.0037E-04	3.0146E-04	1.7532E-03
-8.9	2.4171E-04	1.3637E-04	1.2086E-04	1.3638E-04	1.8130E-04	2.7277E-04	1.5864E-03
-9.0	2.1871E-04	1.2340E-04	1.0936E-04	1.2340E-04	1.6405E-04	2.4681E-04	1.4354E-03
-9.1	1.9790E-04	1.1165E-04	9.8957E-05	1.1166E-04	1.4843E-04	2.2332E-04	1.2988E-03
-9.2	1.7907E-04	1.0103E-04	8.9540E-05	1.0103E-04	1.3431E-04	2.0207E-04	1.1752E-03
-9.3	1.6203E-04	9.1420E-05	8.1020E-05	9.1422E-05	1.2153E-04	1.8284E-04	1.0634E-03
-9.4	1.4661E-04	8.2720E-05	7.3310E-05	8.2722E-05	1.0996E-04	1.6544E-04	9.6221E-04
-9.5	1.3266E-04	7.4849E-05	6.6333E-05	7.4850E-05	9.9502E-05	1.4970E-04	8.7065E-04
-9.6	1.2004E-04	6.7726E-05	6.0021E-05	6.7727E-05	9.0033E-05	1.3545E-04	7.8779E-04
-9.7	1.0861E-04	6.1281E-05	5.4309E-05	6.1282E-05	8.1465E-05	1.2256E-04	7.1282E-04
-9.8	9.8281E-05	5.5450E-05	4.9141E-05	5.5450E-05	7.3713E-05	1.1090E-04	6.4499E-04
-9.9	8.8929E-05	5.0173E-05	4.4465E-05	5.0174E-05	6.6698E-05	1.0034E-04	5.8361E-04
-10.0	8.0466E-05	4.5398E-05	4.0233E-05	4.5399E-05	6.0351E-05	9.0799E-05	5.2807E-04

ETA*	F(-0.5)	F(0.0)	F(0.5)	F(1.0)	F(1.5)	F(2.0)	F(3.5)
0.0	1.0721E+00	6.9314E-01	6.7740E-01	8.2246E-01	1.1528E+00	1.8030E+00	1.1183E+01
.1	1.1405E+00	7.4439E-01	7.3267E-01	8.9438E-01	1.2586E+00	1.9746E+00	1.2314E+01
.2	1.2108E+00	7.9813E-01	7.9141E-01	9.7148E-01	1.3730E+00	2.1611E+00	1.3555E+01
.3	1.2829E+00	8.5435E-01	8.5370E-01	1.0540E+00	1.4964E+00	2.3636E+00	1.4916E+01
.4	1.3566E+00	9.1301E-01	9.1964E-01	1.1424E+00	1.6295E+00	2.5832E+00	1.6408E+01
.5	1.4316E+00	9.7407E-01	9.8930E-01	1.2367E+00	1.7728E+00	2.8210E+00	1.8043E+01
.6	1.5078E+00	1.0374E+00	1.0627E+00	1.3373E+00	1.9267E+00	3.0783E+00	1.9834E+01
.7	1.5850E+00	1.1031E+00	1.1400E+00	1.4443E+00	2.0921E+00	3.3563E+00	2.1792E+01
.8	1.6630E+00	1.1711E+00	1.2211E+00	1.5580E+00	2.2692E+00	3.6565E+00	2.3934E+01
.9	1.7415E+00	1.2411E+00	1.3062E+00	1.6786E+00	2.4589E+00	3.9800E+00	2.6275E+01
1.0	1.8203E+00	1.3132E+00	1.3952E+00	1.8063E+00	2.6616E+00	4.3284E+00	2.8831E+01
1.1	1.8994E+00	1.3873E+00	1.4882E+00	1.9413E+00	2.8780E+00	4.7030E+00	3.1620E+01
1.2	1.9785E+00	1.4632E+00	1.5851E+00	2.0838E+00	3.1086E+00	5.1054E+00	3.4660E+01
1.3	2.0574E+00	1.5410E+00	1.6859E+00	2.2340E+00	3.3541E+00	5.5371E+00	3.7973E+01
1.4	2.1361E+00	1.6204E+00	1.7907E+00	2.3921E+00	3.6150E+00	5.9996E+00	4.1579E+01
1.5	2.2143E+00	1.7014E+00	1.8995E+00	2.5582E+00	3.8919E+00	6.4945E+00	4.5502E+01
1.6	2.2920E+00	1.7839E+00	2.0121E+00	2.7324E+00	4.1854E+00	7.0234E+00	4.9766E+01
1.7	2.3690E+00	1.8677E+00	2.1286E+00	2.9150E+00	4.4962E+00	7.5880E+00	5.4396E+01
1.8	2.4453E+00	1.9529E+00	2.2489E+00	3.1060E+00	4.8246E+00	8.1900E+00	5.9419E+01
1.9	2.5207E+00	2.0393E+00	2.3730E+00	3.3056E+00	5.1715E+00	8.8310E+00	6.4865E+01
2.0	2.5953E+00	2.1269E+00	2.5009E+00	3.5139E+00	5.5372E+00	9.5129E+00	7.0764E+01
2.1	2.6690E+00	2.2155E+00	2.6325E+00	3.7310E+00	5.9224E+00	1.0237E+01	7.7147E+01
2.2	2.7416E+00	2.3050E+00	2.7677E+00	3.9571E+00	6.3276E+00	1.1005E+01	8.4048E+01
2.3	2.8133E+00	2.3955E+00	2.9066E+00	4.1921E+00	6.7534E+00	1.1820E+01	9.1503E+01
2.4	2.8838E+00	2.4868E+00	3.0490E+00	4.4362E+00	7.2002E+00	1.2683E+01	9.9550E+01
2.5	2.9534E+00	2.5788E+00	3.1949E+00	4.6895E+00	7.6688E+00	1.3595E+01	1.0822E+02
2.6	3.0219E+00	2.6716E+00	3.3443E+00	4.9520E+00	8.1594E+00	1.4559E+01	1.1757E+02
2.7	3.0893E+00	2.7650E+00	3.4970E+00	5.2238E+00	8.6727E+00	1.5577E+01	1.2763E+02
2.8	3.1556E+00	2.8590E+00	3.6531E+00	5.5050E+00	9.2092E+00	1.6650E+01	1.3845E+02
2.9	3.2209E+00	2.9535E+00	3.8125E+00	5.7957E+00	9.7694E+00	1.7779E+01	1.5008E+02
3.0	3.2851E+00	3.0485E+00	3.9752E+00	6.0958E+00	1.0353E+01	1.8968E+01	1.6256E+02
3.1	3.3484E+00	3.1440E+00	4.1410E+00	6.4054E+00	1.0962E+01	2.0218E+01	1.7595E+02
3.2	3.4106E+00	3.2399E+00	4.3099E+00	6.7246E+00	1.1596E+01	2.1531E+01	1.9030E+02
3.3	3.4718E+00	3.3362E+00	4.4820E+00	7.0534E+00	1.2256E+01	2.2909E+01	2.0566E+02
3.4	3.5320E+00	3.4328E+00	4.6570E+00	7.3918E+00	1.2942E+01	2.4353E+01	2.2209E+02
3.5	3.5913E+00	3.5297E+00	4.8351E+00	7.7400E+00	1.3654E+01	2.5866E+01	2.3966E+02
3.6	3.6496E+00	3.6269E+00	5.0161E+00	8.0978E+00	1.4393E+01	2.7450E+01	2.5842E+02
3.7	3.7071E+00	3.7244E+00	5.2000E+00	8.4654E+00	1.5159E+01	2.9106E+01	2.7845E+02

ETA*	F(-0.5)	F(0.0)	F(0.5)	F(1.0)	F(1.5)	F(2.0)	F(3.5)
3.8	3.7637E+00	3.8221E+00	5.3868E+00	8.8427E+00	1.5954E+01	3.0837E+01	2.9979E+02
3.9	3.8194E+00	3.9200E+00	5.5763E+00	9.2298E+00	1.6776E+01	3.2644E+01	3.2254E+02
4.0	3.8743E+00	4.0181E+00	5.7687E+00	9.6267E+00	1.7627E+01	3.4529E+01	3.4675E+02
4.1	3.9284E+00	4.1164E+00	5.9637E+00	1.0033E+01	1.8507E+01	3.6495E+01	3.7251E+02
4.2	3.9817E+00	4.2148E+00	6.1615E+00	1.0450E+01	1.9417E+01	3.8543E+01	3.9988E+02
4.3	4.0343E+00	4.3134E+00	6.3618E+00	1.0876E+01	2.0357E+01	4.0676E+01	4.2896E+02
4.4	4.0861E+00	4.4122E+00	6.5648E+00	1.1312E+01	2.1326E+01	4.2895E+01	4.5981E+02
4.5	4.1373E+00	4.5110E+00	6.7704E+00	1.1758E+01	2.2327E+01	4.5202E+01	4.9253E+02
4.6	4.1877E+00	4.6100E+00	6.9785E+00	1.2214E+01	2.3358E+01	4.7599E+01	5.2721E+02
4.7	4.2375E+00	4.7090E+00	7.1891E+00	1.2680E+01	2.4421E+01	5.0088E+01	5.6393E+02
4.8	4.2867E+00	4.8081E+00	7.4022E+00	1.3156E+01	2.5516E+01	5.2672E+01	6.0279E+02
4.9	4.3352E+00	4.9074E+00	7.6178E+00	1.3642E+01	2.6643E+01	5.5352E+01	6.4388E+02
5.0	4.3832E+00	5.0067E+00	7.8357E+00	1.4138E+01	2.7802E+01	5.8130E+01	6.8730E+02
5.2	4.4774E+00	5.2055E+00	8.2787E+00	1.5159E+01	3.0220E+01	6.3988E+01	7.8155E+02
5.4	4.5694E+00	5.4045E+00	8.7311E+00	1.6220E+01	3.2772E+01	7.0262E+01	8.8638E+02
5.6	4.6593E+00	5.6036E+00	9.1925E+00	1.7321E+01	3.5461E+01	7.6969E+01	1.0026E+03
5.8	4.7474E+00	5.8030E+00	9.6628E+00	1.8461E+01	3.8289E+01	8.4125E+01	1.1314E+03
6.0	4.8337E+00	6.0024E+00	1.0141E+01	1.9642E+01	4.1260E+01	9.1744E+01	1.2735E+03
6.2	4.9183E+00	6.2020E+00	1.0629E+01	2.0862E+01	4.4377E+01	9.9844E+01	1.4300E+03
6.4	5.0012E+00	6.4016E+00	1.1125E+01	2.2123E+01	4.7640E+01	1.0844E+02	1.6021E+03
6.6	5.0827E+00	6.6013E+00	1.1629E+01	2.3423E+01	5.1054E+01	1.1754E+02	1.7909E+03
6.8	5.1628E+00	6.8011E+00	1.2141E+01	2.4763E+01	5.4620E+01	1.2718E+02	1.9976E+03
7.0	5.2415E+00	7.0009E+00	1.2662E+01	2.6144E+01	5.8341E+01	1.3736E+02	2.2234E+03
7.2	5.3189E+00	7.2007E+00	1.3190E+01	2.7564E+01	6.2220E+01	1.4810E+02	2.4696E+03
7.4	5.3951E+00	7.4006E+00	1.3725E+01	2.9024E+01	6.6258E+01	1.5942E+02	2.7376E+03
7.6	5.4702E+00	7.6005E+00	1.4268E+01	3.0524E+01	7.0458E+01	1.7133E+02	3.0287E+03
7.8	5.5441E+00	7.8004E+00	1.4819E+01	3.2064E+01	7.4822E+01	1.8384E+02	3.3446E+03
8.0	5.6171E+00	8.0003E+00	1.5377E+01	3.3644E+01	7.9352E+01	1.9698E+02	3.6866E+03
8.2	5.6890E+00	8.2002E+00	1.5942E+01	3.5264E+01	8.4051E+01	2.1076E+02	4.0564E+03
8.4	5.7599E+00	8.4002E+00	1.6515E+01	3.6924E+01	8.8920E+01	2.2520E+02	4.4557E+03
8.6	5.8299E+00	8.6001E+00	1.7094E+01	3.8624E+01	9.3962E+01	2.4031E+02	4.8860E+03
8.8	5.8990E+00	8.8001E+00	1.7681E+01	4.0364E+01	9.9179E+01	2.5610E+02	5.3493E+03
9.0	5.9673E+00	9.0001E+00	1.8274E+01	4.2144E+01	1.0457E+02	2.7261E+02	5.8473E+03
9.2	6.0348E+00	9.2001E+00	1.8874E+01	4.3964E+01	1.1014E+02	2.8983E+02	6.3818E+03
9.4	6.1015E+00	9.4000E+00	1.9481E+01	4.5824E+01	1.1590E+02	3.0778E+02	6.9550E+03
9.6	6.1674E+00	9.6000E+00	2.0094E+01	4.7724E+01	1.2183E+02	3.2649E+02	7.5687E+03
9.8	6.2326E+00	9.8000E+00	2.0714E+01	4.9664E+01	1.2796E+02	3.4597E+02	8.2251E+03
10.0	6.2971E+00	1.0000E+01	2.1341E+01	5.1644E+01	1.3426E+02	3.6623E+02	8.9262E+03

ETA*	F(-0.5)	F(0.0)	F(0.5)	F(1.0)	F(1.5)	F(2.0)	F(3.5)
10.5	6.4553E+00	1.0500E+01	2.2935E+01	5.6769E+01	1.5087E+02	4.2041E+02	1.0889E+04
11.0	6.6097E+00	1.1000E+01	2.4568E+01	6.2144E+01	1.6868E+02	4.7985E+02	1.3183E+04
11.5	6.7604E+00	1.1500E+01	2.6239E+01	6.7769E+01	1.8774E+02	5.4479E+02	1.5846E+04
12.0	6.9077E+00	1.2000E+01	2.7948E+01	7.3644E+01	2.0806E+02	6.1547E+02	1.8920E+04
12.5	7.0518E+00	1.2500E+01	2.9693E+01	7.9769E+01	2.2967E+02	6.9216E+02	2.2449E+04
13.0	7.1930E+00	1.3000E+01	3.1473E+01	8.6144E+01	2.5261E+02	7.7510E+02	2.6481E+04
13.5	7.3314E+00	1.3500E+01	3.3289E+01	9.2769E+01	2.7690E+02	8.6453E+02	3.1066E+04
14.0	7.4672E+00	1.4000E+01	3.5138E+01	9.9644E+01	3.0256E+02	9.6072E+02	3.6257E+04
14.5	7.6005E+00	1.4500E+01	3.7022E+01	1.0676E+02	3.2962E+02	1.0639E+03	4.2109E+04
15.0	7.7314E+00	1.5000E+01	3.8938E+01	1.1414E+02	3.5811E+02	1.1743E+03	4.8684E+04
15.5	7.8602E+00	1.5500E+01	4.0887E+01	1.2176E+02	3.8804E+02	1.2922E+03	5.6041E+04
16.0	7.9868E+00	1.6000E+01	4.2868E+01	1.2964E+02	4.1945E+02	1.4179E+03	6.4248E+04
16.5	8.1115E+00	1.6500E+01	4.4880E+01	1.3776E+02	4.5236E+02	1.5516E+03	7.3373E+04
17.0	8.2342E+00	1.7000E+01	4.6923E+01	1.4614E+02	4.8679E+02	1.6935E+03	8.3488E+04
17.5	8.3551E+00	1.7500E+01	4.8997E+01	1.5476E+02	5.2276E+02	1.8440E+03	9.4667E+04
18.0	8.4743E+00	1.8000E+01	5.1101E+01	1.6364E+02	5.6030E+02	2.0032E+03	1.0699E+05
18.5	8.5918E+00	1.8499E+01	5.3234E+01	1.7276E+02	5.9943E+02	2.1714E+03	1.2054E+05
19.0	8.7077E+00	1.8999E+01	5.5396E+01	1.8214E+02	6.4016E+02	2.3488E+03	1.3540E+05
19.5	8.8220E+00	1.9499E+01	5.7587E+01	1.9176E+02	6.8253E+02	2.5357E+03	1.5166E+05
20.0	8.9349E+00	1.9999E+01	5.9807E+01	2.0164E+02	7.2656E+02	2.7324E+03	1.6941E+05
21.0	9.1564E+00	2.0999E+01	6.4329E+01	2.2214E+02	8.1966E+02	3.1560E+03	2.0979E+05
22.0	9.3727E+00	2.1999E+01	6.8962E+01	2.4364E+02	9.1962E+02	3.6217E+03	2.5735E+05
23.0	9.5841E+00	2.2999E+01	7.3701E+01	2.6614E+02	1.0266E+03	4.1313E+03	3.1296E+05
24.0	9.7908E+00	2.3999E+01	7.8545E+01	2.8964E+02	1.1408E+03	4.6869E+03	3.7755E+05
25.0	9.9933E+00	2.4999E+01	8.3490E+01	3.1414E+02	1.2623E+03	5.2905E+03	4.5214E+05
26.0	1.0191E+01	2.5999E+01	8.8537E+01	3.3964E+02	1.3913E+03	5.9442E+03	5.3777E+05
27.0	1.0386E+01	2.6999E+01	9.3681E+01	3.6614E+02	1.5280E+03	6.6498E+03	6.3559E+05
28.0	1.0577E+01	2.7999E+01	9.8922E+01	3.9364E+02	1.6724E+03	7.4094E+03	7.4678E+05
29.0	1.0765E+01	2.8999E+01	1.0425E+02	4.2214E+02	1.8248E+03	8.2250E+03	8.7261E+05
30.0	1.0949E+01	2.9999E+01	1.0968E+02	4.5164E+02	1.9853E+03	9.0986E+03	1.0144E+06
31.0	1.1130E+01	3.0999E+01	1.1520E+02	4.8214E+02	2.1539E+03	1.0032E+04	1.1735E+06
32.0	1.1309E+01	3.1999E+01	1.2081E+02	5.1364E+02	2.3309E+03	1.1027E+04	1.3516E+06
33.0	1.1484E+01	3.2999E+01	1.2651E+02	5.4614E+02	2.5164E+03	1.2087E+04	1.5500E+06
34.0	1.1657E+01	3.3999E+01	1.3229E+02	5.7964E+02	2.7106E+03	1.3213E+04	1.7705E+06
35.0	1.1828E+01	3.4999E+01	1.3817E+02	6.1414E+02	2.9134E+03	1.4406E+04	2.0147E+06
36.0	1.1996E+01	3.5999E+01	1.4412E+02	6.4964E+02	3.1251E+03	1.5670E+04	2.2844E+06
37.0	1.2161E+01	3.6999E+01	1.5016E+02	6.8614E+02	3.3459E+03	1.7006E+04	2.5814E+06
38.0	1.2325E+01	3.7999E+01	1.5628E+02	7.2364E+02	3.5757E+03	1.8415E+04	2.9077E+06

ETA*	F(-0.5)	F(0.0)	F(0.5)	F(1.0)	F(1.5)	F(2.0)	F(3.5)
39.0	1.2486E+01	3.8999E+01	1.6249E+02	7.6214E+02	3.8148E+03	1.9901E+04	3.2653E+06
40.0	1.2645E+01	3.9999E+01	1.6877E+02	8.0164E+02	4.0633E+03	2.1464E+04	3.6563E+06
41.0	1.2803E+01	4.0999E+01	1.7513E+02	8.4214E+02	4.3212E+03	2.3108E+04	4.0829E+06
42.0	1.2958E+01	4.1999E+01	1.8157E+02	8.8364E+02	4.5887E+03	2.4834E+04	4.5473E+06
43.0	1.3111E+01	4.2999E+01	1.8809E+02	9.2614E+02	4.8660E+03	2.6643E+04	5.0518E+06
44.0	1.3263E+01	4.3999E+01	1.9468E+02	9.6964E+02	5.1531E+03	2.8539E+04	5.5989E+06
45.0	1.3413E+01	4.4999E+01	2.0135E+02	1.0141E+03	5.4501E+03	3.0523E+04	6.1912E+06
46.0	1.3562E+01	4.5999E+01	2.0809E+02	1.0596E+03	5.7572E+03	3.2596E+04	6.8311E+06
47.0	1.3708E+01	4.6999E+01	2.1491E+02	1.1061E+03	6.0745E+03	3.4762E+04	7.5214E+06
48.0	1.3853E+01	4.7999E+01	2.2180E+02	1.1536E+03	6.4021E+03	3.7021E+04	8.2649E+06
49.0	1.3997E+01	4.8999E+01	2.2876E+02	1.2021E+03	6.7400E+03	3.9377E+04	9.0643E+06
50.0	1.4139E+01	4.9999E+01	2.3580E+02	1.2516E+03	7.0885E+03	4.1831E+04	9.9228E+06
55.0	1.4830E+01	5.4999E+01	2.7202E+02	1.5141E+03	8.9918E+03	5.5639E+04	1.5209E+07
60.0	1.5490E+01	5.9999E+01	3.0992E+02	1.8016E+03	1.1173E+04	7.2197E+04	2.2469E+07
65.0	1.6122E+01	6.4999E+01	3.4944E+02	2.1141E+03	1.3645E+04	9.1755E+04	3.2177E+07
70.0	1.6731E+01	6.9999E+01	3.9051E+02	2.4516E+03	1.6419E+04	1.1456E+05	4.4876E+07
75.0	1.7319E+01	7.4999E+01	4.3308E+02	2.8141E+03	1.9506E+04	1.4087E+05	6.1172E+07
80.0	1.7887E+01	7.9999E+01	4.7709E+02	3.2016E+03	2.2919E+04	1.7092E+05	8.1742E+07
85.0	1.8438E+01	8.4999E+01	5.2250E+02	3.6141E+03	2.6667E+04	2.0498E+05	1.0733E+08
90.0	1.8972E+01	8.9999E+01	5.6926E+02	4.0516E+03	3.0760E+04	2.4329E+05	1.3876E+08
95.0	1.9492E+01	9.4999E+01	6.1734E+02	4.5141E+03	3.5209E+04	2.8610E+05	1.7692E+08
100.0	1.9999E+01	9.9999E+01	6.6671E+02	5.0016E+03	4.0024E+04	3.3366E+05	2.2279E+08
200.0	2.8285E+01	1.9999E+02	1.8855E+03	2.0001E+04	2.2630E+05	2.6673E+06	5.0315E+09

ETA*	F(0.5)	F(0.5)/LIM	R(-0.5)	R(0.5)	R(1.5)
0.0	6.7740E-01	.7643	1.1337	1.0822	1.7477
-.1	6.2615E-01	.7808	1.1375	1.0846	1.7613
-.2	5.7747E-01	.7958	1.1401	1.0860	1.7728
-.3	5.3193E-01	.8102	1.1426	1.0872	1.7838
-.4	4.8941E-01	.8238	1.1449	1.0884	1.7943
-.5	4.4979E-01	.8367	1.1472	1.0895	1.8043
-.6	4.1293E-01	.8490	1.1494	1.0906	1.8136
-.7	3.7871E-01	.8605	1.1515	1.0916	1.8224
-.8	3.4698E-01	.8713	1.1534	1.0926	1.8308
-.9	3.1762E-01	.8815	1.1553	1.0935	1.8387
-1.0	2.9050E-01	.8910	1.1570	1.0944	1.8462
-1.1	2.6547E-01	.8999	1.1587	1.0952	1.8531
-1.2	2.4241E-01	.9081	1.1602	1.0959	1.8596
-1.3	2.2119E-01	.9158	1.1617	1.0967	1.8656
-1.4	2.0169E-01	.9228	1.1630	1.0972	1.8712
-1.5	1.8380E-01	.9294	1.1642	1.0979	1.8764
-1.6	1.6739E-01	.9355	1.1653	1.0985	1.8811
-1.7	1.5237E-01	.9411	1.1665	1.0989	1.8856
-1.8	1.3862E-01	.9462	1.1675	1.0994	1.8897
-1.9	1.2606E-01	.9510	1.1684	1.0999	1.8936
-2.0	1.1458E-01	.9553	1.1693	1.1002	1.8969
-2.1	1.0411E-01	.9593	1.1701	1.1007	1.9001
-2.2	9.4566E-02	.9630	1.1707	1.1011	1.9031
-2.3	8.5864E-02	.9663	1.1713	1.1012	1.9057
-2.4	7.7938E-02	.9694	1.1719	1.1015	1.9081
-2.5	7.0724E-02	.9722	1.1725	1.1018	1.9105
-2.6	6.4161E-02	.9747	1.1730	1.1020	1.9126
-2.7	5.8193E-02	.9770	1.1734	1.1023	1.9144
-2.8	5.2769E-02	.9791	1.1738	1.1025	1.9160
-2.9	4.7841E-02	.9810	1.1743	1.1026	1.9176
-3.0	4.3366E-02	.9828	1.1746	1.1028	1.9189
-3.1	3.9303E-02	.9844	1.1750	1.1030	1.9202
-3.2	3.5615E-02	.9858	1.1752	1.1031	1.9214
-3.3	3.2268E-02	.9871	1.1754	1.1032	1.9224
-3.4	2.9233E-02	.9883	1.1757	1.1033	1.9234
-3.5	2.6480E-02	.9894	1.1759	1.1034	1.9243
-3.6	2.3984E-02	.9904	1.1761	1.1035	1.9250
-3.7	2.1721E-02	.9913	1.1763	1.1036	1.9257

ETA*	F(0.5)	F(0.5)/LIM	R(-0.5)	R(0.5)	R(1.5)
-3.8	1.9670E-02	.9921	1.1765	1.1037	1.9264
-3.9	1.7811E-02	.9928	1.1766	1.1037	1.9269
-4.0	1.6127E-02	.9935	1.1768	1.1038	1.9276
-4.1	1.4601E-02	.9941	1.1769	1.1038	1.9279
-4.2	1.3219E-02	.9946	1.1769	1.1039	1.9284
-4.3	1.1967E-02	.9951	1.1771	1.1040	1.9289
-4.4	1.0833E-02	.9956	1.1772	1.1041	1.9291
-4.5	9.8066E-03	.9960	1.1774	1.1040	1.9296
-4.6	8.8767E-03	.9964	1.1774	1.1042	1.9299
-4.7	8.0346E-03	.9967	1.1774	1.1041	1.9303
-4.8	7.2722E-03	.9970	1.1774	1.1041	1.9305
-4.9	6.5820E-03	.9973	1.1775	1.1042	1.9307
-5.0	5.9571E-03	.9976	1.1776	1.1042	1.9310
-5.1	5.3914E-03	.9978	1.1775	1.1042	1.9311
-5.2	4.8794E-03	.9980	1.1776	1.1042	1.9314
-5.3	4.4158E-03	.9982	1.1777	1.1042	1.9313
-5.4	3.9963E-03	.9983	1.1777	1.1043	1.9315
-5.5	3.6165E-03	.9985	1.1777	1.1042	1.9316
-5.6	3.2728E-03	.9986	1.1778	1.1043	1.9317
-5.7	2.9617E-03	.9987	1.1778	1.1043	1.9317
-5.8	2.6802E-03	.9989	1.1779	1.1043	1.9318
-5.9	2.4254E-03	.9990	1.1779	1.1043	1.9319
-6.0	2.1948E-03	.9991	1.1779	1.1043	1.9320
-6.1	1.9861E-03	.9992	1.1779	1.1043	1.9321
-6.2	1.7972E-03	.9992	1.1780	1.1043	1.9321
-6.3	1.6263E-03	.9993	1.1779	1.1044	1.9322
-6.4	1.4716E-03	.9993	1.1780	1.1044	1.9322
-6.5	1.3316E-03	.9994	1.1779	1.1044	1.9322
-6.6	1.2050E-03	.9995	1.1780	1.1043	1.9324
-6.7	1.0903E-03	.9994	1.1779	1.1043	1.9322
-6.8	9.8666E-04	.9995	1.1780	1.1044	1.9324
-6.9	8.9280E-04	.9996	1.1781	1.1044	1.9324
-7.0	8.0787E-04	.9996	1.1780	1.1044	1.9326
-7.1	7.3101E-04	.9996	1.1780	1.1043	1.9326
-7.2	6.6146E-04	.9997	1.1779	1.1044	1.9326
-7.3	5.9853E-04	.9997	1.1779	1.1044	1.9327
-7.4	5.4159E-04	.9997	1.1780	1.1044	1.9326
-7.5	4.9006E-04	.9997	1.1780	1.1044	1.9329

ETA*	F(0.5)	F(0.5)/LIM	R(-0.5)	R(0.5)	R(1.5)
-7.6	4.4343E-04	.9998	1.1780	1.1044	1.9327
-7.7	4.0124E-04	.9998	1.1780	1.1044	1.9326
-7.8	3.6306E-04	.9998	1.1780	1.1044	1.9326
-7.9	3.2851E-04	.9998	1.1780	1.1044	1.9326
-8.0	2.9726E-04	.9998	1.1781	1.1044	1.9327
-8.1	2.6897E-04	.9998	1.1780	1.1044	1.9327
-8.2	2.4338E-04	.9998	1.1781	1.1044	1.9327
-8.3	2.2022E-04	.9998	1.1781	1.1044	1.9327
-8.4	1.9926E-04	.9998	1.1780	1.1044	1.9326
-8.5	1.8030E-04	.9998	1.1781	1.1044	1.9326
-8.6	1.6314E-04	.9998	1.1781	1.1044	1.9326
-8.7	1.4762E-04	.9999	1.1780	1.1045	1.9327
-8.8	1.3357E-04	.9998	1.1780	1.1045	1.9326
-8.9	1.2086E-04	.9999	1.1781	1.1044	1.9326
-9.0	1.0936E-04	.9999	1.1780	1.1045	1.9327
-9.1	9.8957E-05	.9999	1.1782	1.1044	1.9328
-9.2	8.9540E-05	.9999	1.1781	1.1045	1.9327
-9.3	8.1020E-05	.9999	1.1780	1.1044	1.9328
-9.4	7.3310E-05	.9999	1.1780	1.1044	1.9329
-9.5	6.6333E-05	.9999	1.1780	1.1044	1.9328
-9.6	6.0021E-05	.9999	1.1780	1.1044	1.9329
-9.7	5.4309E-05	.9999	1.1780	1.1044	1.9329
-9.8	4.9141E-05	.9999	1.1780	1.1044	1.9328
-9.9	4.4465E-05	.9999	1.1781	1.1044	1.9330
-10.0	4.0233E-05	.9999	1.1781	1.1044	1.9327

ETA*	F(0.5)	F(0.5)/LIM	R(-0.5)	R(0.5)	R(1.5)
0.0	6.7740E-01	.7643	1.1337	1.0822	1.7477
.1	7.3267E-01	34.7530	1.1310	1.0807	1.7354
.2	7.9141E-01	13.2720	1.1282	1.0793	1.7227
.3	8.5370E-01	7.7931	1.1253	1.0780	1.7095
.4	9.1964E-01	5.4527	1.1224	1.0764	1.6959
.5	9.8930E-01	4.1972	1.1195	1.0750	1.6822
.6	1.0627E+00	3.4298	1.1166	1.0733	1.6682
.7	1.1400E+00	2.9197	1.1136	1.0718	1.6540
.8	1.2211E+00	2.5598	1.1104	1.0701	1.6394
.9	1.3062E+00	2.2947	1.1075	1.0686	1.6249
1.0	1.3952E+00	2.0928	1.1045	1.0670	1.6102
1.1	1.4882E+00	1.9349	1.1015	1.0654	1.5956
1.2	1.5851E+00	1.8087	1.0986	1.0638	1.5808
1.3	1.6859E+00	1.7061	1.0954	1.0622	1.5660
1.4	1.7907E+00	1.6215	1.0926	1.0605	1.5513
1.5	1.8995E+00	1.5509	1.0897	1.0590	1.5368
1.6	2.0121E+00	1.4912	1.0868	1.0574	1.5224
1.7	2.1286E+00	1.4404	1.0841	1.0559	1.5082
1.8	2.2489E+00	1.3968	1.0814	1.0543	1.4941
1.9	2.3730E+00	1.3591	1.0787	1.0528	1.4802
2.0	2.5009E+00	1.3263	1.0760	1.0514	1.4667
2.1	2.6325E+00	1.2975	1.0735	1.0499	1.4534
2.2	2.7677E+00	1.2722	1.0711	1.0485	1.4405
2.3	2.9066E+00	1.2499	1.0687	1.0471	1.4277
2.4	3.0490E+00	1.2300	1.0663	1.0458	1.4151
2.5	3.1949E+00	1.2123	1.0641	1.0444	1.4030
2.6	3.3443E+00	1.1965	1.0619	1.0432	1.3912
2.7	3.4970E+00	1.1823	1.0598	1.0419	1.3795
2.9	3.8125E+00	1.1579	1.0557	1.0395	1.3576
2.8	3.6531E+00	1.1695	1.0577	1.0407	1.3683
3.0	3.9752E+00	1.1475	1.0538	1.0383	1.3470
3.1	4.1410E+00	1.1380	1.0520	1.0372	1.3368
3.2	4.3099E+00	1.1293	1.0502	1.0361	1.3269
3.3	4.4820E+00	1.1214	1.0485	1.0351	1.3172
3.4	4.6570E+00	1.1142	1.0468	1.0341	1.3079
3.5	4.8351E+00	1.1076	1.0453	1.0331	1.2989
3.6	5.0161E+00	1.1015	1.0437	1.0321	1.2902
3.7	5.2000E+00	1.0959	1.0422	1.0312	1.2818

ETA*	F(0.5)	F(0.5)/LIM	R(-0.5)	R(0.5)	R(1.5)
3.8	5.3868E+00	1.0908	1.0408	1.0303	1.2736
3.9	5.5763E+00	1.0860	1.0395	1.0294	1.2658
4.0	5.7687E+00	1.0816	1.0382	1.0286	1.2583
4.1	5.9637E+00	1.0775	1.0369	1.0279	1.2509
4.2	6.1615E+00	1.0737	1.0357	1.0270	1.2439
4.3	6.3618E+00	1.0702	1.0345	1.0264	1.2370
4.4	6.5648E+00	1.0669	1.0334	1.0257	1.2304
4.5	6.7704E+00	1.0638	1.0323	1.0250	1.2240
4.6	6.9785E+00	1.0610	1.0313	1.0243	1.2178
4.7	7.1891E+00	1.0583	1.0303	1.0236	1.2119
4.8	7.4022E+00	1.0558	1.0294	1.0230	1.2062
4.9	7.6178E+00	1.0534	1.0284	1.0224	1.2006
5.0	7.8357E+00	1.0512	1.0276	1.0217	1.1953
5.2	8.2787E+00	1.0472	1.0259	1.0206	1.1851
5.4	8.7311E+00	1.0436	1.0244	1.0196	1.1757
5.6	9.1925E+00	1.0405	1.0230	1.0186	1.1667
5.8	9.6628E+00	1.0376	1.0216	1.0177	1.1585
6.0	1.0141E+01	1.0350	1.0204	1.0167	1.1507
6.2	1.0629E+01	1.0327	1.0193	1.0160	1.1435
6.4	1.1125E+01	1.0306	1.0182	1.0152	1.1367
6.6	1.1629E+01	1.0287	1.0172	1.0145	1.1305
6.8	1.2141E+01	1.0270	1.0163	1.0138	1.1245
7.0	1.2662E+01	1.0255	1.0155	1.0132	1.1190
7.2	1.3190E+01	1.0240	1.0147	1.0126	1.1138
7.4	1.3725E+01	1.0227	1.0140	1.0120	1.1088
7.6	1.4268E+01	1.0214	1.0133	1.0115	1.1041
7.8	1.4819E+01	1.0203	1.0126	1.0110	1.0998
8.0	1.5377E+01	1.0193	1.0121	1.0106	1.0957
8.2	1.5942E+01	1.0183	1.0115	1.0101	1.0918
8.4	1.6515E+01	1.0175	1.0110	1.0097	1.0882
8.6	1.7094E+01	1.0166	1.0105	1.0093	1.0847
8.8	1.7681E+01	1.0159	1.0101	1.0090	1.0815
9.0	1.8274E+01	1.0152	1.0096	1.0086	1.0783
9.2	1.8874E+01	1.0145	1.0092	1.0082	1.0754
9.4	1.9481E+01	1.0139	1.0089	1.0080	1.0727
9.6	2.0094E+01	1.0133	1.0085	1.0076	1.0700
9.8	2.0714E+01	1.0127	1.0081	1.0074	1.0675
10.0	2.1341E+01	1.0122	1.0078	1.0071	1.0652

ETA*	F(0.5)	F(0.5)/LIM	R(-0.5)	R(0.5)	R(1.5)
10.5	2.2935E+01	1.0111	1.0071	1.0065	1.0597
11.0	2.4568E+01	1.0101	1.0065	1.0060	1.0549
11.5	2.6239E+01	1.0092	1.0059	1.0055	1.0506
12.0	2.7948E+01	1.0084	1.0055	1.0051	1.0469
12.5	2.9693E+01	1.0078	1.0050	1.0047	1.0435
13.0	3.1473E+01	1.0071	1.0046	1.0044	1.0404
13.5	3.3289E+01	1.0066	1.0043	1.0041	1.0377
14.0	3.5138E+01	1.0061	1.0040	1.0038	1.0352
14.5	3.7022E+01	1.0057	1.0037	1.0037	1.0329
15.0	3.8938E+01	1.0053	1.0034	1.0034	1.0310
15.5	4.0887E+01	1.0050	1.0032	1.0032	1.0291
16.0	4.2868E+01	1.0047	1.0030	1.0030	1.0274
16.5	4.4880E+01	1.0044	1.0028	1.0029	1.0258
17.0	4.6923E+01	1.0041	1.0026	1.0026	1.0244
17.5	4.8997E+01	1.0039	1.0025	1.0025	1.0230
18.0	5.1101E+01	1.0037	1.0024	1.0024	1.0218
18.5	5.3234E+01	1.0035	1.0023	1.0023	1.0207
19.0	5.5396E+01	1.0033	1.0022	1.0021	1.0196
19.5	5.7587E+01	1.0031	1.0021	1.0020	1.0187
20.0	5.9807E+01	1.0029	1.0020	1.0019	1.0178
21.0	6.4329E+01	1.0026	1.0018	1.0017	1.0161
22.0	6.8962E+01	1.0024	1.0016	1.0015	1.0147
23.0	7.3701E+01	1.0022	1.0015	1.0014	1.0135
24.0	7.8545E+01	1.0020	1.0014	1.0013	1.0124
25.0	8.3490E+01	1.0018	1.0012	1.0012	1.0115
26.0	8.8537E+01	1.0017	1.0011	1.0011	1.0106
27.0	9.3681E+01	1.0016	1.0010	1.0010	1.0098
28.0	9.8922E+01	1.0014	1.0009	1.0009	1.0092
29.0	1.0425E+02	1.0013	1.0008	1.0008	1.0085
30.0	1.0968E+02	1.0012	1.0008	1.0007	1.0079
31.0	1.1520E+02	1.0011	1.0007	1.0006	1.0074
32.0	1.2081E+02	1.0010	1.0007	1.0006	1.0071
33.0	1.2651E+02	1.0010	1.0006	1.0006	1.0066
34.0	1.3229E+02	1.0009	1.0005	1.0005	1.0061
35.0	1.3817E+02	1.0009	1.0006	1.0005	1.0060
36.0	1.4412E+02	1.0008	1.0005	1.0004	1.0055
37.0	1.5016E+02	1.0007	1.0004	1.0004	1.0052
38.0	1.5628E+02	1.0007	1.0004	1.0004	1.0050

ETA*	F(0.5)	F(0.5)/LIM	R(-0.5)	R(0.5)	R(1.5)
39.0	1.6249E+02	1.0007	1.0004	1.0004	1.0047
40.0	1.6877E+02	1.0006	1.0004	1.0004	1.0045
41.0	1.7513E+02	1.0006	1.0004	1.0003	1.0043
42.0	1.8157E+02	1.0006	1.0003	1.0003	1.0040
43.0	1.8809E+02	1.0005	1.0003	1.0003	1.0039
44.0	1.9468E+02	1.0005	1.0003	1.0003	1.0037
45.0	2.0135E+02	1.0005	1.0003	1.0003	1.0035
46.0	2.0809E+02	1.0004	1.0003	1.0003	1.0034
47.0	2.1491E+02	1.0004	1.0002	1.0003	1.0032
48.0	2.2180E+02	1.0004	1.0002	1.0003	1.0031
49.0	2.2876E+02	1.0004	1.0002	1.0002	1.0029
50.0	2.3580E+02	1.0004	1.0002	1.0003	1.0028
55.0	2.7202E+02	1.0003	1.0002	1.0002	1.0023
60.0	3.0992E+02	1.0002	1.0001	1.0001	1.0019
65.0	3.4944E+02	1.0002	1.0000	1.0001	1.0016
70.0	3.9051E+02	1.0001	1.0000	1.0001	1.0014
75.0	4.3308E+02	1.0001	1.0000	1.0000	1.0012
80.0	4.7709E+02	1.0001	1.0000	1.0000	1.0012
85.0	5.2250E+02	1.0001	1.0000	1.0000	1.0010
90.0	5.6926E+02	1.0000	1.0000	1.0000	1.0008
95.0	6.1734E+02	1.0000	1.0000	1.0000	1.0007
:8 .50016000E+04					
:8 .40024000E+03					
100.0	1.9999E+01	99.9990	666.7100		